DOI:10.14753/SE.2015.1713

The role of matrix substrate-level phosphorylation during anoxia

PhD thesis

Gergely Kiss

Semmelweis University
János Szentágothai Doctoral School of Neurosciences
Functional Neurosciences Program

Supervisor:	Christos Chinopoulos, PhD
Official reviewers:	Ferenc Gallyas Jr, DSc
	Tamás Kardon, PhD
Chairman of the final examination board:	József Mandl, DSc
Members of the final examination board:	Erzsébet Ligeti, DSc
	Olivér Ozohanics, PhD

Budapest

2014

DOI:10.14753/SE.2015.1713

TABLE OF CONTENTS

DOI:10.14753/SE.2015.1713

DOI:10.14753/SE.2015.1713

1. ABBREVIATIONS

β-OHBDH:	β-hydroxybutyrate dehydrogenase
ΔΨm:	transmembrane potential difference
ΔG:	change in Gibbs free energy (ΔG = 0 means equilibrium)
$\Delta G^{0'}$:	change in standard Gibbs free energy
ΔG_p:	mitochondrial phosphorylation potential
ΔpH:	transmembrane proton concentration gradient
1,2/1,4-NQ:	1,2- or 1,4-naphthoquinone
AC:	aconitase
AcAc:	acetoacetate
ADP:	adenosine 5'-(trihydrogen diphosphate)
a-Kg:	α-ketoglutarate
ANOVA:	analysis of variance
ANT:	adenine nucleotide translocase
Ap_5A:	P^1,P^5-di(adenosine-5') pentaphosphate
ASAT:	aspartate aminotransferase
asp:	aspartate
A-SUCL:	ADP-forming succinate-CoA ligase
ATP:	adenosine 5'-(tetrahydrogen triphosphate)
BCECF-AM:	2',7'-bis-(2-carboxyethyl)-5-(and-6)-carboxyfluorescein, acetoxymethyl ester
BKA:	bongkrekic acid
bOH:	β-hydroxybutyrate
BQ:	*p*-benzoquinone
BSA:	bovine serum albumin
cATR:	carboxyatractyloside
CBQ:	2-chloro-1,4-benzoquinone
CHAPS:	3-[(3-cholamidopropyl)dimethylammonio]-1-propanesulfonate
CO_2:	carbon dioxide
CoASH:	coenzyme A
complex I:	NADH-ubiquinone oxidoreductase
complex II:	succinate dehydrogenase
complex III:	ubiquinone-cytochrome *c* oxidoreductase
complex IV:	cytochrome *c* oxidase
complex V:	F_O-F_1 ATP synthase
CoQ_1:	coenzyme Q_1 = ubiquinone 5
CoQ_{10}:	coenzyme Q_{10} = ubiquinone 50 = ubidecarenone
CS:	citrate synthase

Cyb5r2: NADH:cytochrome *b*5 reductase isoform 2
CYPD: cyclophilin D
CysA: cyclosporin A
DCBQ: 2,6-dichloro-1,4-benzoquinone
DCIP: 2,6-dichloroindophenol
DDM: n-Dodecyl-β-D-maltopyranoside
DMBQ: 2,6-dimethylbenzoquinone
DNP: 2,4-dinitrophenol
DLD: dihydrolipoyl dehydrogenase
DLST: dihydrolipoyl succinyltransferase
DQ: duroquinone
DSP: 3,3'-dithiobis(sulfosuccinimidyl propionate)
DTNB: 5,5'-dithiobis(2-nitrobenzoic acid)
EGTA: ethylene glycol-bis(2-aminoethylether)-N,N,N',N'-tetraacetic acid
E_{rev_ANT}: reversal potential of the adenine nucleotide translocase
E_{rev_ATPase}: reversal potential of the F_O-F_1 ATP synthase
F: Faraday constant = 9.64×10^4 C × mol^{-1}
FCCP: carbonyl cyanide 4-(trifluoromethoxy)phenylhydrazone
FerrCyan: ferricyanide = hexacyanoferrate(III), $K_3[Fe(CN)_6]$
FSE: fumarase
GDH: glutamate dehydrogenase
glut: glutamate
GPD2: mitochondrial glycerol-3-phosphate dehydrogenase
G-SUCL: GDP-forming succinate-CoA ligase
GTP: guanosine 5'-(tetrahydrogen triphosphate)
HEPES: 2-[4-(2-hydroxyethyl)piperazin-1-yl]ethanesulfonic acid
IDH: isocitrate dehydrogenase
IDH(2 or 3): isocitrate dehydrogenase, isoform 2 or 3, respectively
IF1: mitochondrial ATPase inhibitory factor 1
KGDH(C): α-ketoglutarate dehydrogenase (complex)
K_M: affinity constant
KO: knock-out
LED: light-emitting diode
mal: malate
MBQ: methyl-*p*-benzoquinone
MDH: malate dehydrogenase
MgG: Magnesium Green™, pentapotassium salt
MIRTD: mitochondrial respiration generator of truncated DLST
mitoQ: mitoquinone mesylate

MnSOD:	manganese superoxide dismutase
n:	coupling ratio (H^+/ATP)
$NaASO_2$:	sodium arsenite
NAD^+:	nicotinamide adenine dinucleotide (oxidized form)
NADH:	nicotinamide adenine dinucleotide (reduced form)
NQO:	NAD(P)H dehydrogenase = NAD(P)H:quinone oxidoreductase
NQO(1 or 2):	NAD(P)H dehydrogenase, quinone 1 or 2, respectively
OCR:	oxygen consumption rate
olgm:	oligomycin
PAGE:	polyacrylamide gel electrophoresis
PC:	pyruvate carboxylase
PEPCK:	phosphoenolpyruvate carboxykinase
PDH(C):	pyruvate dehydrogenase (complex)
P_i:	inorganic phosphate
pmf:	protonmotive force/electrochemical gradient
PTP:	mitochondrial permeability transition pore
PVDF:	polyvinylidene difluoride
pyr:	pyruvate
R:	universal gas constant = 8.31 J $mol^{-1} \times K^{-1}$
RCR:	respiratory control ratio
ROS:	reactive oxygen species
rot:	rotenone
SDH:	succinate dehydrogenase
SDS:	sodium dodecyl sulfate
SEM:	standard error of the mean
SF 6847:	3,5-di-tert-butyl-4-hydroxybenzylidenemalononitrile
State 1:	mitochondria in a P_i containing buffer without substrates and adenylates
State 2:	State 1 + ADP; depletion of endogenous substrates, no respiration
State 2':	State 1 + substrates; low respiration and high $\Delta\Psi m$ due to lack of ADP
State 3:	State 1 + ADP + substrates; high respiration and phosphorylation
State 4:	all ADP has been converted to ATP; low respiration and high $\Delta\Psi m$
State 5:	anoxia
stigm:	stigmatellin
STK, SUCL:	succinyl-CoA synthetase = succinate-CoA ligase = succinate thiokinase
T:	absolute temperature in Kelvin
TMRM:	tetramethylrhodamine methyl ester
TPP:	tetraphenylphosphonium
UCP:	uncoupling protein
WT:	wild-type

DOI:10.14753/SE.2015.1713

2. INTRODUCTION

In 1957 Philip Siekevitz termed mitochondria the “powerhouses of the cell” [1] as the most important function of these organelles is ATP provision. However they contribute to cellular homeostasis in many other ways: mitochondria modulate intracellular Ca^{2+} levels, generate and eliminate reactive oxygen species (ROS), serve as metabolic hubs and participate in thermoregulation. In addition, mitochondria could integrate and release signals leading to cell demise. Substantial body of evidence has accumulated over the past two decades pointing out that impaired mitochondrial function is involved in cellular deterioration associated with pathological conditions such as ischemia/reperfusion, excitotoxicity, neurodegenerative diseases or trauma (see [2] and references within). Dysfunction of these organelles is characterized by depolarization, energy deficit, impaired Ca^{2+} handling, oxidative stress and changes in the permeability of the inner membrane [3]. Depolarized mitochondria are thought to precipitate cell death by avidly depleting cytosolic ATP pools [2, 4, 5]. In several pathological settings, mitochondria indeed revert to ATP consumption, aggravating an existing cellular pathology [6-10]. However, for as long as the inner mitochondrial membrane remains intact and ATP production is substantiated by a segment of the citric acid cycle without eliciting the need of oxidative phosphorylation, mitochondrial consumption of cytosolic ATP is hindered by an endogenous fail safe mechanism dedicated to increase the survival chances of the cell. The aim of my thesis is to elaborate on this mechanism, focusing on its main features and the implications in aforementioned pathologies.

2.1 The mitochondrial proton circuit

In intact mitochondria as part of the proton circuit [9, 11], respiratory complexes I (NADH-ubiquinone oxidoreductase, EC 1.6.5.3), III (ubiquinone-cytochrome *c* oxidoreductase, EC 1.10.2.2) and IV (cytochrome *c* oxidase, EC 1.9.3.1) comprise the energy-conserving core of the respiratory chain residing within the inner membrane (Fig. 1). As electrons flow through, a drop in *redox potential* – a measure of the tendency of a chemical species to acquire electrons and thereby be reduced [12] – at each complex is coupled to the extrusion of protons across the membrane; from the matrix to the intermembrane space. Complex II (succinate dehydrogenase, EC 1.3.5.1), the mitochondrial glycerol-3-phosphate dehydrogenase (GPD2, EC 1.1.5.3) and the

electron-transferring-flavoprotein dehydrogenase of β-oxidation (EC 1.5.5.1) also contribute to the electron flow through the respiratory chain, however these enzymes energetically and mechanistically incapable of proton translocation [13]. The total redox potential difference across the entire respiratory chain is approximately 1100 mV, and the maximal protonmotive force (*pmf*) across the inner membrane is 180-220 mV [14]. The *pmf* consists of a transmembrane potential difference (ΔΨm, inside negative) and a transmembrane proton concentration gradient (ΔpH):

$$pmf = \Delta\Psi m - \left(\frac{2.3RT}{F}\right)\Delta pH \quad (1)$$

where "R", "T" and "F" refer to the universal gas constant, the absolute temperature, and the Faraday constant, respectively (for values, see **Chapter 1**). At the same time, in the presence of sufficiently high concentration of inorganic phosphate (P_i), as it is the case *in vivo* [15], ΔpH is very small (< 0.15) [16], [Vajda *et al.* 2009: publication not closely related to this thesis]. Therefore, under most conditions, the major component of *pmf* is the ΔΨm, accounting for 150-180 mV of the total gradient [9].

The outward (extrusion) and inward (re-entry) proton currents balance under steady-state conditions. The dominant pathway of proton re-entry in intact mitochondria is the F_O-F_1 ATP synthase (**Chapter 2.3**); yet uncoupling proteins (UCPs) and the endogenous proton leak as parallel channels are also in place ([17, 18] and references in **Chapter 2.2**). In the absence of oxidative phosphorylation, the proton circuit is mostly discharged via these channels, limiting the *pmf* in order to prevent electrical breakdown of the membrane as well as restrict single-electron leakage from the respiratory chain to form superoxide [19]. Ca^{2+}-cycling, metabolite transport and proton-translocating transhydrogenase (EC 1.6.1.1) all use the proton current (Fig. 1). The proton pumps of the respiratory chain together with the F_O-F_1 ATP synthase and other *pmf*-consuming processes thus create a proton circuit across the inner membrane, which is fundamental to mitochondrial bioenergetics.

Figure 1. The mitochondrial proton circuit. The primary, ATP-generating proton pathway is depicted as bold, while the flow of electrons as dashed lines/arrows. Metabolite transport via the phosphate carrier, the proton-translocating trans-hydrogenase reaction and endogenous/UCP-mediated proton leaks as secondary pathways of proton re-entry are shown by thin lines/arrows. Ca^{2+} cycles between the uniporter and the Na^+/Ca^{2+} exchanger. The Na^+ circuit integrates the proton and Ca^{2+} circuits. Figure modified from [14], by permission. ↓

DOI:10.14753/SE.2015.1713

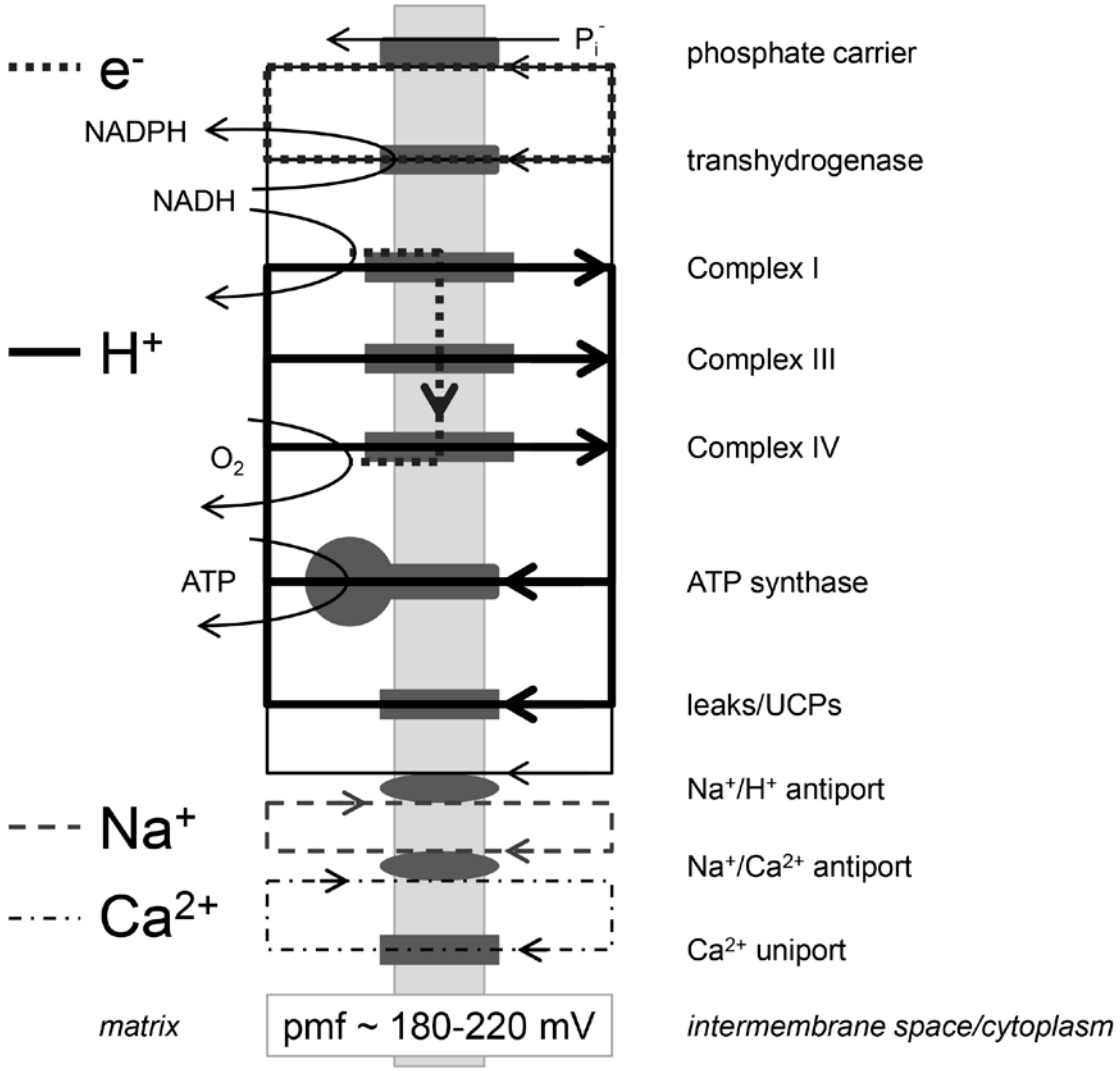

2.2 Defining the mitochondrial respiratory steady states

In oxidative phosphorylation, the endergonic process of phosphorylating ADP to ATP is coupled to the exergonic process of electron transfer to oxygen. As explained above, coupling is achieved through outward currents generating and inward currents utilizing the *pmf* in the proton circuit across the inner membrane (Fig. 1). However, this coupling is not complete, as protons can return to the matrix independently of F_O-F_1 ATP synthase. [20-22]. Uncoupling is the induction of proton permeability in the inner mitochondrial membrane without affecting the respiratory chain and F_O-F_1 ATP synthase. Different means of uncoupling can be distinguished: i) intrinsic uncoupling under physiological conditions is a property of the inner membrane (endogenous proton leak) [20], proton pumps (proton slip) [21, 22], and molecular uncouplers (UCPs) [23-26] (**Chapter 2.1**); ii) defective respiration under pathological and toxicological

conditions is related to mitochondrial dysfunction [14], [Kiss *et al.* 2013: thesis-related publication No. 3]; iii) fully uncoupled state is induced experimentally by application of established uncouplers (protonophores, such as FCCP, DNP or SF 6847) [27], with the aim of obtaining a reference state with collapsed *pmf*, for the evaluation of the respiratory capacity through the respiratory chain [28]. The coupling (or uncoupling) state of mitochondria is a key bioenergetic parameter; a component of the mitochondrial respiratory control [28, 29] (Fig. 2).

Respiratory steady states have been originally defined by Chance and Williams [30-37] according to a protocol for measuring the oxygen consumption of isolated mitochondria, summarized in Table 1. The protocol starts with *State 1*, where mitochondria are suspended in an isosmotic experimental medium with P_i but without adenylates and respiratory substrates. It proceeds to *State 2* after the addition of ADP, inducing a transient activation to effectively exhaust endogenous substrates, after which *State 2* is a substrate-depleted state of residual oxygen consumption. ADP- and substrate activation is achieved in *State 3* by adding respiratory substrates to the medium, *e.g.* in the classical protocol β-hydroxybutyrate was used. In this state, respiration is high and ADP is gradually depleted by conversion to ATP. Respiration drops in the transition to *State 4*, which is an ADP-limited resting state. Finally, respiration becomes oxygen-limited after the aerobic-anoxic transition in the closed chamber (*State 5*).

Table 1. Original definition of respiratory steady states by Chance and Williams [33]. ↓

State	$[O_2]$	ADP level	Substrate level	Respiration rate	Rate-limiting substance
1	> 0	Low	Low	Slow	ADP
2	> 0	High	~0	Slow	Respiratory substrates
3	> 0	High	High	Fast	Respiratory chain
4	> 0	Low	High	Slow	ADP
5	< 0	Low	High	0	Oxygen

Table 2. Definition of mitochondrial respiratory states in *Bioenergetics 3* textbook. *"Chance and Williams proposed a convention following the typical order of addition of agents during an experiment:"* (Nicholls and Ferguson) [11]. ↓

State 1	mitochondria alone (in the presence of P_i)
State 2	substrate added, respiration low due to lack of ADP
State 3	a limited amount of ADP added, allowing rapid respiration
State 4	all ADP converted to ATP, respiration slows
State 5	anoxia

In an alternative, conventional protocol introduced by Estabrook [38], the sequence starts with the above defined *State 1* (mitochondrial suspension in a P_i containing buffer without adenylates and respiratory substrates), but continues with the addition of respiratory substrates to reach *State 2'*. Since adenylates are absent, in this state respiration merely compensates for the proton leaks. Addition of ADP initiates *State 3*. Without further addition of reactants, *State 4* is attained upon exhaustion of ADP. *States 3* and *4* here are identical to the ones defined by Chance and Williams [30-37].

The original definition of *State 2* [30-37] (Table 1) is opposite to the *State 2'* obtained in the absence of ADP but presence of respiratory substrates (Table 2), because they are functionally different states of residual oxygen consumption and compensatory respiration, respectively. *"We have sought independent controls on whether State 2 corresponds to complete oxidation of the system. It is logical that this be so, for respiration is zero in State 2 because substrate, not phosphate acceptor, is limiting."* (Chance and Williams) [33]. On the contrary, *State 2'* and *4* represent ADP-limited steady states with well-defined oxygen consumption by the respiratory chain to compensate for the proton leaks, in the absence or presence of ATP, respectively. Despite the clear definitions elaborated above, *State 2*, *2'* and *4* terminologies have become confusing even among the scientists of the field: *"Also, the controlled respiration prior to addition of ADP, which is strictly termed "state 2", is functionally the same as state 4, and the latter term is usually used for both states."* (Nicholls and Ferguson) [11] (see also Table 2). Since "Bioenergetics" is one of the most fundamental textbooks of mitochondriology, misinterpretation of the terminology became widespread, giving rise to an endless debate among mitochondria-related scientists. Certainly, this state of terminology urges reconsideration for clarification, particularly for extending bioenergetics to the oxygen consumption kinetics of the living cell [28, 39].

The respiratory control ratio (RCR) is defined as *State 3* / *State 4*. Ever since it has been established by Chance and Williams [40], it is widely used as a measure to describe the degree of coupling, respiratory control and intactness of the mitochondrial preparation.

DOI:10.14753/SE.2015.1713

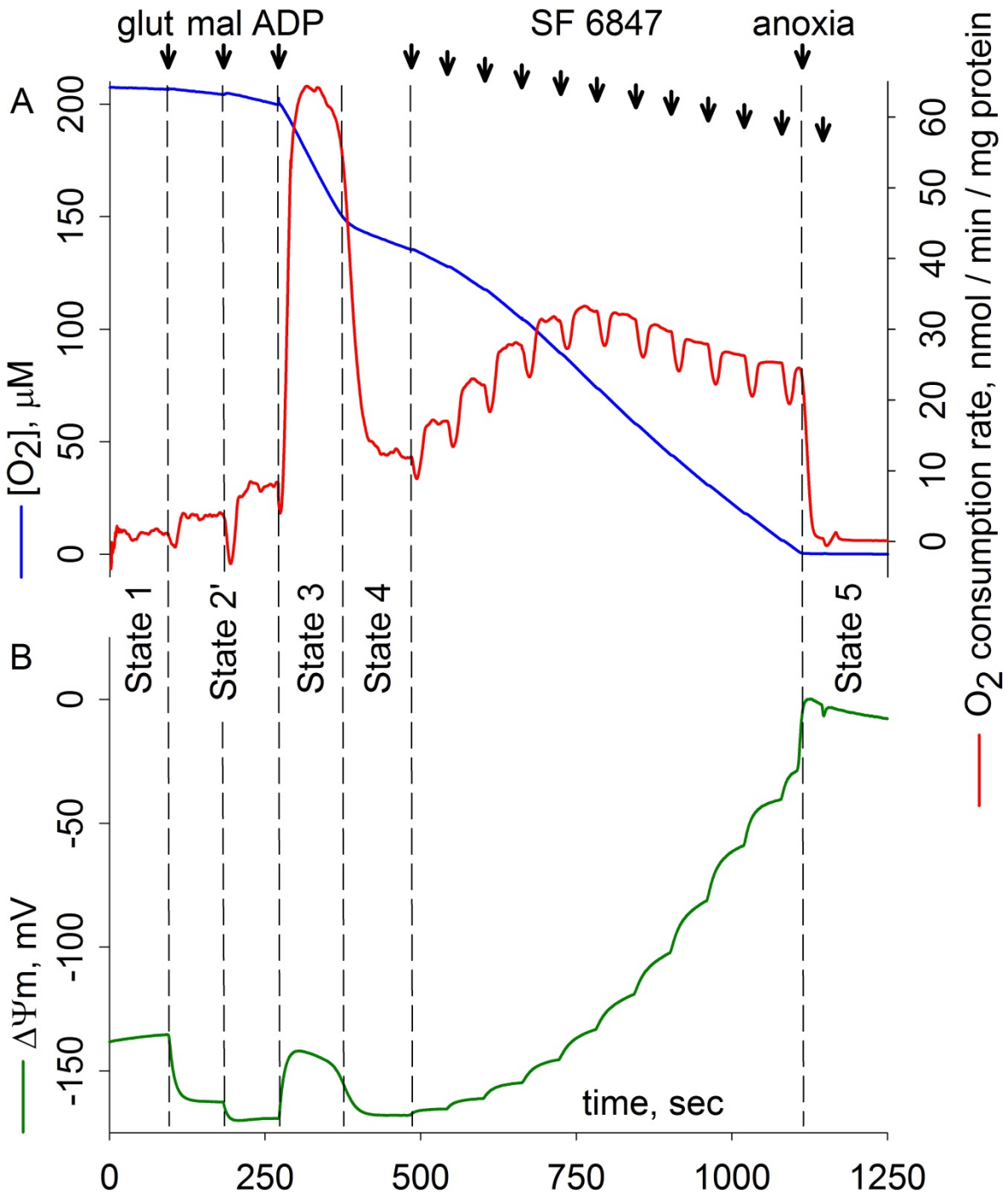

Figure 2. Parallel measurements of oxygen consumption **(A)** and membrane potential (ΔΨm) **(B)** of isolated mouse liver mitochondria. The experiment was performed in an OROBOROS Oxygraph-2k equipped with the O2k-Fluorescence LED2-Module to monitor ΔΨm with the cationic dye safranin O (2.5 µM); at 37°C. 1 mg mitochondria were suspended in 4 ml incubation medium (0.25 mg/ml; the composition is given in **Chapter 4.5**) before the closure of the chamber. Oxygen concentration, flux (negative time derivative of oxygen concentration) and fluorescence were recorded using DatLab software provided by Oroboros Instruments GmbH. Additions: glutamate (glut), 5 mM; malate (mal), 5 mM; ADP, 0.25 mM; SF 6847, 10 nM steps (12) where indicated. ΔΨm was calculated from safranin O fluorescence signal as it is described in **Chapter 4.5**. ↑

The rate of respiration is mostly controlled by the thermodynamic disequilibrium between the redox potential difference across the respiratory chain and ΔΨm. In the absence of ATP synthesis, respiration is regulated so that the rate of proton extrusion balances the rate of proton leak across the inner mitochondrial membrane. If proton extrusion exceeds the rate of re-entry, ΔΨm increases, resulting in an increase in the disequilibrium between the respiratory chain and ΔΨm. The outcome is the decrease of respiratory chain activity and restoration of the steady state. In Fig. 2, respiration is initiated by respiratory substrates glutamate plus malate (*State 2'*), and then disturbed by the addition of ADP (*State 3*). The added ADP exchanges with matrix ATP via the adenine nucleotide translocase (ANT), and as a result, the phosphorylation potential (ΔG_p) [29, 41] for the ATP synthesis reaction in the matrix is lowered, disturbing the F_O-F_1 ATP synthase equilibrium:

$$\Delta G_p = \Delta G^{0\prime} + 1.36 \log \frac{[ATP]}{[ADP][P_i]} \qquad (2)$$

where $\Delta G^{0'}$ is the standard free energy of ATP hydrolysis at a given pH, and [ATP], [ADP] and [P_i] refer to concentrations in the medium. The F_O-F_1 ATP synthase starts operating in the direction of ATP synthesis at the expense of proton re-entry to the matrix in order to restore ΔG_p. The proton re-entry decreases ΔΨm, thus the thermodynamic disequilibrium between the respiratory chain and ΔΨm increases. Adherent increase of proton current and respiration restores the balance. This accelerated *State 3* respiration is self-regulating in a way that the rate of proton extrusion matches the increased rate of proton re-entry. Since under these circumstances ΔΨm is dissipated by both the F_O-F_1 ATP synthase and ANT (see **Chapters 2.3**, **2.4** and **2.8**), it is set in a new steady state lower than that of *State 2'*; its actual value depending on the respiratory substrates provided [42]. As it is visible in Fig. 2, energy transduction is well regulated: ΔΨm drops by less than 20% upon ADP addition. ATP synthesis, and hence *State 3* respiration can be terminated in the following ways: i) when all the added ADP is phosphorylated to ATP, respiration slows down as it becomes ADP-limited (*State 3* - *State 4* transition in Fig. 2A and 18); ii) by blocking ANT-mediated ADP-ATP exchange with its specific inhibitor carboxyatractyloside (cATR) or bongkrekic acid (BKA) (see Fig. 18 and 26F); iii) by inhibiting the F_O-F_1 ATP synthase *e.g.* with oligomycin (olgm).

Uncoupling agents like SF 6847 uncouple oxidative phosphorylation by increasing the proton permeability of the inner membrane. Therefore, they override the inhibition of proton re-entry, creating a futile cycle wherein protons are extruded by the respiratory chain but shuttled back right away into the matrix; impeding the ΔΨm to build up. As a consequence, uncouplers induce rapid respiration (regardless of the presence of F_O-F_1 ATP synthase and ANT inhibitors, or the absence of ADP) but hinder ATP synthesis. Uncoupling agents thus can be used to i) create a zero reference point for ΔΨm calibration (**Chapter 5.2.1**), ii) establish open-circuit operation of the proton circuit in order to evaluate the maximal flux through the respiratory chain [28], iii) set the ΔΨm to any preferred value with careful titration (**Chapter 5.1**).

2.3 The F_O-F_1 ATP synthase

The F_O-F_1 ATP synthase (EC 3.6.3.14) consists of two coupled rotary molecular motors, called F_O and F_1 (or F_1-ATPase); the former being membrane-bound and the latter solvent exposed. When F_1 is coupled to F_O embedded in a membrane across which there is sufficient *pmf*, the complex generates ATP from ADP and P_i. The energy-requiring step is not the chemical step in ATP synthesis, but the binding of P_i and the release of tightly bound ATP from F_O-F_1 ATP synthase [43]. It seems as though mitochondria are built around this molecular rotary engine to keep it operating in the direction of ATP synthesis by providing the necessary *pmf*. Nevertheless, if respiration or the integrity of the inner membrane becomes compromised and *pmf* dissipates, the F_O-F_1 ATP synthase switches to reverse mode generating a suboptimal ΔΨm at the expense of ATP hydrolysis by pumping protons out of the matrix [44].

Regulatory mechanisms of F_O-F_1 ATP synthase activity can be divided upon whether they are affecting ATP synthesis or ATP hydrolysis rates, or both. ATP synthesis activity by the F_O-F_1 ATP synthase can be modulated by changing the magnitude of *pmf*. This can be achieved by either modulating the complexes of the respiratory chain [45] or the components of the citric acid cycle that provide reducing equivalents to the complexes [46], or by changing the proton permeability of the inner membrane. Coupling factor B is a protein located in the inner mitochondrial membrane that facilitates ATP synthesis by blocking a proton leak [47]. Recently, mitochondrial ATPase inhibitory factor 1 (IF1) – discovered in 1963 by Pullman and Monroy [48] – has also been implicated in modulating ATP synthesis activity by a mechanism that

involves arrangement of F_O-F_1 ATP synthase in dimer formation, creating more efficient conditions for ATP synthesis by local biophysical factors [49-51]. Regarding the hydrolytic activity of the F_1-ATPase, four mechanisms are in place aiming at blocking it upon decrease in *pmf*, mediated by i) a decrease in matrix ATP concentration, ii) a decrease in ATP/ADP ratio, iii) an increase in matrix P_i, and iv) the endogenous factor IF1 [44, 48]. The first two mechanisms converge on the inhibition of the F_1-ATPase by MgADP, reviewed in [44], however, it is not established if this regulation is operational on fully assembled F_O-F_1 ATP synthase within intact mitochondria. The most important regulatory mechanism is sustained by IF1, a protein that is expressed in some tissues of some organisms exhibiting the ability to block the ATP hydrolytic activity of F_1-ATPase [52-54]; however, it must be stressed that IF1 does not operate in an all-or-none manner: the binding and release of this protein in F_1-ATPase are governed by both matrix [ATP] and $\Delta\Psi m$, independently from each other [55-57], apart from the effect of matrix pH [58]. Furthermore, inhibition of F_1-ATPase by IF1 may not be complete; matrix ATP inhibits the unbinding of IF1 from F_1-ATPase with a K_i of 0.14 mM [56]. According to Giorgio *et al.* [59, 60], cyclophilin D (CYPD, EC 5.2.1.8), a ubiquitous matrix-located protein binds to the oligomycin sensitivity-conferring protein subunit of the F_O-F_1 ATP synthase in a phosphate-dependent manner, resulting in a decrease in both ATP synthesis and hydrolysis rates. CYPD is a member of the cyclophilins family encoded by the *PPIF* gene [61], which exhibits peptidyl-prolyl *cis/trans* isomerase activity. Genetic ablation of the *PPIF* gene or inhibition of CYPD binding on F_O-F_1 ATP synthase by cyclosporin A led to disinhibition, resulting in accelerated ATP synthesis and hydrolysis rates. These effects however were demonstrated in either submitochondrial particles or mitochondria permeabilized by alamethicin, representing conditions under which there is direct access to the F_O-F_1 ATP synthase. As discussed in Chinopoulos *et al.* 2011 (thesis-related publication No. 2), in intact mitochondria, changes in ATP synthesis or hydrolysis rates by the F_O-F_1 ATP synthase do not necessarily translate to changes in ATP efflux or influx rates as a result of the presence of the ANT (further explained in **Chapters 2.4** and **5.1.2**). The molecular turnover numbers and the number of active ANT molecules may vary from those of F_O-F_1 ATP synthase molecules per mitochondrion [2, 42]. Furthermore, the steady-state ADP-ATP exchange rates (for ANT) or ADP-ATP conversion rates (for

F_O-F_1 ATP synthase) do not change in parallel as a function of the ΔΨm [62], [Chinopoulos *et al.* 2010: thesis-related publication No. 1]. It is therefore reasonable to assume that a change in matrix ADP-ATP conversion rate caused by a change in F_O-F_1 ATP synthase activity may not result in an altered rate of ADP influx (or ATP influx, in the case of sufficiently de-energized mitochondria) from the extramitochondrial compartment because of the imposing action of the ANT. Addressing the extent of contribution of CYPD on the rates of ADP and ATP fluxes towards the extramitochondrial compartment is one of the objectives of my thesis (**Chapter 5.1**).

Persistent reversal of F_O-F_1 ATP synthase could deplete the cellular ATP reserves, driving the cell into an energy deficit eventually leading to cell death [9]. Under these conditions, glycolysis can provide the ATP required to maintain ATP-dependent cellular functions and the reverse operation of F_O-F_1 ATP synthase; preventing total collapse of ΔΨm and counteracting the consumption of cytosolic ATP pools. Glycolytic ATP production indeed can be accelerated 10-fold when oxidative phosphorylation is abolished and as a result, ATP/ADP ratio decreases by ~70% but not collapses [63]. Survival of cells with impaired respiratory chain thus likely depends on the glycolytic capacity. However – on the basis of findings submitted in this thesis – a novel concept arises: matrix substrate-level phosphorylation could be a mean to preserve the cytosolic ATP reserves produced by glycolysis, which is crucial for survival due to maintaining the operations of vital ATP-dependent transporter such as Na^+/K^+- and Ca^{2+}-ATPases. Since ATP hydrolysis by the F_O-F_1 ATP synthase takes place on the matrix side, in case of an uncompromised inner membrane the directionality of the ANT will define weather cytosolic or matrical ATP pools will drive the reverse operating F_O-F_1 ATP synthase if the respiratory chain becomes defective.

2.4 The adenine nucleotide translocase

The adenine nucleotide translocase (ANT) is the most abundant member of the mitochondrial carrier family: it represents up to 10% of all proteins from the inner membrane of heart mitochondria [64, 65]. There are four known isoforms in humans [66, 67], all encoded by nuclear DNA [64, 68]. ANT assembles in multimeric translocating units [69] and catalyzes the electrogenic, reversible exchange of ADP^{3-} for ATP^{4-} with a 1:1 stoichiometry across the inner membrane [70]. Accordingly, the forward operation of the translocase (ATP export from the mitochondrial matrix in

exchange for extramitochondrial ADP) dissipates, while the reverse operation (ADP export from the mitochondrial matrix in exchange for extramitochondrial ATP) actually generates ΔΨm. The directionality of the ADP-ATP transport through the ANT is determined mostly by the magnitude of the ΔΨm; but influenced by many other parameters elaborated in [62]. In addition, ANT has other roles as well in both physiological and pathological conditions: it is i) thought to be a major conduit of the "proton leak" [71], ii) a regulatory component of the mitochondrial permeability transition pore (PTP) [72, 73], iii) involved in mitochondria-mediated apoptosis [74].

In case of a respiratory chain failure, assuming that i) the inner mitochondrial membrane remains intact, ii) glycolytic ATP production is unhindered and upregulated due to Pasteur effect[1] and iii) substrates are available to support matrix substrate-level phosphorylation, ATP supply for hydrolyzing F_O-F_1 ATP synthase could originate from either side of the inner membrane. Under these settings, the ANT will determine whether cytosolic or matrical ATP pools will be consumed, governed mainly by ΔΨm.

2.5 Directional asynchrony in the operation of F_O-F_1 ATP synthase and ANT

Directionality of the reversible F_O-F_1 ATP synthase is mostly controlled by ΔΨm and its so called "reversal potential" set by the concentrations of the participating reactants. Reversal potential of an enzyme transporting across a membrane may be defined as the ΔΨm, where no net flux of substrates can be detected. In case of F_O-F_1 ATP synthase, its "reversal potential" (E_{rev_ATPase}) gives the value of ΔΨm at which the complex shifts from an ATP-forming to an ATP-consuming entity. The values of E_{rev_ATPase} are given by the following equation [Chinopoulos *et al.* 2010]:

$$E_{rev_{ATPase}} = -\left(\frac{316}{n}\right) - \left(\frac{\frac{2.3RT}{F}}{n}\right) \times \log\left\{\frac{[MgATP^{2-}]_{in}}{[MgADP^{-}]_{in} \times [P_i]_{in}}\right\} - \frac{2.3RT}{F} \times (pH_{out} - pH_{in}) \quad (3)$$

and

$$[P_i]_{in} = \frac{[P_i^{total}]_{in}}{(1 + 10^{pH_{in} - pK_{a2}})} \quad (4)$$

[1] *During his studies on the fermentation of glucose by yeast, Louis Pasteur discovered that both the rate and the total amount of glucose consumption were many times greater under anaerobic than aerobic conditions.*

where “in” and “out” signify inside and outside the mitochondrial matrix, respectively, “n” is the H^+/ATP coupling ratio [75] and “R”, “T” and “F” are the universal gas constant, the absolute temperature, and the Faraday constant, respectively (for values, see **Chapter 1**). $K_{M(ADP)}$ and $K_{M(ATP)}$ are the true affinity constants of Mg^{2+} for ADP and ATP valued $10^{-3.198}$ and $10^{-4.06}$, respectively, according to [76], and $[P_i]$ is the free phosphate concentration (in Molar) given by Eq. (4), where $pK_{a2} = 7.2$ for phosphoric acid. The F_O-F_1 ATP synthase utilizes the Mg^{2+}-bound forms, $MgATP^{2-}$ and $MgADP^-$ [76]. However, $MgATP^{2-}$ can be expressed as $[ATP^{4-}]_{free} \times [Mg^{2+}]/K_{M(ATP)}$, and $MgADP^-$ can be expressed as $[ADP^{3-}]_{free} \times [Mg^{2+}]/K_{M(ADP)}$. By incorporating these to Eq. (3), we obtain:

$$E_{rev_{ATPase}} = -\left(\frac{316}{n}\right) - \left(\frac{\frac{2.3RT}{F}}{n}\right) \times \log\left\{\frac{[ATP^{4-}]_{free_{in}} \times K_{M(ADP)}}{[ADP^{3-}]_{free_{in}} \times K_{M(ATP)} \times [P_i]_{in}}\right\} - \frac{2.3RT}{F} \times (pH_{out} - pH_{in}) \quad (5)$$

Since nucleotide phosphorylation/dephosphorylation takes place on the matrix side of the F_O-F_1 ATP synthase, obviously only ADP and ATP present in the matrix participate in the production/consumption process. Extramitochondrial adenine nucleotides can contribute to the matrical adenine nucleotide pools only through the ANT. Therefore, if the F_O-F_1 ATP synthase hydrolyzes ATP originating not from matrix substrate-level phosphorylation [77, 78], but from cytosolic ATP reserves [2], it must be preceded by ANT reversal [Chinopoulos *et al.* 2010]. By a minor fraction, the ATP-Mg/P_i carrier could also transport extramitochondrial ATP into the matrix [79]. The ANT utilizes the free forms of ADP^{3-} and ATP^{4-}, and exhibits its own reversal potential (E_{rev_ANT}), which is in turn governed by the participating reactants [62]:

$$E_{rev\_ANT} = \frac{2.3RT}{F} \times log\left\{\frac{[ADP^{3-}]_{free_{out}} \times [ATP^{4-}]_{free_{in}}}{[ADP^{3-}]_{free_{in}} \times [ATP^{4-}]_{free_{out}}}\right\} \quad (6)$$

Eqs. (5) and (6) share the common reactants $[ATP^{4-}]free_{in}$ and $[ADP^{3-}]free_{in}$ (gray rectangles), therefore, the reversal potential of the F_O-F_1 ATP synthase and that of ANT can both be expressed as functions of matrix free ATP^{4-} and ADP^{3-}, see Fig. 3 from Chinopoulos *et al.* 2010 and Kiss *et al.* 2013 (thesis-related publications No. 1 and 3).

According to Fig. 3, alterations in $[ATP^{4-}]free_{in}$ and $[ADP^{3-}]free_{in}$ affect E_{rev_ATPase} and E_{rev_ANT} inversely; a decrease in $[ATP^{4-}]free_{in}/[ADP^{3-}]free_{in}$ ratio would shift E_{rev_ATPase} toward more positive and E_{rev_ANT} toward more negative values and *vice versa*. The realization that E_{rev_ATPase} and E_{rev_ANT} are inversely affected by $[ATP^{4-}]free_{in}$ and $[ADP^{3-}]free_{in}$ could also be derived intuitively: a forward-operating F_O-F_1 ATP synthase elevates matrix [ATP], which will favor its own reversal but also compel ANT to convey the generated ATP to the cytosol. Likewise, reversed F_O-F_1 ATP synthase will reduce [ATP], elevating [ADP] in the meantime, which will disfavor ATP hydrolysis but urge ANT to expel accumulated matrix ADP by operating in reverse mode [80].

The $[ATP^{4-}]free_{in}/ [ADP^{3-}]free_{in}$ ratio is a dynamically altering variable, following the actual metabolic demand of the cell. However – as it is suggested in **Chapter 2.9** –, real-time quantification of this valuable parameter is very difficult. The rest of the parameters also exhibit wide fluctuations: phosphate [81], the coupling ratio "n" [82, 83] and $\Delta\Psi m$; "flickering" of the latter could be greater than 100 mV [84-86].

Figure 3. Computational estimation of E_{rev_ANT} and E_{rev_ATPase}. **A**: ATPase forward, ANT forward; **B**: ATP reverse, ANT forward; **C**, **C_1**, **C_2**: ATPase reverse, ANT reverse; **D**: ATPase forward, ANT reverse. Black solid triangles represent E_{rev_ATPase}; white solid triangles represent E_{rev_ANT}. Values were computed for $[ATP^{4-}]free_{out}$=1.2 mM, $[ADP^{3-}]free_{out}$=10 μM, $[P_i]_{in}$=0.01 M, n=3.7 (2.7+1 for the electrogenic ATP^{4-}/ADP^{3-} exchange of the ANT), pH_{in}=7.38, and pH_{out}=7.25. White open triangles represent E_{rev_ANT} values computed for $[ATP^{4-}]free_{out}$=2.2 mM, and all other parameters as above. ↓

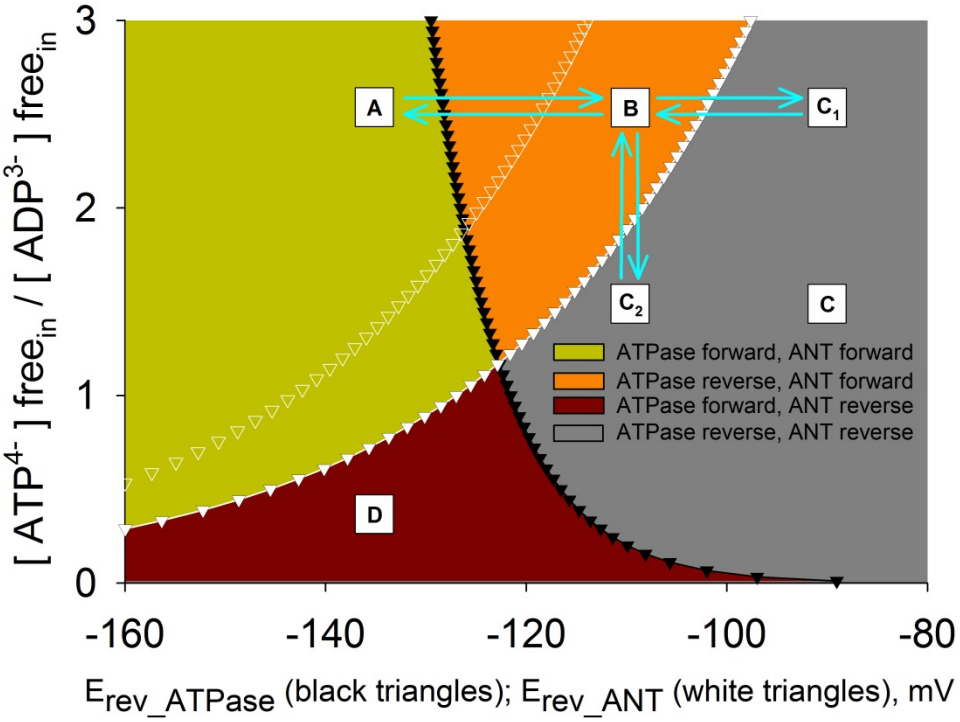

2.6 Computational estimations of E_{rev_ATPase} and E_{rev_ANT}

The concentration of free ATP^{4-} ([L]) can be calculated by the following equation:

$$[L] = \frac{\left\{ \frac{[L]_t}{1 + \frac{[Mg^{2+}]_{free}}{k_{M,app}}} \right\}}{\left(1 + \frac{10^{-pH}}{k_H}\right)} \quad (7)$$

where $[L]_t$ is the total ATP concentration, *i.e.*, $[ATP^{4-}]$ + $[ATP\text{-}H^{3-}]$ + $[ATP\text{-}Mg^{2-}]$ + $[ATP\text{-}H\text{-}Mg^{-}]$; "$k_H$" is the dissociation constant for the reaction $ATP\text{-}H^{3-} \leftrightarrow ATP^{4-} + H^{+}$; and "$k_{M,app}$" is the apparent dissociation constant of $MgATP^{2-}$ measured at pH 7.25 and 37°C [42]. By the same token, $[ADP^{3-}]_{free}$ can be calculated using Eq. (7): [L], $[ADP^{3-}]_{free}$; $[L]_t$ total ADP concentration, *i.e.*, $[ADP^{3-}]$ + $[ADP\text{-}H^{2-}]$ + $[ADP\text{-}Mg^{-}]$ + [ADP-H-Mg]; k_H is the dissociation constant for the reaction $ADP\text{-}H^{2-} \leftrightarrow ADP^{3-} + H^{+}$; and $k_{M,app}$ is the apparent dissociation constant of $MgADP^{-}$ measured at pH 7.25 and 37°C [42]. Since k_H and $k_{M,app}$ values for matrical conditions are difficult to determine, it is assumed that they do not differ notably from those found outside the matrix. Because the matrix $[Mg^{2+}]$ and pH_{in} are only slightly different from the extramitochondrial $[Mg^{2+}]$ and pH_{out} [42], it is assumed that both ANT and F_O-F_1 ATP synthase handle the measured free [ATP] and [ADP]. Results of the computations using Eqs. (3-7) are depicted in Fig. 3: E_{rev_ATPase} (black triangles) and E_{rev_ANT} (white triangles) are plotted as functions of matrix ATP/ADP ratio. The two curves define four spaces: A, B, C, and D. Mitochondria exhibiting a free matrix ATP/ADP ratio for a given ΔΨm that would place them anywhere within the A space (green space) have their F_O-F_1 ATP synthase and ANT operating in forward mode; *i.e.*, F_O-F_1 ATP synthase combines ADP and P_i to generate ATP and ANT brings that ATP into the extramitochondrial compartment in exchange for ADP. Mitochondria exhibiting values that would place them anywhere within the C space (gray space) have both their ANT and F_O-F_1 ATP synthase operate in reverse mode; *i.e.*, ANT brings ATP into the matrix in exchange for ADP, and F_O-F_1 ATP synthase hydrolyzes that ATP to ADP and P_i. Mitochondria exhibiting values that would place them anywhere within the B space (orange space) have the F_O-F_1 ATP synthase of these organelles operating in reverse mode, whereas the ANT still operates in forward mode. Under these circumstances, mitochondria could i) either return to the A space or ii) proceed to the C space and gain

access to extramitochondrial ATP pools by one or more of the following 3 routes: further change in ΔΨm toward more depolarizing values, so that they would reach point C_1; further decrease in the matrix ATP/ADP ratio, so that they would reach point C_2; or shift of E_{rev_ANT} to the left (Fig. 3, white open triangles; *i.e.*, by increasing $[ATP^{4-}]free_{out}$ or decreasing $[ADP^{3-}]free_{out}$ or decreasing pH_o), so that the existing ΔΨm and matrix ATP/ADP ratio pair values now fall within the C space. From Eq. (6), it is evident that because E_{rev_ANT} encompasses the terms $[ATP^{4-}]free_{in}$ and $[ADP^{3-}]free_{in}$, a change in matrix ATP/ADP ratio is bound to affect E_{rev_ANT} as well. In other words, a change in matrix ATP/ADP ratio may not be the only reason for a mitochondrion becoming extramitochondrial ATP consumer; the accompanying shift in E_{rev_ANT} will also contribute. It is unlikely for mitochondria to exhibit such a high ΔΨm but so low ATP/ADP ratio *in vivo* that would place them within the D space (red space), and therefore this part of the graph has presumably no biological representation. For the estimations, other parameters were assumed to be static, specifically those of $[ATP^{4-}]free_{out}$, $[ADP^{3-}]free_{out}$, $[P_i]_{in}$, n, pH_{in} and pH_{out}. Some of these values have been chosen on the basis of reports on cytosolic estimations or computational predictions [87]. A Windows-based software has been generated by our group (*Erev estimator*), in which the user can enter any value for any parameter participating in Eqs. (4-6), and observe the changes in E_{rev_ATPase} and E_{rev_ANT}. The software and instructions on how to use it can be downloaded (*http://www.tinyurl.com/Erev-estimator*). These computer simulations have been verified by experimental results in isolated and *in situ* mitochondria, showing that E_{rev_ATPase} is almost always more negative than E_{rev_ANT}, implying that progressively depolarizing mitochondria will first exhibit reversal of the F_O-F_1 ATP synthase, followed by reversal of the ANT [Chinopoulos *et al.* 2010], thereby proving the existence of the B space.

It is worth mentioning here that from Fig. 3 only the directionalities but not the activities of the ANT and the F_O-F_1 ATP synthase can be deduced. As ΔΨm approaches E_{rev_ATPase} or E_{rev_ANT} values, respective activities decrease indeed; still, the characteristics of ΔΨm-dependent activity changes require further clarification. The ADP-ATP exchange rate of intact mitochondria as a function of several physiological parameters including ΔΨm however, has been described [42], [Chinopoulos *et al.* 2010] and modeled already [62], as well as F_O-F_1 ATP synthase activity [88, 89]. Fig. 4

presents a typical ADP-ATP exchange rate profile of intact mitochondria as a function of ΔΨm: black squares are experimental data points obtained from parallel ADP-ATP exchange rate and ΔΨm measurements in isolated mitochondria titrated with an uncoupler [90]. The same experimental protocol performed on *in situ* mitochondria in permeabilized cells provided similar results [91]. Although predictions of thermodynamic *vs.* kinetic analyses cannot be used interchangeably, the ΔΨm values at which the F_O-F_1 ATP synthase and ANT yield a net rate of zero deduced by i) thermodynamic (at ΔG = 0) and ii) kinetic analysis [62], are identical [62, 88, 92], [Chinopoulos *et al.* 2010]. Along these lines, when ΔΨm matches or approximate E_{rev_ATPase} or E_{rev_ANT} values according to thermodynamic analysis, it can be assumed that respective ANT and F_O-F_1 ATP synthase activities are also minute.

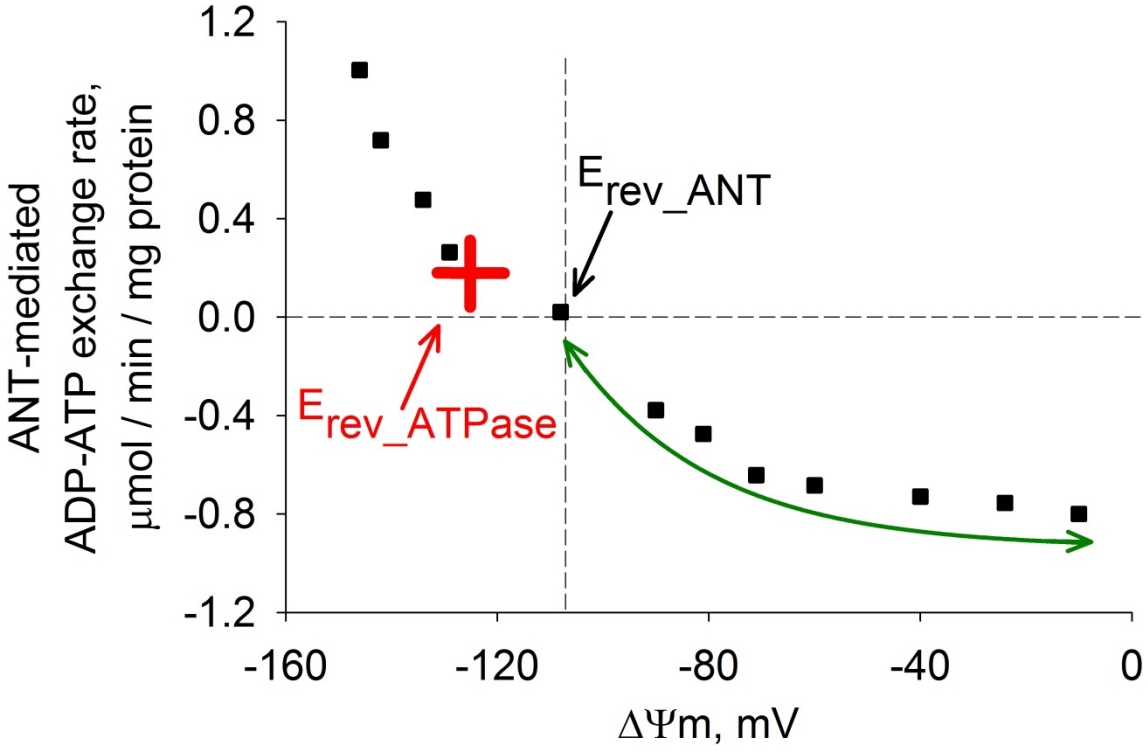

Figure 4. Plot of the ADP-ATP exchange rate mediated by the ANT *vs.* ΔΨm in isolated rat liver mitochondria depolarized to various voltages by increasing amounts of an uncoupler. Black cross indicates E_{rev_ANT}, red cross indicates E_{rev_ATPase}. ↑

2.7 Contribution of matrix substrate-level phosphorylation

The F_O-F_1 ATP synthase is the major player in controlling matrix ATP and ADP levels, but it is itself controlled by ΔΨm [44], the variable that defines the x-axis of the graph in Fig. 3. However, ATP can also be generated by substrate-level phosphorylation, a pathway that is independent from *pmf*. In the mitochondrial matrix there are two reactions capable of substrate-level phosphorylation: the mitochondrial phosphoenolpyruvate carboxykinase (PEPCK, EC 4.1.1.32) and the succinate-CoA ligase (SUCL, or succinate thiokinase or succinyl-CoA synthetase). Mitochondrial PEPCK is thought to participate in the transfer of the phosphorylation potential from the matrix to cytosol and *vice versa* [93-96]. SUCL catalyzes the reversible conversion of succinyl-CoA and ADP or GDP to CoASH, succinate and ATP or GTP [97]. ΔG for this reaction is 0.07 kJ/mol, therefore, it is reversible [98]. It plays a key role in the citric acid cycle [99], ketone metabolism [100], and heme synthesis [101] as well as being a phosphate target for the activation of mitochondrial metabolism [102]. The enzyme is a heterodimer, being composed of an invariant α subunit encoded by the *SUCLG1* gene and a substrate-specific β subunit encoded by either the *SUCLA2* or *SUCLG2* gene. This dimer combination results in either an ADP-forming succinate-CoA ligase (A-SUCL; EC 6.2.1.5) or a GDP-forming succinate-CoA ligase (G-SUCL; EC 6.2.1.4). A-SUCL is mostly expressed in skeletal muscle, brain and heart, while G-SUCL is barely detected in brain and muscle, but strongly expressed in liver and kidney [96]. In the human brain, A-SUCL is expressed exclusively in the neurons [103]. The ADP-forming succinate-CoA ligase is potentially the only matrix enzyme generating ATP in the absence of *pmf*, capable of maintaining matrix ATP levels under energy-limited conditions, such as transient hypoxia [104-106]. However, GDP-forming succinate-CoA ligase may also support ATP formation in the matrix through the concerted action with a mitochondrial isoform of a nucleotide diphosphate kinase known as NM23-H4 (NDPK-D, EC 2.7.4.6); this kinase complexates with either ADP- or GDP-forming succinate-CoA ligase [107, 108].

How would ADP-forming succinate-CoA ligase mediated increase in matrix [ATP] affect the reversal potentials of F_O-F_1 ATP synthase and that of ANT? As it is apparent from Fig. 3, an increase in matrix ATP/ADP ratio increases E_{rev_ATPase} and decreases E_{rev_ANT}. Along these lines, an increase in matrix ATP/ADP ratio carries a particularly

beneficial effect: assuming that a mitochondrion in a cell exhibits a ΔΨm of -100 mV, a matrix [ATP] = 4 mM, and a matrix [ADP] = 2 mM, that would make an ATP/ADP ratio of 2. Assuming that all other parameters are as for Fig. 3, this mitochondrion would reside in the C space; *i.e.*, it would consume cytosolic ATP, because both the ANT and the F_O-F_1 ATP synthase operate in reverse mode. In this case, an increase in substrate-level phosphorylation by 25% (arbitrarily chosen) will elevate matrix ATP/ADP ratio to 3.3, and that will "relocate" this mitochondrion to the B space. This mitochondrion will still consume ATP because of a reversed F_O-F_1 ATP synthase, but this ATP cannot come from the cytosolic compartment, because the ANT operates in forward mode. In this case, the F_O-F_1 ATP synthase consumes the ATP that comes from substrate-level phosphorylation, sparing the cytosolic reserves.

From the work described in this thesis, which integrates the findings of all the thesis-related publications as well as earlier reports by the groups of Sanadi [109], Lambeth [97], Weinberg [105], Chinnery [110] and Balaban [102], the concept is being established that matrix substrate-level phosphorylation could be a mitochondrial endogenous fail safe mechanism supporting the reverse operation of F_O-F_1 ATP synthase, with the benefit of maintaining ΔΨm at a suboptimal level, when mitochondria are depolarized but not sufficiently for the ANT to reverse. This assists in preserving glycolytic ATP pools that could otherwise be suppressed during prolonged ischemia [111] but are evidently crucial for the survival chances of cells because of maintaining the function of vital ATP-dependent mechanisms, such as Na^+/K^+-ATPase and Ca^{2+}-ATPases. The importance of SUCL can be better appreciated by the severe phenotype observed in patients suffering from *SUCLA2* (or *SUCLG1*) deficiencies [112]. Mutations in the *SUCLG2* gene have never been reported, as they are most probably incompatible with life. However, it would be difficult to attribute the phenotype exclusively to the provision of ATP by SUCL *vs.* other very important metabolic branches, such as the maintenance of the citric acid cycle [99], ketone metabolism [100], or heme synthesis [101]. It is also noteworthy that recent experiments by the group of Balaban [102] showed that SUCL is activated by matrix P_i. Support for a P_i-induced activation of SUCL is also lent by the study of Siess and colleagues [113], who determined the effects of P_i on matrix metabolite concentrations. In that study, P_i was found to increase [malate] but to decrease [α-ketoglutarate] and [succinyl-CoA],

implying activation of SUCL. By the same token, during cardiac ischemia, succinate is known to accumulate [104, 114], a phenomenon that is consistent with an increase in SUCL activity, possibly as a result of activation by P_i. Activation of SUCL toward the formation of ATP and succinate would obviously have the implication of providing ATP for the consuming F_O-F_1 ATP synthase, thereby maintaining a moderate $\Delta\Psi m$ that, if more negative than E_{rev_ANT}, could contribute to sparing cytosolic ATP pools. A beneficial byproduct is the provision of matrix P_i from matrix ATP hydrolysis that could activate SUCL toward extra ATP formation. Finally, as the elevation of matrix [P_i] shifts E_{rev_ATPase} toward more depolarizing $\Delta\Psi m$ values [80], an additional benefit would be the priming of mitochondria to reverse ATP hydrolysis at more positive potentials, thereby rendering them less prone to matrix ATP consumption.

Considering Eqs. (3-7) and the computer simulations in Chinopoulos *et al.* 2010 showing that the F_O-F_1 ATP synthase reverses at more negative potentials than the ANT, E_{rev_ATPase} must be positioned in the proximity of the red cross in Fig. 4. This means if $\Delta\Psi m$ discharges to a value less negative than E_{rev_ATPase}, F_O-F_1 ATP synthase will inevitably switch to reverse mode. The questions arise here though: how is it possible for respiration-impaired but still intact mitochondria generating membrane potential by a reverse-operating F_O-F_1 ATP synthase to hinder further cytosolic ATP import and consumption? What are the impediments of the transition from the B to the C space in Fig. 3?

2.8 Barriers preventing mitochondrial consumption of cytosolic ATP

The first barrier emerges when depolarization of the inner membrane reaches the potential of the E_{rev_ATPase}, prompting reversal of F_O-F_1 ATP synthase. The reversal itself counters further depolarization since it implies $\Delta\Psi m$ generation by pumping protons out of the matrix at the expense of ATP hydrolysis. However, if the initial depolarization is robust enough to overcome the repolarization due to reversed-operating F_O-F_1 ATP synthase, $\Delta\Psi m$ will drop further to reach E_{rev_ANT}.

Exceeding E_{rev_ANT} causes ANT reversal and by virtue, gives rise to the second barrier: the electrogenic nucleotide exchange through the reverse-operating ANT (exchanging cytosolic ATP^{4-} for matrix ADP^{3-}) antagonizes the initial depolarization stimulus. Assuming the magnitude of the initial depolarization is severe enough to force further decrease in $\Delta\Psi m$, a third barrier emerges: the more positive the $\Delta\Psi m$ value

becomes, the higher the reverse activity of the ANT will be, as indicated by the bidirectional green arrow in Fig. 4. Likewise, decreasing ΔΨm favors acceleration of the reverse-operating F_O-F_1 ATP synthase as well [Chinopoulos *et al.* 2010]. Isolated and *in situ* mitochondria treated with inhibitors of the respiratory chain, exhibited magnitudes of ΔΨm that were clamped very near to the predicted E_{rev_ANT} values, which makes sense as the reverse operation of the ANT cannot increase ΔΨm higher than E_{rev_ANT}. Accordingly, under these conditions reverse ATP-ADP exchange rates mediated by the ANT were either zero or very small, depending on the type of substrates provided to mitochondria. Substrates can be divided into two groups, whether they support or bypass substrate-level phosphorylation [Chinopoulos *et al.* 2010]. Glutamate and α-ketoglutarate are typical respiratory substrates that support ATP formation from substrate-level phosphorylation, while substrates such as succinate and β-hydroxybutyrate do not support this reaction (elaborated further in **Chapters 2.7** and **5.2.2**). As shown in Fig. 5A, when mitochondria respire on substrates supporting matrix substrate-level phosphorylation (black trace “a”), no cytosolic ATP consumption can be measured upon the addition of the complex III inhibitor stigmatellin (stigm). On the other hand, when mitochondria respire on succinate, stigmatellin not only ceases their ATP output, but it causes them to take up and hydrolyze the previously generated ATP. Note, that even in case of an evidently reverse-operating ANT, consumption of ATP occurs 12-15 times slower than its production (red trace “b”). Even so, if mitochondria are provided with succinate, inhibition of ANT activity by carboxyatractyloside (cATR) still causes prompt and complete depolarization (Fig. 5B, trace “b”). These experimental results are in accordance with the above interpreted conclusion: in the absence of substrate-level phosphorylation ANT reverses indeed and by doing so it contributes to ΔΨm (maintained by the reversals of both ANT and F_O-F_1 ATP synthase); meanwhile, allowing only moderate mitochondrial ATP uptake. This is because ADP-ATP exchange generated membrane potential restricts the nucleotide exchange rates themselves (bidirectional green arrow in Fig. 4). Contrary to succinate, in the presence of substrate-level phosphorylation supportive respiratory substrates, carboxyatractyloside induces only a minor depolarization (Fig. 5B, trace “a”); implying that ANT is operating close to its thermodynamic equilibrium.

DOI:10.14753/SE.2015.1713

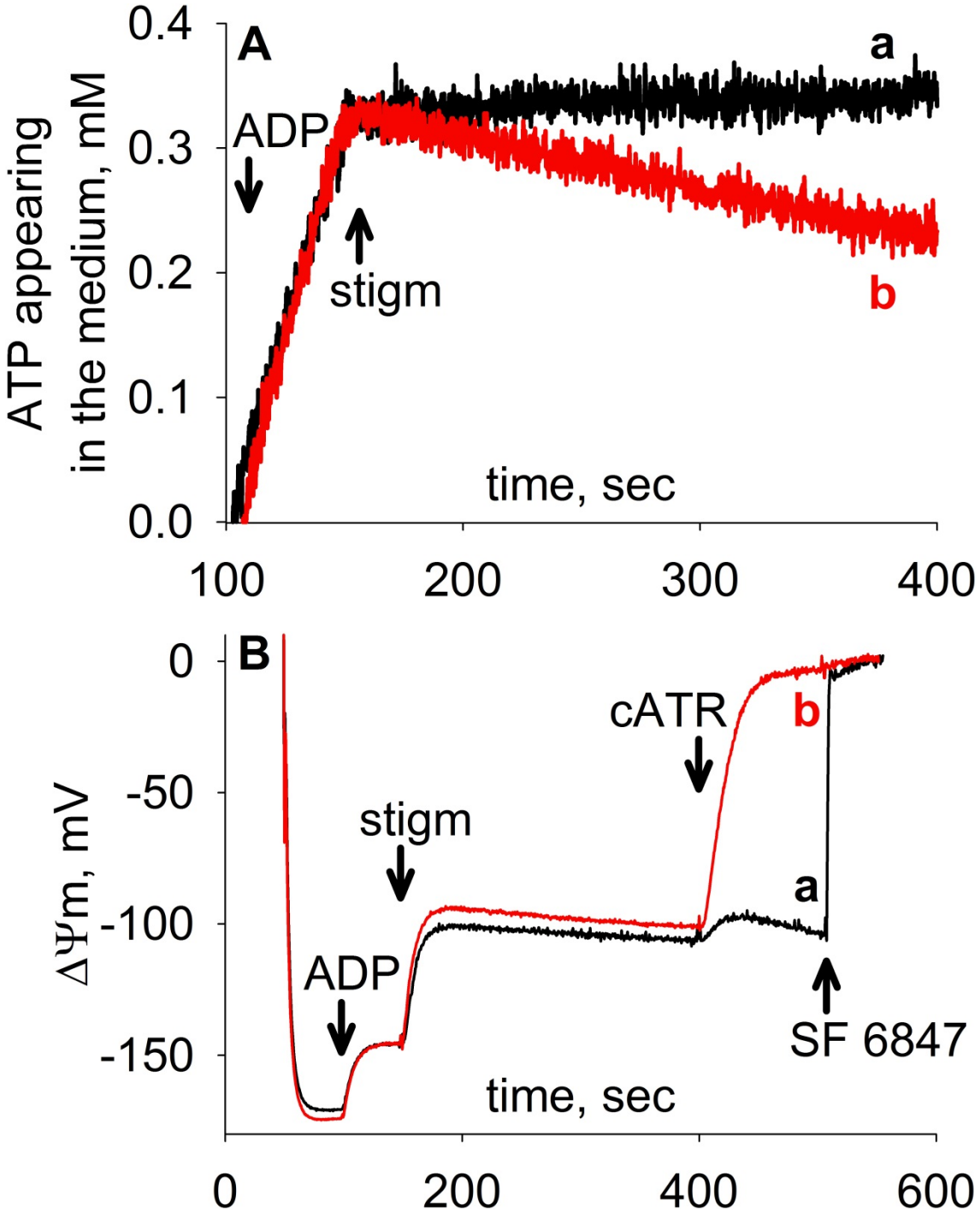

Figure 5. (A) Reconstructed time courses of ATP appearing in the medium after the addition of 1 mM ADP to isolated rat liver mitochondria respiring on 5-5 mM glutamate plus malate (a) or 5 mM succinate plus 1 μM rotenone (b), followed by addition of the complex III inhibitor, stigmatellin (stigm); 1.2 μM. **(B)** Time course of changes in safranin O fluorescence, calibrated to ΔΨm in isolated rat liver mitochondria respiring on 5-5 mM glutamate plus malate (a) or 5 mM succinate plus 1 μM rotenone (b). 1 mM ADP, 1.2 μM stigmatellin and 2 μM carboxyatractyloside (cATR) were added where indicated. At the end of the experiments, 200 nM of the uncoupler SF 6847 was added to achieve complete depolarization. ↑

This thesis builds on the concept soundly established according to argumentations above and in [2, 5, 80] and [Chinopoulos *et al.* 2010], postulating that if the reasons for mitochondrial depolarization are not great enough to overcome the membrane potential-generating actions of the reverse-operating ANT and F_O-F_1 ATP synthase (such as during inhibition of the four complexes of the respiratory chain by drugs or anoxia), mitochondria will consume cytosolic ATP at a very low rate, and only in the absence of matrix substrate-level phosphorylation. ATP uptake will be restricted by the extent of $\Delta\Psi m$ deviations from E_{rev_ANT} towards more depolarizing values: greater deviation will entail greater opposition by the reversed ANT, as indicated by the green double arrow in Fig. 4. In the presence of sufficient matrix substrate-level phosphorylation, moderately depolarized mitochondria with an intact inner membrane cannot consume cytosolic ATP [Chinopoulos *et al.* 2010]. Nonetheless, accepting that the mechanism(s) causing the initial depolarization can be great enough to overcome the repolarization posed by the reversed F_O-F_1 ATP synthase and the ANT, mitochondria could become significant cytosolic ATP consumers. Such could be the case during activation of a low-conductance permeability or extensive uncoupling [115, 116], always assuming that the inner mitochondrial integrity is uncompromised. If there is no exogenous factor or endogenous molecular entity (see **Chapter 2.3**) to mediate a large decrease in $\Delta\Psi m$, the barriers to overcome in order to force mitochondria to eventually consume cytosolic ATP are the potential-generating action(s) of the ANT and/or the F_O-F_1 ATP synthase.

2.9 What is the actual value of $[ATP^{4-}]free_{in}/[ADP^{3-}]free_{in}$ ratio?

The determination of free matrix [ATP] and [ADP] is a challenging task, because of several limitations. First, in order to quantify matrix ATP and ADP values during phosphorylation, addition of ADP to the mitochondrial suspension is required, which will be converted to ATP. The fact that the matrix volume is likely several thousand times smaller than the experimental volume creates a technical challenge; as the matrix adenylate concentrations are many-fold lower than those appearing in the extramitochondrial compartment, therefore the smallest contamination from the experimental volume – which is inevitable – will lead to an overestimation of the matrix ATP/ADP ratio. This can be addressed by centrifuging phosphorylating mitochondria through lipid layers (*e.g.*, silicon oil), thus excluding as much as possible the water-soluble extramitochondrial nucleotides. However, corrections still have to be made for

nucleotides residing in the intermembrane space that would be carried along the lipid layers. For isolated mitochondria, reports of matrix ATP/ADP ratios during phosphorylation range from 0.01 to 12 [94, 117-130]. For mitochondria *in situ* or *in vivo*, the consensus is in the 1-3 ratio range ([131-133] and y-axis of Fig. 3). Second, it is highly probable that results obtained after separation of intra- and extramitochondrial compartments are not relevant because of the time used for the separation process and possible interconversions of adenine nucleotides even in the presence of inhibitors [120, 127, 128, 134]. Third, matrix adenine nucleotides are bound to proteins [135], a notion supported by the fact that isolated mitochondria retain more than 50% of their total adenine nucleotide content after permeabilization by toluene [136]. Due to this potential binding of adenine nucleotides to intramitochondrial proteins [137-140], it is difficult if not impossible to estimate the relationship between the measured total ATP/ADP ratio to free intramitochondrial ATP/ADP ratio. Fourth, matrix micro-compartmentalization of adenine nucleotides has been reported by several groups independently from each other [123, 141-144], still this concept is yet to be accepted unequivocally [127, 145, 146]. It is perhaps better to predict free matrix ATP/ADP ratios using mathematical modeling, depending on parameters that can be reliably quantified [62].

Along these lines and for reasons elaborated in [62], predicting the concentration of free P_i in the mitochondrial matrix is also very challenging. Keeping in mind the uncertainty and fluctuation of the values that dictate E_{rev_ANT} and E_{rev_ATPase}, it cannot be overemphasized that the actual behavior of mitochondria in terms of ATP production or consumption and in terms of whether it is cytosolic or matrix in origin is the convergent result of many complex mechanisms.

2.10 The critical role of α-ketoglutarate dehydrogenase complex in maintaining mitochondrial phosphorylation potential during respiratory arrest

The α-ketoglutarate dehydrogenase complex (KGDHC) is an enzyme consisting of multiple copies of three subunits: α-ketoglutarate dehydrogenase (KGDH or E1k, EC 1.2.4.2), dihydrolipoyl succinyltransferase (DLST or E2k, EC 2.3.1.61) and dihydrolipoyl dehydrogenase (DLD or E3, EC 1.8.1.4). It participates in the citric acid cycle, where it irreversibly catalyzes the conversion of α-ketoglutarate, CoASH, and NAD^+ to succinyl-CoA, NADH, and CO_2. It may exhibit a high flux-control

coefficient[2] in the generation of reducing equivalents [147] and is also crucial for maintenance of the mitochondrial redox state [148]. In addition, KGDHC is involved in transaminations, glutamate metabolism [149]. Furthermore, it provides succinyl-CoA for heme synthesis, a pathway commencing in mitochondria [150, 151], and mitochondrial substrate-level phosphorylation. Finally, the *DLST* gene also encodes a truncated mRNA for another protein, designated as mitochondrial respiration generator of truncated DLST (MIRTD), that is localized in mitochondria, where it regulates the biogenesis of the respiratory chain [152]. A decline in KGDHC activity has been associated with a number of neurodegenerative diseases; however, activity decline is not universal for all citric acid cycle enzymes [153-155]. In search of an association between a decrease in KGDHC activity and incidence of neurodegeneration, two transgenic mouse strains have been generated, one lacking the DLST subunit [156], and the other lacking the DLD subunit [157]. Disruption of both alleles of either gene results in perigastrulation lethality; heterozygote mice exhibit no apparent behavioral phenotypes. A deficiency in the DLD or DLST subunit has been shown to cause increased vulnerability to mitochondrial toxins modeling neurodegenerative diseases [156, 158, 159], and to result in reduced numbers of neural progenitor cells in the hippocampi of adult mice [160]. In transgenic mice carrying human mutations prompting them to develop amyloid deposits, DLST deficiency aggravates amyloid plaque burden [161]. In addition, increased levels of the lipid peroxidation marker, malondialdehyde, was found in $DLD^{+/-}$ [158] but not $DLST^{+/-}$ mice [160]. KGDHC is known to generate reactive oxygen species (ROS), and $DLD^{+/-}$ mice exhibited diminished rates of ROS production [162, 163].

Although these findings establish a link between KGDHC deficiency and brain pathology, they stop short in identifying the molecular mechanisms underlying the propensity for neurodegeneration. So far, the focus of this association has been biased toward diminished provision of reducing equivalents and excess production of ROS. The results presented in **Chapter 5.2** demonstrate that in KGDHC-deficient mice, the decreased provision of succinyl-CoA diminishes matrix substrate-level phosphorylation, resulting in impaired mitochondrial ATP output and consumption of cytosolic ATP by

[2] *Flux-control coefficient is defined – for infinitesimally small changes – as the percentage change in the steady state rate of the pathway divided by the percentage change in the enzyme activity causing the flux change.*

respiration-impaired mitochondria; in line with the predictions deduced in **Chapter 2.6** according to thesis-related publications No. 1 and 3.

2.11 Provision of NAD^+ to KGDHC is essential for the uninterrupted generation of matrix ATP by substrate-level phosphorylation

As it was discussed in **Chapter 2.7**, a functional matrix substrate-level phosphorylation generates ATP, elevates the ATP/ADP ratio in the mitochondrial matrix, thus shifts E_{rev_ATPase} toward more polarizing, while E_{rev_ANT} toward more depolarizing potentials. The overall outcome is an expanded B space (see Fig. 3), implying that for progressively depolarizing mitochondria supported by matrix substrate-level phosphorylation, it is more likely that they will be prevented from consuming cytosolic ATP [Chinopoulos *et al.* 2010]. However, the question arises of whether, and to what extent, this mechanism can remain operational during metabolic compromise, given that it utilizes succinyl-CoA, which is a product of KGDHC that in turn requires provision of NAD^+. In a metabolic standstill, the respiratory complexes are inactive and do not oxidize NADH. Still, in the experiments with isolated and *in situ* mitochondria in Chinopoulos *et al.* 2010 and Kiss *et al.* 2013, the beneficial contribution of substrate-level phosphorylation was readily evident even after tens of minutes of complete respiratory chain inhibition. Mitochondria probed from $DLST^{+/-}$ or $DLD^{+/-}$ mice showed that, during complete respiratory chain inhibition, provision of substrates favoring the SUCL reaction toward ATP formation is critical for shifting E_{rev_ANT} toward more polarized $\Delta\Psi m$ values [Kiss *et al.* 2013]. That can only mean that, during respiratory arrest, KGDHC remained operational, which in turn implies that NAD^+ was available. **Chapter 5.3** focuses on identifying the sources of NAD^+ in the absence of oxidative phosphorylation, and considers primarily the i) oxidation of NADH by mitochondrial diaphorases; nevertheless, ii) the reversed action of isocitrate dehydrogenase [164, 165], iii) the nicotinamide nucleotide transhydrogenase reaction [166], iv) the malate dehydrogenase reaction that can yield NAD^+ and malate by oxidizing NADH and oxaloacetate [164, 165] and v) ROS-mediated direct and/or indirect oxidation of NADH to NAD^+ [162, 163] are also examined. NAD^+ providers are key components of the fail safe mechanism proposed in this thesis, as they assure the continuous operation of KGDHC, which will supply SUCL with succinyl-CoA, eventually generating high-energy phosphates even if the respiratory chain becomes

inoperable, *e.g.* in the absence of oxygen [Kiss *et al.* 2014: thesis-related publication No. 4].

In general, diaphorase activity is attributed to a flavoenzyme catalyzing the oxidation of reduced pyridine nucleotides by endogenous or artificial electron acceptors called “DT diaphorase” because of its reactivity with both DPNH (NADH) and TPNH (NADPH) discovered by Lars Ernster *et al.* [167, 168], now known as NAD(P)H:quinone oxidoreductase (NQO). It has also been identified in parallel by Märki and Martius, called “vitamin K reductase” [169] and later confirmed to be the same enzyme [170]. A “quinone reductase” with properties similar to the enzyme described by Ernster *et al.* also appears in earlier literature by Wosilait *et al.* [171, 172], as well as a microsomal “TPNH-neotetrazolium diaphorase”, described by Williams *et al.* [173], and a “brain diaphorase” by Giuditta and Strecker [174, 175]. Finally, a “menadione reductase” has been reported by Koli *et al.* [176]. DT diaphorase (EC 1.6.5.2, formerly assigned to EC 1.6.99.2) catalyzes a two-electron reductive metabolism (unlike other NAD(P)-linked quinone reductases [177]) detoxifying quinones and their derivatives [178]. Several isoforms have been identified [179, 180]; among them, NQO1 and NQO2 have been most extensively characterized [180]. A striking difference between them is that NQO2 uses dihydronicotinamide riboside (NRH) while NQO1 utilizes NAD(P)H for an electron donor [181, 182]. NQO1 has been found to localize not only in the cytosol, but also in mitochondria from several tissues [170, 183-193]. Mitochondrial diaphorase corresponds to 3-15% of total cellular activity [170, 187, 190, 192-194] and is localized in the matrix, since it reacts only with intramitochondrial reduced pyridine nucleotides, but is inaccessible to those added from the outside [191, 195]. However, it must be emphasized that mitochondrial diaphorase activity may not be exclusively due to NQO1; other mitochondrial enzymes may also exhibit diaphorase-like activity as a moonlighting function; for example, the isolated DLD subunit of KGDHC exhibits diaphorase activity and it is known to exist in the matrix as such, without being part of the KGDHC [196-201].

Finally, the pathway responsible for providing oxidized substrates to the diaphorase(s) is scrutinized and the conclusion is drawn that re-oxidation is mediated by complex III of the respiratory chain.

DOI:10.14753/SE.2015.1713

3. AIMS AND OBJECTIVES

As soon as the respiratory chain ceases to operate, the F_O-F_1 ATP synthase starts to hydrolyze ATP in order to compensate for the loss of $\Delta\Psi m$. In this thesis my intention is to confirm, if CYPD – a ubiquitous matrix-located protein with an ill-defined physiological function – binds to and modulates the F_O-F_1 ATP synthase not only in submitochondrial particles and permeabilized mitochondria, as it was shown already [59], but in intact mitochondria as well. The binding occurs in a phosphate-dependent manner and decreases both ATP synthesis and hydrolysis rates. However, modulation of F_O-F_1 ATP synthase by CYPD not necessarily increases the ANT-mediated ATP efflux rate in energized mitochondria or the ATP influx rate in de-energized mitochondria. I wish to demonstrate and, if so, to explain this lack of an effect of CYPD on the ANT-mediated adenine nucleotide exchange, by means of a recent kinetic model of the mitochondrial phosphorylation system [62]. One of the three aims of my thesis is to seek evidence that in mitochondria exhibiting intact inner membranes, the absence of CYPD or the inhibition of its binding to F_O-F_1 ATP synthase by cyclosporin A affects only matrix P_i and adenine nucleotide levels. By modulating matrix [ATP], [ADP], and [P_i], CYPD-F_O-F_1 ATP synthase interaction may fine-tune E_{rev_ANT} and E_{rev_ATPase}, adjusting them to the actual metabolic circumstances of the cell.

Provision of succinyl-CoA by the KGDHC is essential for the generation of matrix ATP or GTP by substrate-level phosphorylation via SUCL. This is especially important when the respiratory chain becomes inoperable due to chemical inhibition or anoxia, during which substrate-level phosphorylation becomes the only means of intramitochondrial ATP provision. Along this line, our group has recently identified that matrix substrate-level phosphorylation plays a major role in determining E_{rev_ANT} and E_{rev_ATPase}, essentially dictating the $\Delta\Psi m$ at which mitochondria switch from ATP producers to ATP consumers [Chinopoulos *et al.* 2010]. Since KGDHC may exhibit a high flux-control coefficient in the citric acid cycle, it is reasonable to assume that a decreased succinyl-CoA supply due to an impaired KGDHC would result in compromised substrate-level phosphorylation, rendering mitochondria more prone to consume cytosolic ATP in case of respiratory chain failure. This hypothesis is to be tested on transgenic mice with a deficiency in the dihydrolipoyl dehydrogenase (DLD) and/or dihydrolipoyl succinyltransferase (DLST) subunits of KGDHC exhibiting a 20-

62% decrease in the enzymatic activity. Do these respiration-impaired mitochondria prepared from KGDHC-deficient transgenic mice consume extramitochondrial ATP? If this is the case, I intend to examine if mitochondria from these transgenic mice respiring on substrates supporting substrate-level phosphorylation exhibit lower ADP-ATP exchange rates compared to those from WT littermates. My second aim in this thesis is to corroborate that the diminished matrix [ATP] in KGDHC-deficient mitochondria shifts E_{rev_ANT} towards more negative values, eventually causing the translocase to reverse prematurely. As the decline in KGDHC activity has been associated with neurodegeneration, I wish to investigate, if these pathologies are a consequence of the inability of respiration-impaired mitochondria to rely on matrical ATP reserves.

By means of a recently developed device able to measure in parallel oxygen consumption and $\Delta\Psi m$ in the same sample, it has become possible to address sources of NAD^+ provision during respiratory inhibition. Assuming NAD^+ is available, KGDHC may still remain functional under these circumstances [202]. As KGDHC operation generates CO_2, to verify above assumption, I intend to demonstrate acidification of the incubation medium due to CO_2 production by respiration-impaired mitochondria. A set of enzymes called diaphorases reduce a large variety of endogenous substrates, most notably quinones, generating NAD^+ from NADH in the process. By using specific pharmacological inhibitors and substrates, and examining tissues from pigeon liver exhibiting no diaphorase activity the third aim of my thesis is to test the hypothesis that diaphorases in the mitochondrial matrix utilize endogenous quinones for the regeneration of NAD^+ from NADH during respiratory arrest. However, as these enzymes may not be the sole contributors to the maintenance of KGDHC operation, it is reasonable to consider alternative sources for NAD^+ provision as well. I also intend to examine the possibility that reduced quinones are re-oxidized by complex III of the respiratory chain. The prime purpose is to identify mitochondrial diaphorases as potential providers of NAD^+ for KGDHC that in turn maintains provision of succinyl-CoA to SUCL; yielding matrix ATP. If the above reasoning is correct, obtained results might substantiate the concept that dietary provision of diaphorase substrates able to accumulate in mitochondria may be tissue-protective in energy crisis, as it occurs in pathological conditions.

DOI:10.14753/SE.2015.1713

4. MATERIALS AND METHODS

4.1 Animals

Mice (*Mus musculus*) were of either i) only C57Bl/6 ($WT_{(dld)}$ in **Chapter 5.2**), or ii) C57BL/6 and 129SV/EV hybrid ($WT_{(dlst)}$ in **Chapter 5.2**), or iii) mixed FVB and C57Bl/6 genetic background (WT in **Chapters 5.1** and **5.3**), or iv) only C57Bl/6J or v) only C57Bl/6N (**Chapter 5.3**); as indicated throughout the text. CYPD KO mice and WT littermates were a kind gift from Anna Schinzel [203] (**Chapter 5.1**). Mice deficient in the DLD subunit ($DLD^{+/-}$; C57BL/6) have been developed and characterized [157] (**Chapter 5.2**). $DLD^{+/-}$ and WT littermates were obtained from Jackson Laboratory (JAX® mice; Jackson Laboratory Repository, Bar Harbor, ME, USA), deposited by Dr. Mulchand S. Patel (State University of New York at Buffalo, Buffalo, NY, USA). Mice deficient in the DLST subunit ($DLST^{+/-}$; C57BL/6 and 129SV/EV hybrid) and WT littermates were obtained from Lexicon Pharmaceuticals (The Woodlands, TX, USA) (**Chapter 5.2**). $DLD^{+/-}$ and $DLST^{+/-}$ mice have no apparent behavioral phenotype. Double-transgenic $DLD^{+/-}$/$DLST^{+/-}$ mice were produced by cross-breeding $DLD^{+/-}$ and $DLST^{+/-}$ mice, and they also exhibited no apparent behavioral phenotype. Transgenic mice overexpressing the human superoxide dismutase 2 (MnSOD) under the control of the mouse myosin, heavy polypeptide 6, cardiac muscle, alpha, Myh6, promoter were obtained from Jackson Laboratory (JAX® mice; Jackson Laboratory Repository), deposited by Dr. Paul N. Epstein, University of Louisville, KY, USA (**Chapter 5.3**). Transgene expression is specific to the heart mitochondria. SOD activity is increased by 20-fold in heart and cardiac catalase activity is increased 2-fold. The animals were of a mixed FVB and C57Bl/6 background, backcrossed for at least 5 generations. Wild-type (WT) control animals were in most cases littermates. NADH:cytochrome *b*5 reductase isoform 2 (Cyb5r2) heterozygote mice of C57BL/6 background were obtained from the European Mouse Mutant Archive (EMMA) node at the MRC-Harwell and the European Conditional Mouse Mutagenesis Program (EUCOMM) consortium (**Chapter 5.3**). They were backcrossed for at least 5 generations with FVB mice, yielding WT, heterozygote, and viable, fertile homozygote knock-out (KO) $Cyb5r2^{-/-}$ mice. The animals used for the experiments presented in this thesis were of either sex and between 2 and 3 months of age. Mice were housed in a room maintained at 20-22°C on a 12/12-hour light/dark cycle with food and water

available *ad libitum*. Pigeons (*Columba livia domestica*) were obtained from a local vendor and used on the same or next day (**Chapter 5.3**). All experiments were carried out in compliance with the Guide for the Care and Use of Laboratory Animals of the National Institute of Health and were approved by the Institutional Animal Care and Use Committee of the Weill Cornell Medical College and the Animal Care and Use Committee of the Semmelweis University (Egyetemi Állatkísérleti Bizottság).

4.2 Isolation of mitochondria from mouse and pigeon liver, mouse heart and brain

Nonsynaptic brain mitochondria from adult male and female mice were isolated on a Percoll gradient as described in [204], with minor modifications detailed in [205]. Mitochondria from the hearts and livers of all animals were isolated as described in [206], with minor modifications. The animals were sacrificed by decapitation and the organs were rapidly removed, minced, washed and homogenized using a glass/PTFE Potter-Elvehjem tissue grinder in ice-cold isolation buffer containing 225 mM mannitol, 75 mM sucrose, 5 mM HEPES (free acid), 1 mM EGTA and 1 mg/ml bovine serum albumin (BSA, essentially fatty acid-free), with the pH adjusted to 7.4 with Trizma® (Sigma-Aldrich, St. Louis, MO, USA). The homogenate was centrifuged at 1,250 ***g*** for 10 min; the upper fatty layer of the supernatant was aspirated and the pellet was discarded, then the remaining supernatant was centrifuged at 10,000 ***g*** for 10 min; this step was repeated once. At the end of the third centrifugation, the supernatant was discarded, and the pellet was suspended in 0.15 ml of the same buffer with 0.1 mM EGTA. The mitochondrial protein concentration was determined using the bicinchoninic acid assay, calibrated with BSA standards [207], using a Tecan Infinite 200 PRO series plate reader (Tecan Deutschland GmbH, Crailsheim, Germany). Yields were typically 0.2 ml of ~15 mg/ml per 2 brains; 0.2 ml of ~15 mg/ml per 4 hearts; 0.4 ml of ~80 mg/ml per mouse liver and 0.8 ml of ~80 mg/ml per pigeon liver.

4.3 Isolation of synaptosomes from mouse brain

Synaptosomes were prepared from adult male and female mice by Percoll gradient purification as detailed previously [208]. Protein concentration was determined as detailed in the previous chapter; yields were typically 0.2 ml of ~20 mg/ml per 2 brains.

4.4 Neuronal cultures

Mixed primary cultures of cortical neurons and astrocytes (~20% of total cell count were astrocytes) were prepared from mouse pups (P0-P1), as detailed elsewhere [209]. Cultures were prepared from each pup individually; subsequent genotyping of the pups identified whether the culture was from a WT or a transgenic mouse. Cells were grown on poly-l-ornithine-coated 8-well Lab-Tek II chambered coverglasses (Nunc, Rochester, NY, USA) for 7-12 days, at a density of 105 cells/well in Neurobasal medium containing 2% B27 supplement and 2 mM glutamine.

4.5 Determination of membrane potential in isolated liver, heart, brain, *in situ* synaptic and *in situ* neuronal somal mitochondria

Mitochondrial membrane potential ($\Delta\Psi m$) of isolated mitochondria was estimated using fluorescence quenching of the cationic dye safranin O, due to its accumulation inside energized mitochondria [210]. Mitochondria (0.5 mg/ml for liver, 0.25 mg/ml for heart and 0.125 mg/ml for brain; in these and all subsequent experiments, a wet weight of mitochondrial amount is implied) were suspended in 2 or 4 ml (depending on the experimental setting; see below) of an incubation medium containing 110 mM K-gluconate, 10 mM HEPES (free acid), 10 mM KH_2PO_4, 10 mM mannitol, 10 mM NaCl, 8 mM KCl, 1 mM $MgCl_2$, 0.01 mM EGTA, 0.5 mg/ml BSA (essentially fatty acid-free), with the pH adjusted to 7.25 with KOH, plus 5 μM safranin O. Substrates and their combinations were used as indicated throughout the text. Fluorescence was recorded in either a PTI Deltascan fluorescence spectrophotometer (Photon Technology International, Inc., Lawrenceville, NJ, USA) or in Hitachi F-4500 or F-7000 fluorescence spectrophotometers (Hitachi High Technologies, Maidenhead, UK) in 2 ml disposable plastic cuvettes at a 5 Hz acquisition rate, using 495 and 585 nm excitation and emission wavelengths, respectively. To convert safranin O fluorescence into millivolts, a voltage-fluorescence calibration curve was constructed. To this end, safranin O fluorescence was recorded in the presence of 2 nM valinomycin and stepwise increasing $[K^+]$ (in the 0.2-120 mM range), which allowed calculation of $\Delta\Psi m$ by the Nernst equation, assuming a matrix $[K^+]$ = 120 mM [210]. Safranin O is known to increase *State 4* respiration [211], decrease maximum Ca^{2+} uptake capacity and exhibit an appreciable non-specific binding component if used at concentrations above 5 μM [90]. However, at concentrations below 5 μM, calibration of the safranin O fluorescence

signal to ΔΨm deviates significantly from linearity, thereby more complex fitting functions are required, decreasing the faithfulness of the conversion. Therefore – for the experiments in this thesis –, 5 μM of safranin O was used at the expense of diminishing the respiratory control ratio by approximately one unit (from 7.5 to 6.5 using glutamate plus malate), but the signal-to-noise ratio was optimal and the calibration of the fluorescence signal to ΔΨm highly reproducible.

Alternatively, safranin O fluorescence was also detected – in parallel with oxygen consumption – at a 2 Hz acquisition rate using the O2k-Fluorescence LED2-Module of the OROBOROS Oxygraph-2k (Oroboros Instruments GmbH, Innsbruck, Austria) equipped with a light-emitting diode (LED) exhibiting a wavelength maximum of 465 +/- 25 nm (current for light intensity was adjusted to 2 mA, *i.e.*, level "4") and a < 505 nm shortpass excitation filter (dye-based, filter set "Safranin"). Emitted light was detected by a photodiode (range of sensitivity: 350-700 nm), through a > 560 nm longpass emission filter (dye-based). Chamber volume of the Oxygraph-2k was 4 ml.

Estimation of ΔΨm from tetraphenylphosphonium (TPP^+) ion distribution was measured using a custom-made TPP^+-selective electrode [212]. For these experiments, the assay medium (identical to that for safranin O experiments) was supplemented with 2 μM TPP^+Cl^- and mitochondrial protein concentration was 2 mg/ml. The electrode was calibrated by sequential additions of TPP^+Cl^-. TPP^+Cl^- appeared to be less toxic than safranin O in terms of an effect on mitochondrial respiration; however, the signal-to-noise ratio was not as satisfactory as that obtained from safranin O, and it could not be improved by increasing the concentration of TPP^+ (from a total 2 to a total 4 μM).

ΔΨm of *in situ* mitochondria of synaptosomes was qualitatively estimated fluorimetrically by loading synaptosomes with 100 nM of the potentiometric fluorescent dye tetramethylrhodamine methyl ester (TMRM). Synaptosomes (0.5 mg) were added to 2 ml of incubation medium containing 140 mM NaCl, 10 mM PIPES (Na^+), 3 mM KCl, 2 mM $MgCl_2$, 1.5 mM $CaCl_2$, plus 15 mM glucose, with the pH adjusted to 7.4 with NaOH. Fluorescence was recorded in a Hitachi F-4500 fluorescence spectrophotometer (Hitachi High Technologies) at a 5-Hz acquisition rate, using 546 and 573 nm excitation and emission wavelengths, respectively.

ΔΨm of *in situ* mitochondria of neurons was qualitatively determined by wide-field fluorescence imaging, or confocal imaging. Briefly, the TMRM fluorescence (7.5 nM)

was followed in time over cell bodies (see below). Experiments were performed in a medium containing 120 mM NaCl, 3.5 mM KCl, 1.3 mM $CaCl_2$, 1 mM $MgCl_2$, 20 mM HEPES (free acid), 15 mM glucose, and 1 μM tetraphenylboron, with the pH adjusted to 7.4 with NaOH. To prevent excitotoxicity, all experiments were performed in the presence of 1 μM tetrodotoxin, 10 μM MK801, 10 μM 2,3-dihydroxy-6-nitro-7-sulfamoylbenzo(f)quinoxaline and 1 μM nifedipine. All ΔΨm determinations of isolated, *in situ* synaptic and neuronal somal mitochondria were performed at 37°C.

4.6 Fluorescence imaging

Imaging was performed either with confocal imaging (on a Leica TCS SP5 confocal system; Leica Microsystems Inc., Buffalo Grove, IL, USA) or epifluorescent imaging. During the confocal imaging, full frames (using a Leica HC PL Fluotar ×10 air 0.3NA lens) were taken at 3-min intervals; 9-18 view fields in 3-6 wells of the Lab-Tek chamber were recorded cyclically using the inbuilt acquisition feature of the Leica Microsystems software. Epifluorescence imaging was performed on an Olympus IX-81 inverted microscope (Olympus, Tokyo, Japan) equipped with a UAPO ×20 air 0.75NA lens, a Lambda LS Xe-arc light source (175 W), Lambda 10-2 excitation and emission filter wheels (Sutter Instruments, Novato, CA, USA), a Bioprecision-2 linear encoded *xy* stage (Ludl Electronic Products Ltd., Hawthorne, NY, USA), and an ORCA-ER2 cooled digital charge-coupled device camera (-60°C, 10-MHz readout, low gain, 12-bit depth; Hamamatsu Photonics, Hamamatsu, Japan). Full frames at 4 × 4 binning (1.3 μm/pixel resolution) were taken at 3-min intervals. Eight to 16 view fields in 4-8 wells of the Lab-Tek chamber were recorded cyclically using the Multi-Dimensional Acquisition feature of Metamorph 6.3 software (Molecular Devices, Sunnyvale, CA, USA). The filter sets, given as excitationdichroic mirror-emission (nm) for TMRM were 535/20-555LP-590/20 (all from Chroma, Rockingham, VT, USA).

4.7 $[Mg^{2+}]_{free}$ determination from Magnesium Green™ (MgG) fluorescence in the extramitochondrial volume of isolated mitochondria and conversion to ADP-ATP exchange rate

Mitochondria (1 mg) were added to 2 ml of the incubation medium specified in **Chapter 4.5** without safranin O, plus 50 μM of the adenylate kinase inhibitor Ap_5A (Mg^{2+} activates adenylate kinase in the intermembrane space) and 2 μM MgG, a Mg^{2+}-sensitive fluorescent indicator (Invitrogen, Carlsbad, CA, USA). Substrates and their

combinations were used as indicated in the text, or in the figures and in their legends. MgG fluorescence was recorded in a PTI Deltascan fluorescence spectrophotometer (Photon Technology International, Inc.) at a 5 Hz acquisition rate, using excitation and emission wavelengths of 506 nm and 531 nm, respectively. MgG exhibits an extremely high molar extinction coefficient (ε_{max} [MgG] = 75,000 $cm^{-1} \times M^{-1}$), therefore, slits were opened to widths of no more than 1 nm. After stabilization of the signal at 37°C, 2 mM ADP was added, and the fluorescence (*F*) was recorded for 50 sec, followed by addition of 2 μM cATR (**Chapter 5.2**). At the end of each experiment, minimum fluorescence (F_{min}) was measured after the addition of 4 mM EDTA, followed by the recording of maximum fluorescence (F_{max}) elicited by addition of 20 mM $MgCl_2$. Free Mg^{2+} concentration ($[Mg^{2+}]_{free}$) was calculated from the following equation:

$$[Mg^{2+}]_{free} = \frac{K_d \times (F - F_{min})}{F_{max} - F} - 0.055\ mM \tag{8}$$

assuming a "K_d" of 0.9 mM for the MgG-Mg^{2+} complex [213]. The correction term -0.055 mM is empirical, and possibly reflects the chelation of other ions by EDTA that have an affinity for MgG and alter its fluorescence. The ADP-ATP exchange rate was estimated using a method described by our group [42], exploiting the differential affinity of ADP and ATP to Mg^{2+}. The rate of ATP appearing in the medium after the addition of ADP to energized mitochondria (or *vice versa* in the case of de-energized mitochondria) is calculated from the measured rate of change in free extramitochondrial [Mg^{2+}] using the equation:

$$[ATP]_t = \frac{\frac{[Mg^{2+}]_t}{[Mg^{2+}]_{free}} - 1 - \frac{[ADP]_t(t=0) + [ATP]_t(t=0)}{K_{ADP} + [Mg^{2+}]_{free}}}{\frac{1}{K_{ATP} + [Mg^{2+}]_{free}} - \frac{1}{K_{ADP} + [Mg^{2+}]_{free}}} \tag{9}$$

where, $[ADP]_t$ and $[ATP]_t$ are the total concentrations of ADP and ATP, respectively, in the medium, and $[ADP]_t(t = 0)$ and $[ATP]_t(t = 0)$ are $[ADP]_t$ and $[ATP]_t$ in the medium at time zero. The assay is designed such that the ANT is the sole mediator of changes in [Mg^{2+}] in the extramitochondrial volume, as a result of ADP-ATP exchange [42]. For the calculation of [ATP] or [ADP] from $[Mg^{2+}]_{free}$, the apparent K_d values are identical to those reported in [42] as a result of identical experimental conditions (K_{ADP} = 0.906 ± 0.023 mM, and K_{ATP} = 0.114 ± 0.005 mM). $[Mg^{2+}]_t$ is the total amount of Mg^{2+} present in the medium (1 mM). Eq. (9) – termed "ANT calculator" – is available as an

executable file for download (*http://www.tinyurl.com/ANT-calculator*). A variant of this method involving an improved calibration step introduced to minimize errors that may arise during the conversion of the MgG signal to extramitochondrial $[Mg^{2+}]_{free}$ and ATP is described in Chinopoulos *et al.* 2014 (publication not closely related to this thesis).

In the case of permeabilized mitochondria by alamethicin, the ATP hydrolysis rate by the F_O-F_1 ATP synthase was estimated by the same principle because one molecule of ATP hydrolyzed yields one molecule of ADP (plus P_i). In **Chapter 5.1**, the rates of ATP efflux, influx and hydrolysis have been estimated sequentially from the same mitochondria: first mitochondria were energized, a small amount of uncoupler was added prior to the addition of ADP, and ATP efflux was recorded; 150 sec later, 1 μM of SF 6847 was added, and ATP influx was recorded; after 150 sec, alamethicin was added, and ATP hydrolysis by the F_O-F_1 ATP synthase was recorded. F_{min} and F_{max} were subsequently recorded as detailed above. For conversion of calibrated free $[Mg^{2+}]$ to free [ADP] and [ATP] appearing in the medium, the initial values of total [ADP] and $[Mg^{2+}]$ were considered because $[ADP]_{free}$ and $[ATP]_{free}$ are added parameters in the numerator of Eq. (9).

4.8 Mitochondrial respiration

Oxygen consumption was monitored polarographically using an OROBOROS Oxygraph-2k (Oroboros Instruments GmbH). Mouse brain (**Chapter 5.2**; 0.125 mg) mitochondria were suspended in 2 ml, or mouse (1 mg in **Chapter 5.2** and 2 mg in **5.3**) or pigeon (**Chapter 5.3**; 2 mg) liver mitochondria were suspended in 4 ml incubation medium, the composition of which was the following: 110 mM K-gluconate, 10 mM HEPES (free acid), 10 mM KH_2PO_4, 10 mM mannitol, 10 mM NaCl, 8 mM KCl, 1 mM $MgCl_2$, 0.01 mM EGTA, 0.5 mg/ml BSA (essentially fatty acid-free), with the pH adjusted to 7.25 with KOH. As in **Chapter 5.3** mitochondrial oxygen consumption was measured in parallel with $\Delta\Psi m$, 5 μM safranin O was added to the incubation medium. Substrates and their combinations were used as indicated throughout the text. Experiments were performed at 37°C. Oxygen concentration (μM) and flux (pmol × sec^{-1} × ml^{-1}; negative time derivative of oxygen concentration) were recorded using DatLab software (Oroboros Instruments GmbH). Flux was converted to nmol × min^{-1} × mg^{-1} in order to normalize for mitochondrial mass; in this manner different mitochondrial preparations became comparable.

DOI:10.14753/SE.2015.1713

4.9 Determination of extramitochondrial pH changes

The pH of the medium in which mouse liver mitochondria were suspended (0.5 mg/ml in the 4 ml chamber volume) was recorded by connecting a combination pH microelectrode (Radiometer Analytical, Lyon, France) to the BNC connector of the OROBOROS Oxygraph-2k (Oroboros Instruments GmbH). The medium used for this purpose had to have a low buffering capacity as the intent was to detect the minor pH changes caused by mitochondrial CO_2 production. The composition of this medium was the following: 120 mM KCl, 10 mM mannitol, 10 mM NaCl, 5 mM KH_2PO_4, 1 mM $MgCl_2$, 0.01 mM EGTA, 0.5 mg/ml BSA (essentially fatty acid-free), with the pH adjusted to 7.25 with KOH. Substrates and their combinations were used as indicated in the respective figures. The voltage signal output of the electrode was converted to pH by calibrating with MeterLab® certified standard solutions of the following pH values: 4.005 ± 0.010 and 7.000 ± 0.010 at 25°C (Radiometer Analytical). Since experiments were performed at 37°C, temperature compensation was applied during voltage-pH calibration according to data provided by the manufacturer.

4.10 Mitochondrial matrix pH (pH_i) determination

The pH_i of isolated liver mitochondria from WT and CYPD KO mice was estimated as described in [214], with minor modifications. Briefly, mitochondria (20 mg) were suspended in 2 ml of an incubation medium containing 225 mM mannitol, 75 mM sucrose, 5 mM HEPES (free acid), 0.1 mM EGTA, with the pH adjusted to 7.4 using Trizma® (Sigma-Aldrich), and incubated with 50 μM BCECF-AM (Invitrogen) at 30°C. After 20 min, mitochondria were centrifuged at 10,600 ***g*** for 3 min (at 4°C), washed once and centrifuged again. The final pellet was suspended in 0.2 ml of the same medium and kept on ice until further manipulation. Fluorescence of hydrolyzed BCECF trapped in the matrix was measured in a Hitachi F-4500 fluorescence spectrophotometer (Hitachi High Technologies) in a ratiometric mode at a 2 Hz acquisition rate, using excitation and emission wavelengths of 450/490 nm and 531 nm, respectively. Buffer composition and temperature were identical to that used for ΔΨm determination, but without the addition of safranin O (see **Chapter 4.5**). Respiratory substrates were 5 mM succinate plus 1 mM glutamate where indicated in **Chapter 5.1**. The BCECF signal was calibrated using a range of buffers of known pH values in the range of 6.8-7.8, and by

equilibrating matrix pH to that of the incubation medium by 250 nM SF 6847 plus 1 μM nigericin. For converting BCECF fluorescence ratio to pH, the function was fitted:

$$f = a \times e^{\frac{b}{x+c}} \quad (10)$$

to BCECF fluorescence ratio values, where "x" is the BCECF fluorescence ratio, "a", "b" and "c" are constants and "f" represents the calculated pH. The fitting of the above function to BCECF fluorescence ratio values obtained by subjecting mitochondria to buffers of known pH returned $r^2 > 0.99$ and the standard error of the estimates of "a" and "c" constants were in the range of 0.07-0.01, and < 0.1 for "b".

4.11 Determination of NADH fluorescence in isolated liver mitochondria

Autofluorescence of reduced mitochondrial pyridine nucleotides was measured using 340 and 435 nm excitation and emission wavelengths, respectively. Fluorescence measurements were performed in a Hitachi F-7000 fluorescence spectrophotometer (Hitachi High Technologies, Maidenhead, UK) in disposable plastic cuvettes at a 5 Hz acquisition rate. Isolated mouse liver mitochondria (0.5 mg/ml, wet weight) were suspended in 2 ml incubation medium, the composition of which was identical to the one described in **Chapter 4.8**. Respiratory substrates were 5 mM glutamate plus 5 mM malate. Experiments were performed at 37°C.

4.12 Determination of KGDHC activity

KGDHC activity in isolated mouse liver and brain mitochondria and isolated nerve terminals was measured fluorimetrically, as detailed in [162], with minor modifications. The reaction medium was composed of 20 mM HEPES (free acid), 0.3 mM thiamine pyrophosphate, 50 μM $CaCl_2$, 0.2 mM $MgCl_2$, 5 mM α-ketoglutarate, 1 mM dithiothreitol and 0.5 mM NAD^+, with the pH adjusted to 7.8 with KOH. The reaction was started by adding 0.12 mM CoASH to freeze-thawed mitochondria (0.1 mg/ml) or synaptosomes (0.5 mg/ml). Reduction of NAD^+ was followed at 30°C in a Hitachi F-4500 fluorescence spectrophotometer (Hitachi High Technologies) at 435 nm emission after excitation at 340 nm. The molar extinction coefficient (ε_{340}) of NADH fluorescence was considered as 6,220 $cm^{-1} \times M^{-1}$.

4.13 Determination of SUCL activity

ATP- and GTP-forming SUCL activities in isolated mouse liver and brain mitochondria were determined at 30°C, as described in [215], with modifications

detailed in [96]. Mitochondria (0.25 mg from brain and 1 mg from liver) were added in an assay mixture (2 ml) containing 20 mM potassium phosphate, 0.4% 3-[(3-cholamidopropyl)dimethylammonio]-1-propanesulfonate (CHAPS; pH 7.2), 10 mM $MgCl_2$, and 2 mM ADP or GDP. The reactions were initiated by adding 0.2 mM succinyl-CoA and 0.2 mM 5,5'-dithiobis(2-nitrobenzoic acid) (DTNB) in quick succession. The molar extinction coefficient value at 412 nm for the 2-nitro-5-thiobenzoate anion formed on reaction of DTNB with CoASH was considered as 13,600 $cm^{-1} \times M^{-1}$. Rates of 2-nitro-5-thiobenzoate formation were followed in a GBC UV/VIS 920 spectrophotometer (GBC Scientific Equipment Pty. Ltd., Braeside, VIC, Australia) during constant stirring by subtracting the rate observed when ADP/GDP was omitted.

4.14 Cross-linking, co-precipitation and western blotting

In **Chapter 5.1**, mitochondria (5 mg/ml) were suspended in the same buffer as for the ΔΨm determination, but without the addition of safranin O (see **Chapter 4.5**) and supplemented with 5 mM succinate and 1 mM glutamate. Cyclosporin A (1 μM) was added where indicated. After 3 min of incubation at 37°C, 2.5 mM DSP was added, and mitochondria were incubated further for 15 min. Subsequently, mitochondria were sedimented at 10,000 ***g*** for 10 min, and resuspended in 1% digitonin, in a buffer containing 50 mM Trizma® (Sigma-Aldrich), 50 mM KCl, with the pH adjusted to 7.6 with KOH. Samples were then incubated overnight under wheel rotation at 4°C in the presence of monoclonal anti-complex V sera covalently linked to protein G-agarose beads (MS501 immunocapture kit; Mitosciences, Eugene, OR, USA). After centrifugation at 2,000 ***g*** for 5 min, the beads were washed twice for 5 min in a solution containing 0.05% (w/v) n-Dodecyl-β-D-maltopyranoside (DDM) in $NaCl/P_i$. The elution was performed in 1% (w/v) sodium dodecyl sulfate (SDS) for 15 min. To reduce the DSP disulfide bond, the cross-linked immunoprecipitates were treated with 150 mM dithiothreitol for 30 min at 37°C and separated by sodium dodecyl sulfate-polyacrylamide gel electrophoresis (SDS-PAGE). Separated proteins were transferred to a methanol-activated polyvinylidene difluoride (PVDF) membrane. Immunoblotting was performed in accordance with the instructions of the manufacturers of the antibodies. Mouse monoclonal anti-CYPD (MSA04; Mitosciences) and anti-β subunit of the F_O-F_1 ATP synthase (MS503; Mitosciences) primary antibodies were used at concentrations of 2 μg/ml. Immunoreactivity was detected using the appropriate

peroxidase-linked secondary antibody (dilution 1:4,000, donkey anti-mouse; Jackson Immunochemicals Europe Ltd., Newmarket, UK) and enhanced chemiluminescence detection reagent (RapidStep^{TM} ECL reagent; Calbiochem, Merck Chemicals, Darmstadt, Germany). In **Chapter 5.2**, frozen mitochondrial and synaptosomal pellets were thawed on ice and separated by SDS-PAGE. Separated proteins were transferred to a methanol-activated PVDF membrane. Immunoblotting was performed as recommended by the manufacturers of the antibodies. Mouse monoclonal anti-cyclophilin D (cypD; Mitosciences), rabbit polyclonals anti-SUCLG1 and anti-SUCLG2 (Abcam, Cambridge, UK), and anti-SUCLA2 (Proteintech Europe Ltd., Manchester, UK) primary antibodies were used at concentrations of 1 μg/ml, and rabbit polyclonal anti-manganese superoxide dismutase (MnSOD; Abcam) at 0.2 μg/ml. Immunoreactivity was detected using the appropriate peroxidase-linked secondary antibody (1:4,000, donkey anti-mouse or donkey anti-rabbit; Jackson Immunochemicals Europe Ltd.) and enhanced chemiluminescence detection reagent (ECL system; Amersham Biosciences GE Healthcare Europe GmbH, Vienna, Austria).

4.15 Statistical analysis

Data are presented as means ± SEM. Significant differences between 2 groups were evaluated by Student's *t* test; significant differences between ≥ 3 groups of data were evaluated by one-way analysis of variance (ANOVA) followed by Tukey's *post hoc* analysis. Values of $p < 0.05$ were considered statistically significant. If normality test failed, ANOVA on ranks was performed. Wherever single graphs are presented, they are representative of ≥ 3 independent experiments.

4.16 Reagents

Standard laboratory chemicals, P^1,P^5-di(adenosine-5') pentaphosphate (Ap_5A), alamethicin, nigericin, safranin O and valinomycin were obtained from Sigma-Aldrich. SF 6847 was from Biomol (BIOMOL GmbH, Hamburg, Germany). DSP was obtained from Piercenet (Thermo Fisher Scientific, Rockford, IL, USA). BCECF-AM, MgG, TMRM, Neurobasal medium and B27 supplement were obtained from Invitrogen. BKA and cATR were from Merck KGaA (Darmstadt, Germany). All mitochondrial substrate stock solutions were dissolved in bi-distilled water and titrated to pH 7.0 with KOH. ATP and ADP were purchased as K^+ salts of the highest purity available (Calbiochem) and titrated to pH 6.9 with KOH.

DOI:10.14753/SE.2015.1713

5. RESULTS

5.1 Modulation of F_O-F_1 ATP synthase activity by cyclophilin D regulates matrix adenine nucleotide levels

This chapter examines the extent of contribution of CYPD on the rates of ADP and ATP flux towards the extramitochondrial compartment. According to experiments outlined below, for as long as the inner mitochondrial membrane integrity remained intact, the absence of CYPD or its inhibition by cyclosporin A did not affect the ATP efflux rate in energized mitochondria or the rate of ATP consumption in de-energized mitochondria. However, the absence of CYPD or its inhibition by cyclosporin A significantly decreased the extent of uncoupler-induced depolarization in ATP-energized intact mitochondria. Functional results are supported by the finding that the CYPD-F_O-F_1 ATP synthase interaction was demonstrated in intact mitochondria using the membrane-permeable cross-linker, 3,3'-dithiobis(sulfosuccinimidyl propionate) (DSP) followed by co-precipitation using an antibody for F_O-F_1 ATP synthase as bait; cyclosporin A was found to diminish the binding of CYPD on the F_O-F_1 ATP synthase. The results indicate that modulation of F_O-F_1 ATP synthase activity by CYPD comprises an "in-house" mechanism regulating matrix adenine nucleotide levels that does not transduce to the extramitochondrial compartment for as long as the inner mitochondrial membrane remains intact.

5.1.1 ADP-ATP exchange rates in intact mitochondria and ATP hydrolysis rates in permeabilized mitochondria

For the most part, ANT-mediated ADP-ATP exchange rate is controlled by the $\Delta\Psi m$, among other parameters elaborated in **Chapter 2.4**. ANT-mediated ADP-ATP exchange rates were measured in intact isolated WT and CYPD KO mouse liver mitochondria, both in the presence and absence of cyclosporin A, in the -130 to -160 mV $\Delta\Psi m$ range, titrated by the uncoupler SF 6847 using different concentrations, and at 0 mV produced by a maximal dose of the uncoupler. ANT-mediated ADP-ATP exchange rates were compared with those obtained by direct ATP hydrolysis rates by the F_O-F_1 ATP synthase in alamethicin-permeabilized mitochondria.

DOI:10.14753/SE.2015.1713

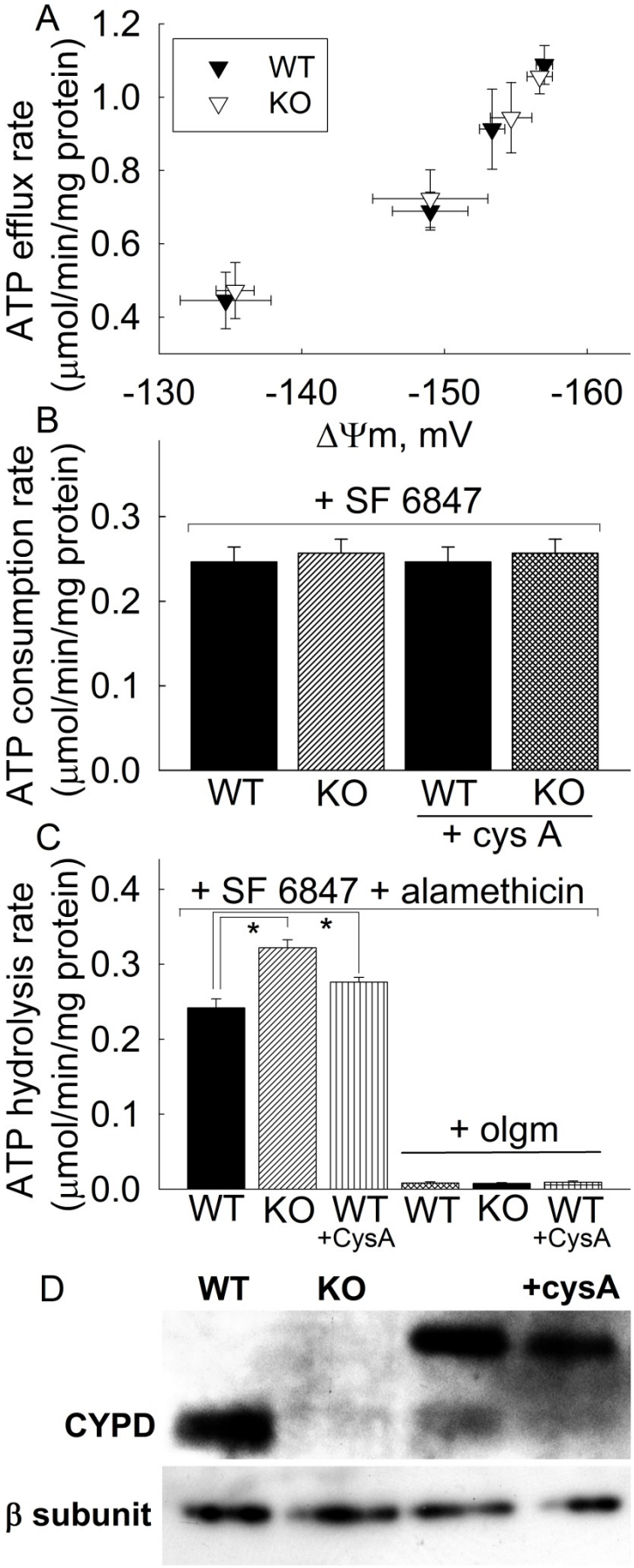

Figure 6. ADP-ATP exchange rates in intact mitochondria and ATP hydrolysis rates in permeabilized mitochondria; CYPD binds on F_O-F_1 ATP synthase in a cyclosporin A-inhibitable manner in intact mouse liver mitochondria. **(A)** ATP efflux rates as a function of ΔΨm in intact, energized mouse liver mitochondria isolated from WT and CYPD KO mice. **(B)** Bar graphs of ATP consumption rates in intact, completely de-energized WT and CYPD KO mouse liver mitochondria, and the effect of cyclosporin A. **(C)** Bar graphs of ATP hydrolysis rates in permeabilized WT ± cyclosporin A and CYPD KO mouse liver mitochondria, and the effect of oligomycin (olgm). *Statistically significant (Tukey's test, $p < 0.05$). **(D)** Lanes 1 and 2 represent CYPD-WT and KO mitochondria, respectively (0.85 µg each). Lanes 3 and 4 represent co-precipitated samples of cross-linked intact mitochondria, treated with 1% digitonin before cross-linking. For lane 4, mitochondria were additionally treated with cyclosporin A before cross-linking. The upper panel is a western blot for CYPD and the lower panel is a western blot for the β subunit of F_O-F_1 ATP synthase. ←

Mitochondria were energized by succinate (5 mM) and glutamate (1 mM) to disfavor matrix substrate-level phosphorylation (explained comprehensively in **Chapter 5.2.2**); ensuring that under these experimental conditions the only ATP generating entity contributing to ATP efflux from mitochondria is the F_O-F_1 ATP synthase. ADP was added (2 mM) and small amounts of the uncoupler SF 6847 were subsequently titrated (10-30 nM) to reduce ΔΨm to not more than -130 mV, whereas ΔΨm was recorded as time courses from fluorescence changes as a result of the redistribution of safranin O across the inner mitochondrial membrane. In parallel experiments, ATP efflux rates were calculated by measuring extramitochondrial changes in free [Mg^{2+}] using a method described in **Chapter 4.7**, exploiting the differential affinities of ADP and ATP to Mg^{2+}. ADP-ATP exchange rates as a function of ΔΨm in the -130 to -160 mV range, comparing mitochondria isolated from the livers of WT *vs.* CYPD KO mice, are shown in Fig. 6A. There was no difference in the ATP efflux-ΔΨm profile of the WT compared to CYPD KO mice, whereas ANT was operating in the forward mode. Similarly, when mitochondria were completely depolarized by 1 μM SF 6847 (Fig. 6B), no statistically significant difference was observed between mitochondria isolated either from WT or CYPD KO mice during ATP influx, irrespective of the presence of cyclosporin A (1 μM) in the medium. However, if mitochondria were subsequently permeabilized by alamethicin (20 μg), mitochondria isolated from CYPD KO mice exhibited a 30.9 ± 1.3% faster ATP hydrolysis rate compared to WT littermates (Fig. 6C). The effect of cyclosporin A (1 μM) was only 14.3%, although nonetheless this was statistically significant (p = 0.027). This ATP hydrolysis rate was 96.7% sensitive to oligomycin, thus supporting the assumption that it was almost entirely a result of the F_O-F_1 ATP synthase.

To further confirm that, in intact mitochondria, the binding of CYPD to F_O-F_1 ATP synthase occurs and is inhibitable by cyclosporin A, we incubated mitochondria with the membrane-permeable cross-linker DSP in the absence or presence of cyclosporin A, extracted proteins with 1% digitonin [59], immunoprecipitated with anti-complex V sera, and finally tested immunocaptured proteins for the presence of CYPD using the β subunit of the F_O-F_1 ATP synthase as loading control. As shown in Fig. 6D, digitonin-treated, cross-linked samples pulled down CYPD (lane 3), and cyclosporin A reduced the amount of CYPD bound to F_O-F_1 ATP synthase (lane 4). In lane 1, mitochondria

from the liver of a CYPD-WT mouse and, in lane 2, mitochondria from the liver of a CYPD-KO mouse were loaded (0.85 μg each), serving as a positive and negative control for the CYPD blot, respectively. The results shown in Fig. 6D point to the fact that CYPD-F_O-F_1 ATP synthase interactions can be observed in intact mitochondria and cyclosporin A disrupts these interactions.

5.1.2 Prediction of alterations in ANT-mediated ADP-ATP exchange rate caused by changing matrix ATP and ADP levels by kinetic modeling

The rate equations of both the electrogenic translocation of adenine nucleotides catalyzed by the ANT [92] and the F_O-F_1 ATP synthase reaction [88, 89] have been derived previously and implemented in a complete mitochondrial phosphorylation system [62]. According to above mentioned equations, the ANT-mediated ADP-ATP exchange rate and F_O-F_1 ATP synthase activity both depend on free matrix ATP and ADP concentrations, therefore it was possible to calculate the changes in free extramitochondrial ATP and ADP concentrations. The increase in F_O-F_1 ATP synthase activity upon CYPD ablation was assumed to be 30% (arbitrarily chosen on the basis of the results in Fig. 6C and in [59]) and its impact on ANT-mediated ADP-ATP exchange rate was estimated for predefined ΔΨm values. Values of ΔΨm were chosen as depicted in Fig. 6A; obtained by the addition of the uncoupler SF 6847 in different concentrations. The results of the calculations are shown in Table 3: the increase in ANT-mediated ADP-ATP exchange rate as a result of a 30% increase in F_O-F_1 ATP synthase activity is in the range of 1.38–7.7%. The percentage change increased for more depolarized ΔΨm values, approaching the reversal potential of the ANT. At 0 mV, during which both the ANT and the F_O-F_1 ATP synthase operate in reverse mode, the increase in ANT-mediated ADP-ATP exchange rate decreases to 1.7%. Since the greatest increase in the ANT-mediated ADP-ATP exchange rate calculated at -134 mV (7.7%) occurs during the lowest ADP-ATP exchange rate (Fig. 6A), it is least likely to lead to statistically significant adenine nucleotide flux rates from mitochondria obtained from WT *vs.* CYPD KO littermates. The above calculations afford the assumption that a 30% increase in F_O-F_1 ATP synthase activity will lead to an insignificant increase (1.38–1.7%) in the ANT-mediated ADP-ATP exchange rate in maximally polarized (forward mode of both ANT and F_O-F_1 ATP synthase) and maximally depolarized (reverse mode of both ANT and F_O-F_1 ATP synthase) mitochondria.

Table 3. Estimation of the change (%) in the ANT-mediated ADP-ATP exchange rate as a function of an increase in F_O-F_1 ATP synthase activity (%) at different ΔΨm values for 1-1 mM free matrix ATP and ADP concentrations (equations in [62]). ↓

Increase in F_O-F_1 ATP synthase activity (%)	Increase in ANT-mediated ADP-ATP exchange rate (%)				
+30	+1.38	+1.94	+3.65	+7.70	+1.70*
ΔΨm (mV)	-157	-154	-147	-134	0

*Reverse mode of operation for both ANT and F_O-F_1 ATP synthase.

5.1.3 Effect of altering matrix pH on adenine nucleotide exchange rates

Uncouplers are by definition protonophores which cycle across the inner mitochondrial membrane dissipating the ΔΨm by shuttling protons back to the matrix, thus acidifying it (see **Chapter 2.2**). This may affect CYPD binding to the inner membrane by means of the decreasing matrix P_i concentration, which is otherwise necessary for CYPD to bind to the F_O-F_1 ATP synthase. In the meantime, matrix acidification increases the binding of IF1 to F_1-ATPase (see **Chapter 2.3**). IF1 inhibits the consumption of ATP by a reverse-operating F_O-F_1 ATP synthase, especially during acidic conditions [53, 58]. IF1 would inhibit ATP hydrolysis independent of the CYPD-F_O-F_1 ATP synthase interaction and, as such, mask activation of ATP hydrolysis as a result of CYPD ablation or displacement by cyclosporin A. As discussed in **Chapter 2.1**, in the presence of abundant P_i, ΔpH across the inner mitochondrial membrane is in the range of 0.11-0.15. Accordingly, since the pH of the experimental medium was 7.25, matrix pH in our hands was 7.39 ± 0.01. That is far from the pH 6.8 optimum of IF1. However, IF1 also binds to the F_O-F_1 ATP synthase at a pH higher than 6.8, promoting the dimerization of two synthase units [50] and thus modulating ATP synthesis [51]. Therefore, matrix pH was manipulated during the application of the uncoupler and ATP influx and efflux rates were recorded. The acidification produced by the uncoupler was either minimized by methylamine (60 μM) or exacerbated by nigericin (1 μM), as also described in one of my publications not closely related to this thesis [Vajda *et al.* 2009]. Matrix pH is shown in the white boxes within the gray bars, for the conditions indicated in the x-axis of Fig. 7. ATP consumption rates were not statistically significantly different between WT and CYPD KO mitochondria, in which the uncoupler-induced acidification has been altered by either methylamine or nigericin (n = 8, for all data bars). No differences were observed for ATP efflux rates in fully

DOI:10.14753/SE.2015.1713

polarized mitochondria (Fig. 7A). The effect of nigericin decreasing ATP efflux rate in mitochondria, even though it yielded a higher membrane potential (at the expense of ΔpH), is explained in [62]. Methylamine did not affect ΔΨm (not shown), although, in the concomitant presence of SF 6847, it decreased ATP consumption rates compared to the effect of SF 6847 alone (Fig. 7B). Nigericin also decreased ATP consumption rates (Fig. 7B).

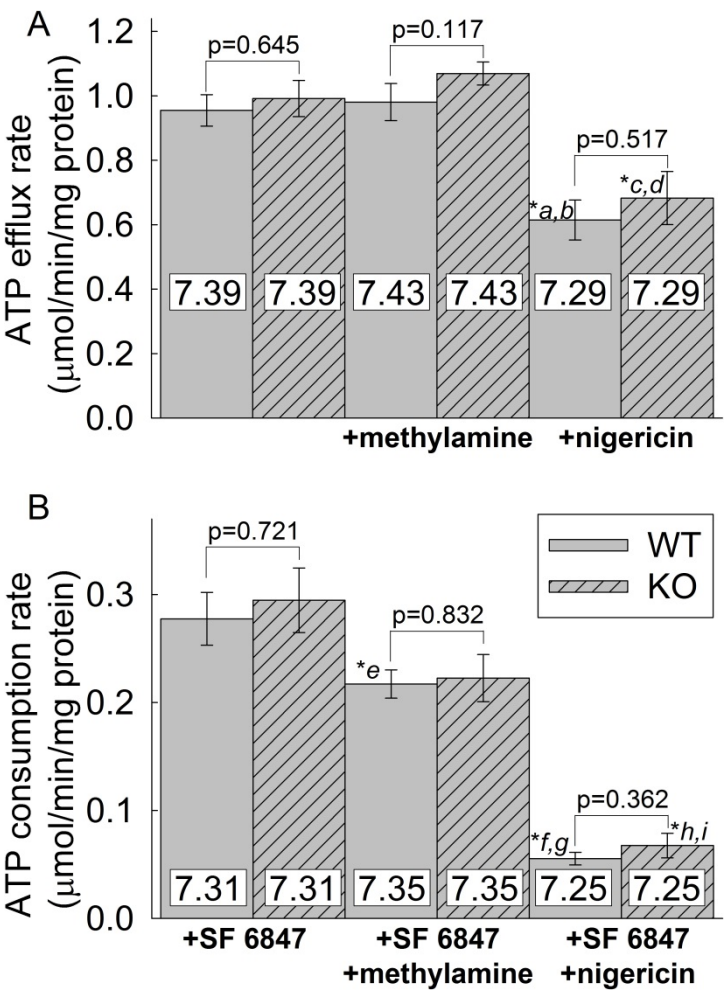

Figure 7. ATP efflux **(A)** and consumption **(B)** rates in WT and CYPD KO (striped bars) mitochondria as a function of matrix pH. Matrix pH is shown in the white box within each bar for the respective condition indicated on the x-axis. *a**, significantly different from WT control. *b**, significantly different from WT + methylamine. *c**, significantly different from KO control. *d**, significantly different from KO + methylamine. *e**, significantly different from WT + SF 6847. *f**, significantly different from WT + SF 6847. *g**, significantly different from WT + SF 6847 + methylamine. *h**, significantly different from KO + SF 6847. *i**, significantly different from KO + SF 6847 + methylamine. ←

5.1.4 CYPD decreases reverse H^+ pumping rate through the F_1-ATPase in partially energized intact mitochondria

To demonstrate the ability of CYPD to modulate F_O-F_1 ATP synthase-mediated ATP hydrolysis rates, intact mouse liver mitochondria were de-energized by substrate deprivation in the presence of the specific complex I inhibitor rotenone, followed by the

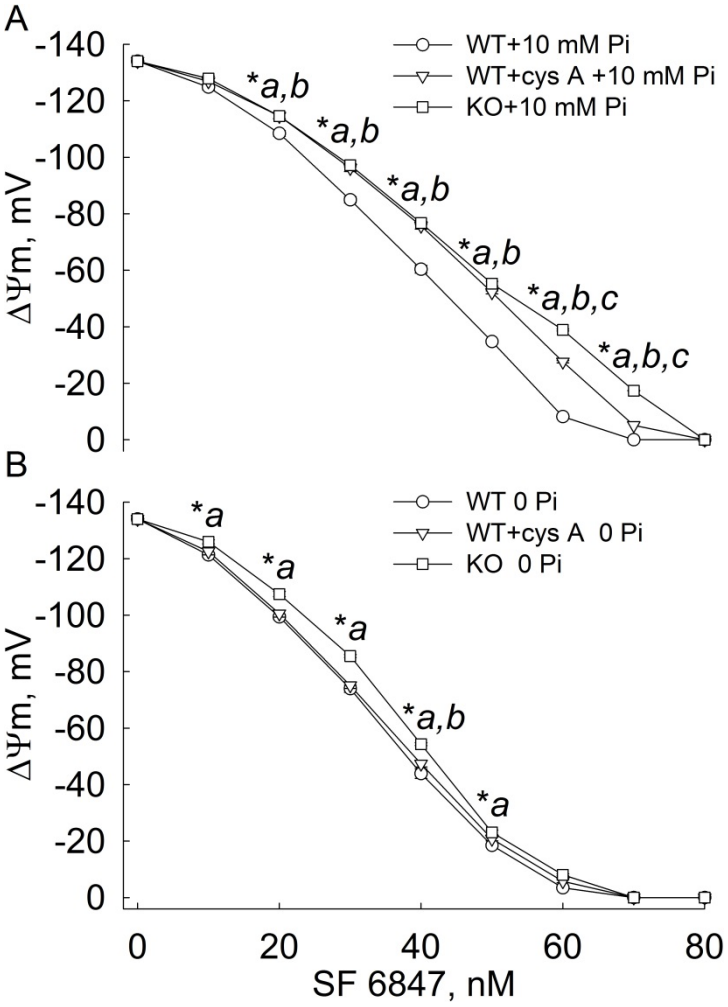

addition of 2 mM ATP. ΔΨm was recorded in order to compare WT ± cyclosporin A *vs.* CYPD KO mice. Under these conditions, and as a result of the sufficiently low ΔΨm values before the addition of ATP, ANT and F_O-F_1 ATP synthase operated in the reverse mode. Provision of exogenous ATP led to ATP influx to mitochondria, followed by its hydrolysis by the reversed F_O-F_1 ATP synthase, which in turn extruded protons to the extra-mitochondrial compartment, thus generating ΔΨm.

Figure 8. Effect of CYPD on F_1-ATPase-mediated H^+ pumping as a result of ATP hydrolysis in intact mitochondria. **(A)** Safranin O fluorescence values converted to mV in intact, de-energized WT and CYPD KO mitochondria by substrate deprivation and rotenone, and subsequently energized by the exogenous addition of 2 mM ATP (with 1 mM total $MgCl_2$ in the buffer), as a function of uncoupler dose (0-80 nM), in the presence of 10 mM P_i in the medium. **(B)** As in (A), although in the absence of P_i from the medium. *a, statistically significant, KO significantly different from WT; *b, statistically significant, WT + cyclosporin A significantly different from WT; *c, statistically significant, KO significantly different from WT + cyclosporin A (Tukey's test, $p < 0.05$). ↑

In this setting, the ability of the F_O-F_1 ATP synthase to pump protons out of the matrix represented the only component opposing the action of an uncoupler. On the basis of the study by Giorgio *et al.* [59] showing that the binding of CYPD to F_O-F_1 ATP synthase occurs only in the presence of P_i, the experiments were performed described below in the presence and absence of 10 mM P_i. As shown in Fig. 8A, in the presence of 10 mM P_i, mitochondria isolated from the livers of CYPD KO mice resisted

the uncoupler-induced depolarization (open quadrangles) more than those obtained from WT littermates (open circles). Cyclosporin A also exhibited a similar effect on WT mitochondria (open triangles) but not on KO mice (not shown). These results also attest to the fact that a possible acidification-mediated IF1 binding on F_O-F_1 ATP synthase, in turn masking the relief of inhibition by CYPD, could not account for the lack of effect on adenine nucleotide flux rates in intact mitochondria, as noted above. In the absence of exogenously added P_i, this effect was much less pronounced (Fig. 8B); however, during endogenous ATP hydrolysis in intact mitochondria, it is anticipated that there may be a significant production of P_i in the vicinity of the F_O-F_1 ATP synthase within the matrix.

5.2 The negative impact of α-ketoglutarate dehydrogenase complex deficiency on matrix substrate-level phosphorylation

The decline in α-ketoglutarate dehydrogenase complex (KGDHC) activity has been associated with neurodegeneration. Provision of succinyl-CoA by KGDHC is essential for generation of matrix ATP or GTP by substrate-level phosphorylation catalyzed by ADP- or GDP-forming succinate-CoA ligase. Experiments outlined in this chapter demonstrate ATP consumption in respiration-impaired mitochondria obtained from KGDHC-deficient transgenic mice. This was attributed to a shift in the reversal potential of the ANT (E_{rev_ANT}, see **Chapters 2.4-2.6**) toward more negative values due to diminished matrix substrate-level phosphorylation, which caused the translocase to reverse prematurely. Since both the expression and maximal enzymatic activity of SUCL were identical in transgenic and WT mice, decreased matrix substrate-level phosphorylation was due to diminished provision of succinyl-CoA. These results – along with the fact that mitochondria from WT mice respiring on substrates supporting substrate-level phosphorylation exhibited ~30% higher ADP-ATP exchange rates compared to KGDHC-deficient littermates – suggest that KGDHC-associated pathologies are a consequence of the inability of respiration-impaired mitochondria to rely on “in-house” mitochondrial ATP reserves.

5.2.1 Identifying mitochondria as extramitochondrial ATP consumers

To label a respiration-impaired mitochondrion as an extramitochondrial ATP consumer, its ΔΨm and matrix ATP/ADP ratio pair of values must be anywhere within the C space of Fig. 3 (for the figure and definition of the “C space”, see **Chapter 2.6**).

Due to the dynamism of ΔΨm, matrix ATP/ADP ratio, E_{rev_ATPase} and E_{rev_ANT} values that define the borders of the C space, it is experimentally exceptionally challenging to measure all these parameters and judge at any given time if a mitochondrion consumes extramitochondrial ATP. Instead, for this purpose it is much simpler and equally informative to examine the effect of ANT inhibitors on ΔΨm during ADP-induced respiration [5, 80], [Chinopoulos *et al.* 2010]. Adenine nucleotide exchange through the ANT is electrogenic, since 1 molecule of ATP^{4-} is exchanged for 1 molecule of ADP^{3-} (**Chapter 2.4**). In fully energized mitochondria, export of ATP in exchange for ADP costs ~25% of the total energy produced [216]. Therefore, during the forward mode of ANT, abolition of its operation by an ANT inhibitor, such as carboxyatractyloside (cATR) or bongkrekic acid (BKA), will lead to a gain of ΔΨm, whereas during the reverse mode of ANT, abolition of its operation by the inhibitor will lead to a loss of ΔΨm. This *biosensor test* (*i.e.*, the effect of cATR on isolated, or BKA on *in situ* mitochondria obtained from WT, $DLD^{+/-}$, $DLST^{+/-}$ and $DLD^{+/-}/DLST^{+/-}$ transgenic mice) was used to address the directionality of ANT during respiratory inhibition. Generalized scheme of this test is depicted in Fig. 9.

Figure 9. Illustrative graph of all safranin O-related experiments from all kinds of mitochondria and conditions (see Figs. 11-16, 21 and 22 in **Chapter 5.2**; Figs. 24, 25 and 27-31 in **Chapter 5.3**). In Figs. 21 and 22, BKA was used instead of cATR. ↓

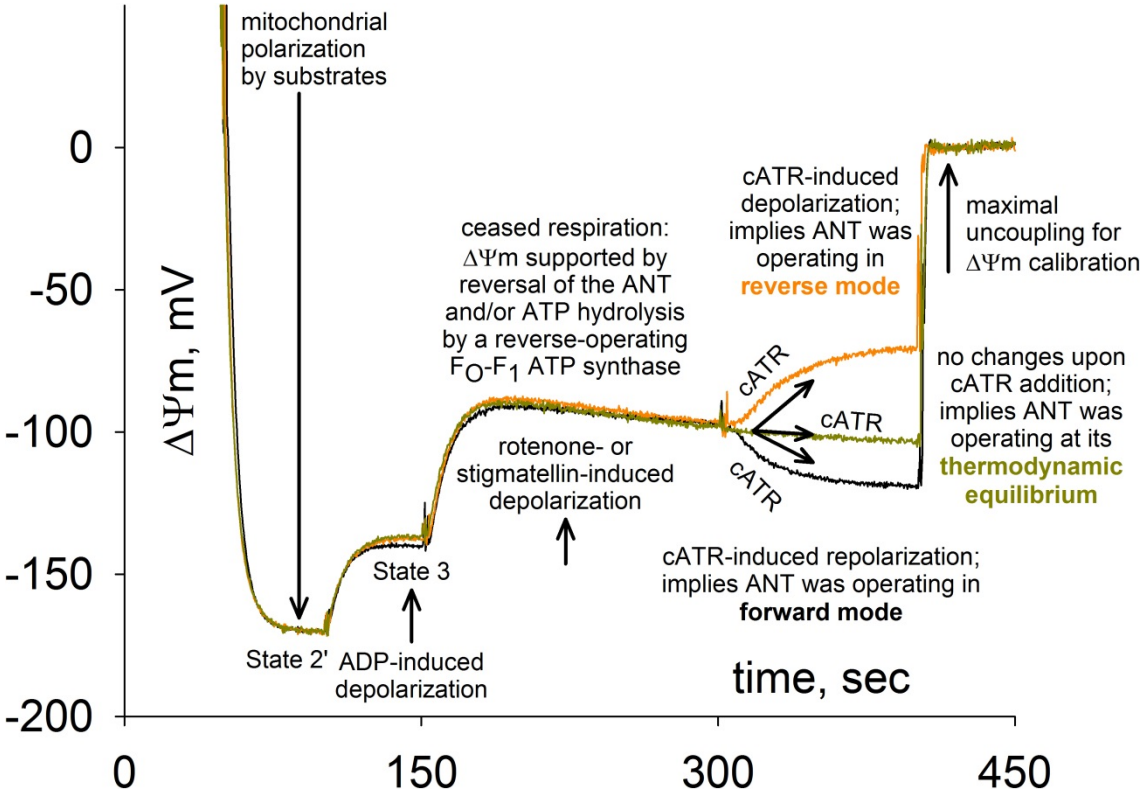

5.2.2 Categorization of substrates used for isolated mitochondria

Using isolated mitochondria enables to manipulate the substrates that the organelles respire on. The substrates used for these experiments and their positions in mitochondrial metabolism are highlighted in orange in Fig. 10. Substrates can be categorized to those that participate directly in the citric acid cycle (α-ketoglutarate, succinate, fumarate, and malate), and those that participate indirectly (pyruvate, aspartate, and glutamate) or not at all (β-hydroxybutyrate and acetoacetate). An alternative categorization is to those that support substrate-level phosphorylation *vs.* those that do not. Glutamate and α-ketoglutarate are the two substrates that support substrate-level phosphorylation to the greatest extent: glutamate could enter the citric acid cycle through conversion to α-ketoglutarate, and become converted by KGDHC to succinyl-CoA, which would in turn be converted to succinate plus ATP by SUCL. This amount of ATP could amend the matrix ATP pools produced by F_O-F_1 ATP synthase. Malate alone does not support substrate-level phosphorylation, but it assists in the entry of many substrates in mitochondria, including glutamate and α-ketoglutarate, thus indirectly supporting substrate-level phosphorylation. Pyruvate and aspartate alone or in combination support substrate-level phosphorylation very weakly. β-hydroxybutyrate and acetoacetate alone do not support substrate-level phosphorylation, but the latter leads to NAD^+ regeneration that could boost substrate-level phosphorylation supported by glutamate (or α-ketoglutarate). β-hydroxybutyrate would work in the exact opposite way; *i.e.*, it does not support substrate-level phosphorylation when glutamate or α-ketoglutarate is used because it competes for NAD^+ with KGDHC. This claim is validated later on, showing that addition of β-hydroxybutyrate to glutamate plus malate exacerbated the differences between cATR-induced changes in ΔΨm of WT and KGDHC-deficient mice during inhibition of complex I; by the same token, addition of acetoacetate to glutamate plus malate decreased the differences between cATR-induced changes in ΔΨm of the WT and the KGDHC-deficient mice during inhibition of complex I (see Figs. 11-16. and for further explanation, **Chapter 5.3**). Likewise, β-hydroxybutyrate or acetoacetate did not assist malate in boosting substrate-level phosphorylation. Succinate disfavors substrate-level phosphorylation, even in the presence of glutamate [Chinopoulos *et al.* 2011] (experimental settings in **Chapters 5.1.1** and **5.1.3**). The reason behind this is that succinate keeps the reversible SUCL

reaction towards succinyl-CoA plus ADP plus P_i formation. This is reflected by the fact that, in the presence of glutamate and succinate, α-ketoglutarate is primarily exported out of mitochondria [217], whereas succinate almost completely suppresses the oxidation of NAD^+-linked substrates, at least in the partially inhibited *State 3* and in *State 4* (the mitochondrial respiratory states has been defined in **Chapter 2.2**) [218]. Furthermore, succinate suppresses glutamate deamination [219]. Fumarate also disfavors substrate-level phosphorylation.

Figure 10. The citric acid cycle and related reactions. Substrates used for isolated mitochondria in this chapter are highlighted in orange. β-OHBDH: β-hydroxybutyrate dehydrogenase; PDH: pyruvate dehydrogenase; PC: pyruvate carboxylase; CS: citrate synthase; ASAT: aspartate aminotransferase; AC: aconitase; GDH: glutamate dehydrogenase; IDH: isocitrate dehydrogenase; KGDHC: α-ketoglutarate dehydrogenase complex; STK: succinate thiokinase (succinate-CoA ligase); SDH; succinate dehydrogenase; FSE: fumarase; MDH; malate dehydrogenase. The interconversion of isocitrate to α-ketoglutarate is depicted as reversible due to the concerted actions of the two mitochondrial IDH isoforms and a transhydrogenase: IDH2, which is $NADP^+$-dependent and reversible [164, 165, 220-222], and IDH3 [223], [224, 225] which is NAD^+-dependent, and considered irreversible [226], and their splice variants [227, 228]; interconversions of $NAD(P)^+$ and NAD(P)H would occur through the transhydrogenase [166, 229]. PC is slightly reversible [230]. Figure modified from [202], by permission. ↓

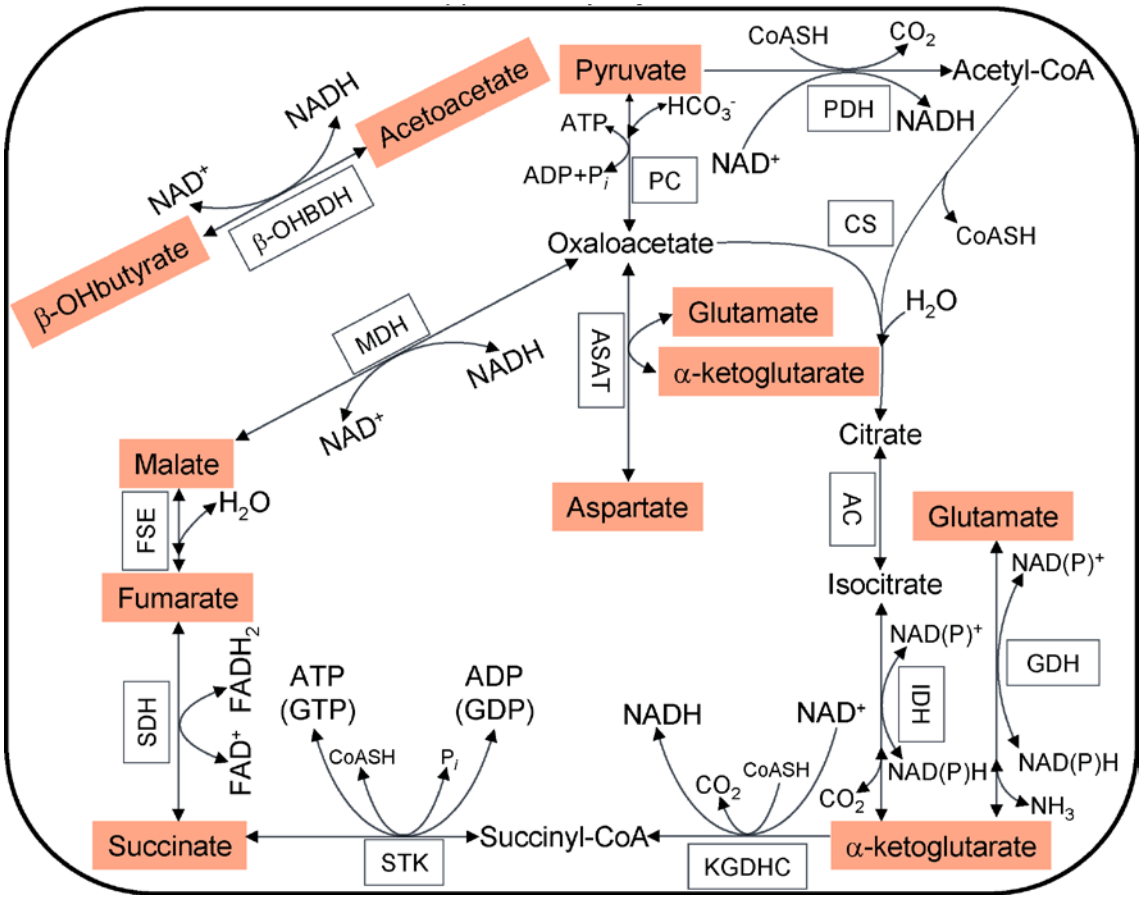

DOI:10.14753/SE.2015.1713

5.2.3 Effect of cATR on ΔΨm during respiratory inhibition in isolated mitochondria from WT, $DLD^{+/-}$, $DLST^{+/-}$ and $DLD^{+/-}/DLST^{+/-}$ mice

As shown in Figs. 11-16 ΔΨm was measured by safranin O fluorescence in isolated liver (Figs. 11-15) and Percoll-purified brain (Fig. 16) mitochondria obtained from WT, $DLD^{+/-}$, $DLST^{+/-}$ and $DLD^{+/-}/DLST^{+/-}$ mice and calibrated as detailed in **Chapter 4.5**. Many respiratory substrates and their combinations were used, detailed in the figures and in their legends. All substrates and their combinations were first examined in liver mitochondria where yields were high. Based on these results, specific substrates and their combinations were selected to investigate brain mitochondria where much lower yields are typically obtained. The sequence of additions was the following, which is identical for all panels: mitochondria were allowed to polarize, followed by the addition of 2 mM ADP, where indicated. ADP would depolarize mitochondria to a variable level depending on the substrate combinations that they respire upon (**Chapter 2.2**). After 50 sec during which a substantial amount of ADP has been converted to ATP, complex I or III was inhibited by rotenone (1 μM) or stigmatellin (1.2 μM), respectively. Data obtained by using stigmatellin were necessary to prove the point that addition of succinate (that would have been pointlessly used with rotenone since complex I is bypassed with this substrate) disfavors substrate-level phosphorylation, thus underlying the ANT reversals. However, with brain mitochondria that have aged on ice for no more than one hour, stigmatellin was causing a very large depolarization leading the organelles directly to the C space, even though they otherwise maintained respiratory control ratios for over 5 hours. Apparently, in mouse brain mitochondria some factor is rapidly consumed, that renders them exquisitely sensitive to inhibition by stigmatellin (**Chapter 5.3** elaborates on this particular subject). Inhibition of the respiratory chain will "clamp" ΔΨm in the -83 – -125 mV range, also depending on the substrate combinations. After an additional 150 sec, cATR (2 μM) or oligomycin (olgm, 10 μg/ml) was added. Towards the end of each experiment SF 6847 (1 μM) was added in order to completely depolarize mitochondria; this would assist in the calibration of the safranin O signal (**Chapter 2.2**). No swelling was observed under any circumstances (not shown, see supplementary material of Kiss *et al.* 2013), therefore the losses of ΔΨm were not due to opening of the permeability transition pore (PTP) [72].

In panels A-K, M-O, Q, S, U of Figs. 11 and 12, panels A, C, E, I, K, M-O, Q, S, U of Figs. 14 and 15, and panels A-J of Fig. 16, it is evident that addition of cATR to respiration-impaired mitochondria obtained from WT mice resulted in the gain of ΔΨm, indicating that the ANT was operating in forward mode, as implied by this *biosensor test*, elaborated in **Chapter 5.2.1**. On the other hand, addition of cATR to respiration-impaired mitochondria obtained from $DLD^{+/-}$, (panels A, H, K, S of Figs. 11 and 12, and panels C and G of Fig. 16), $DLST^{+/-}$ (panels A, G, I, N and Q of Figs. 14 and 15) and $DLD^{+/-}/DLST^{+/-}$ (panels A, B, D, E, H, K, M, N, Q, S of Figs. 11 and 12 and panels B and D of Fig. 16) mice resulted in the loss of ΔΨm, implying that the ANT was operating in reverse mode. Therefore, for the corresponding substrates, respiration-impaired mitochondria of $DLD^{+/-}$, $DLST^{+/-}$ and $DLD^{+/-}/DLST^{+/-}$ mice imported extra-mitochondrial ATP. Since E_{rev_ATPase} is always more negative than E_{rev_ANT}, imported ATP is subject to hydrolysis by F_O-F_1 ATP synthase, unless it is inhibited by IF1 (**Chapters 2.3**, **6.2** and **6.5**). However, addition of oligomycin (10 μg/ml) instead of cATR (trace "o" in panels E and F of Fig. 14 and panels M and N of Fig. 15) caused the ΔΨm to collapse, indicating that the F_O-F_1 ATP synthase was operating in reverse mode. Addition of succinate to any substrate combination in WT or KGDHC-deficient mice resulted in cATR-induced depolarization, attributed to the shifting of the succinate-CoA ligase equilibrium towards ATP consumption, as described in Chinopoulos *et al.* 2010 (not shown for brain, see Figs. 11, 12 and 14 for liver mitochondria: gray (for WT), dark red (for $DLD^{+/-}$), dark blue (for $DLST^{+/-}$) and dark green (for $DLD^{+/-}/DLST^{+/-}$) traces of panels B, D, F, H, J, N in Figs. 11 and 12 and panels B, F, H, J in Fig. 14). By the same token, addition of fumarate – a substrate that also disfavors substrate-level phosphorylation – to any other substrate combination, reverted the cATR-induced re- to a depolarization (implying ANT reversal), or exacerbated the extent of cATR-induced alteration of ΔΨm. This is shown in Fig. 13, all panels. Fumarate did not yield robust cATR-induced depolarizations as succinate did, probably because fumarate is also readily converted to malate, which was shown above to benefit substrate-level phosphorylation caused by other substrates. Note that the extent of mitochondrial membrane polarization of WT *vs.* transgenic mice mitochondria prior to the addition of cATR was nearly identical, with the exception of panels A, C, D, G, I, K, N of Figs. 14 and 15.

Results obtained using the cATR *biosensor test* shown in Figs. 11-16 in conjunction to the thermodynamic considerations mentioned in **Chapter 5.2.1** and shown in Fig. 9 imply that using substrate combinations supporting substrate-level phosphorylation in mitochondria obtained from KGDHC-deficient mice compared to those from WT littermates, either i) E_{rev_ANT} values were more negative, and/or ii) matrix ATP/ADP ratios were lower. Besides the function of the ANT, matrix ATP/ADP ratios are primarily (but not exclusively) affected by the reversible mechanisms producing or consuming ATP. In the mitochondrial matrix the two most significant contributors are the F_O-F_1 ATP synthase and the ADP-forming succinate-CoA ligase. The GDP-forming succinate-CoA ligase also contributes to the matrix ATP pools (see **Chapter 2.7**). The activity of the F_O-F_1 ATP synthase but not of succinate-CoA ligase strongly depends on $\Delta\Psi m$ [62, 88], [Chinopoulos *et al.* 2011]. ATP efflux and respiration rates from fully energized mitochondria of WT, $DLD^{+/-}$, $DLST^{+/-}$ and $DLD^{+/-}/DLST^{+/-}$ mice were therefore investigated for various substrates in the absence of confounding factors, such as respiratory inhibition that would lead to membrane depolarization.

Figure 11. Effect of carboxyatractyloside (cATR, 2 μM) on $\Delta\Psi m$ of mouse liver mitochondria of WT, $DLD^{+/-}$, or $DLD^{+/-}/DLST^{+/-}$ double-transgenic mice compromised at complex I or III by rotenone (1 μM) or stigmatellin (1.2 μM), respectively, in the presence of different respiratory substrate combinations. ADP (2 mM) was added where indicated. Substrate concentrations were: glutamate (glut, 5 mM), malate (mal, 5 mM), acetoacetate, (AcAc, 0.5 mM), β-hydroxybutyrate (bOH, 2 mM), α-ketoglutarate (a-Kg, 5 mM), succinate (succ, 5 mM). At the end of all experiments, 1 μM SF 6847 was added to achieve complete depolarization. ↓

DOI:10.14753/SE.2015.1713

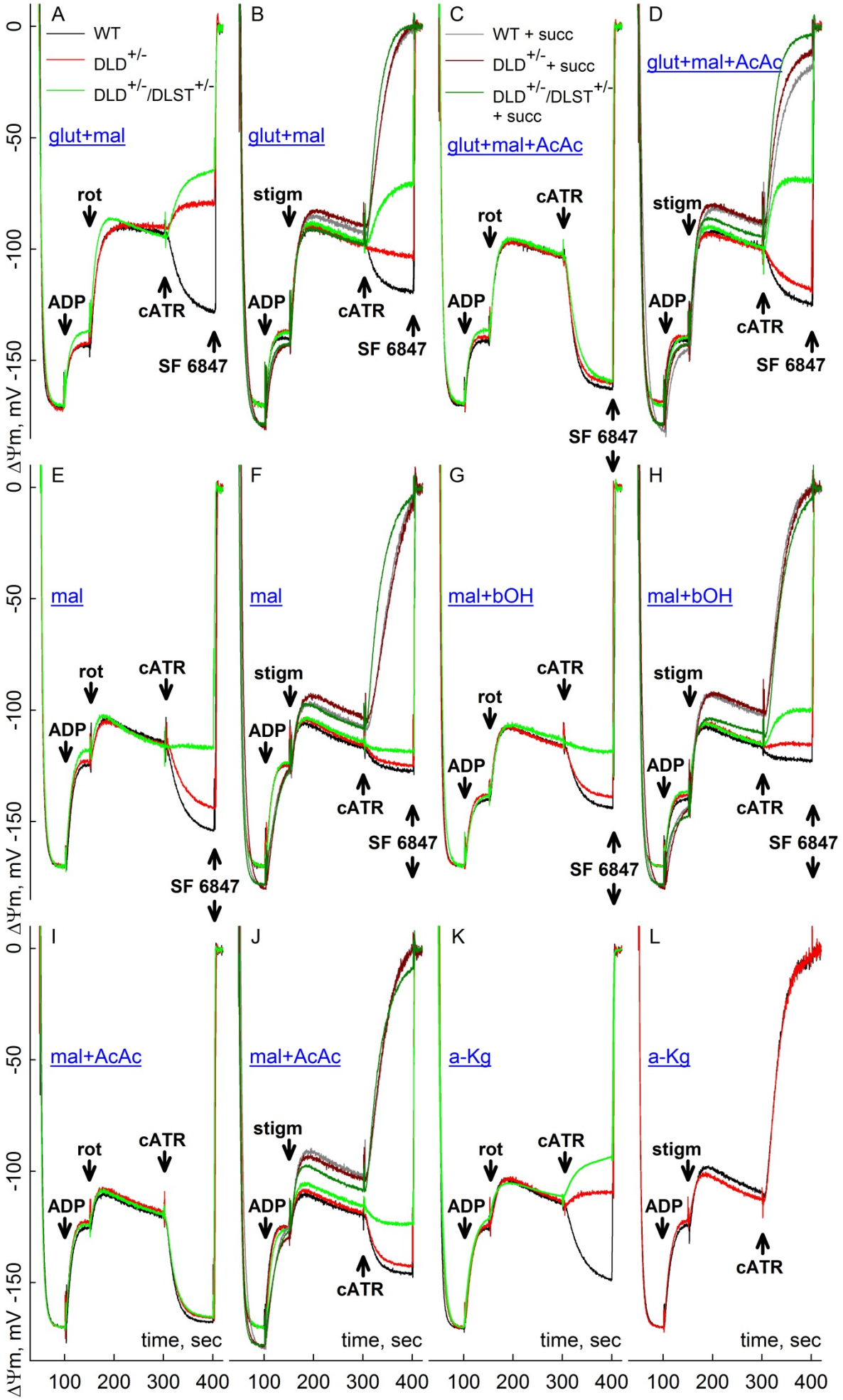

DOI:10.14753/SE.2015.1713

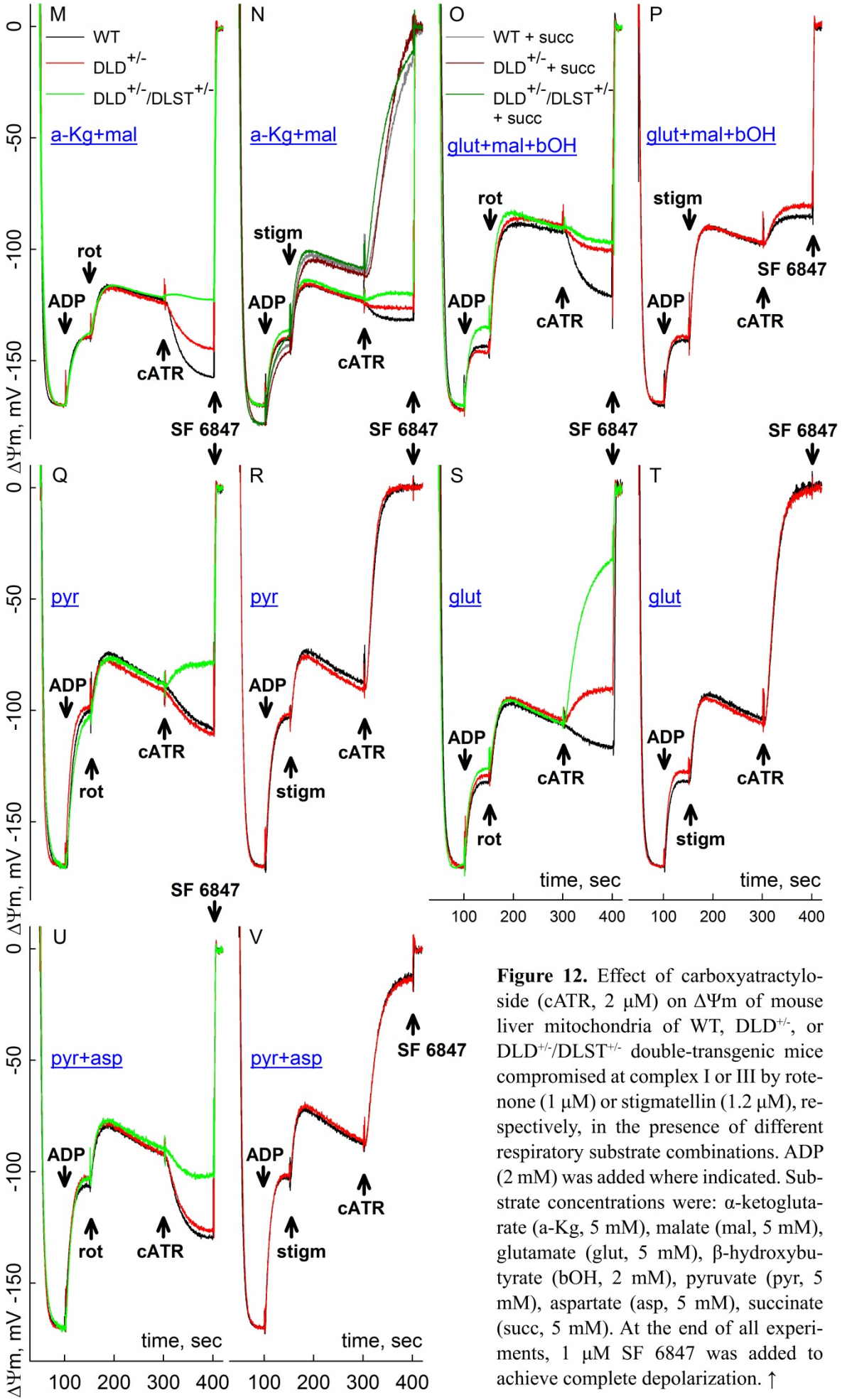

Figure 12. Effect of carboxyatractyloside (cATR, 2 μM) on ΔΨm of mouse liver mitochondria of WT, DLD$^{+/-}$, or DLD$^{+/-}$/DLST$^{+/-}$ double-transgenic mice compromised at complex I or III by rotenone (1 μM) or stigmatellin (1.2 μM), respectively, in the presence of different respiratory substrate combinations. ADP (2 mM) was added where indicated. Substrate concentrations were: α-ketoglutarate (a-Kg, 5 mM), malate (mal, 5 mM), glutamate (glut, 5 mM), β-hydroxybutyrate (bOH, 2 mM), pyruvate (pyr, 5 mM), aspartate (asp, 5 mM), succinate (succ, 5 mM). At the end of all experiments, 1 μM SF 6847 was added to achieve complete depolarization. ↑

Figure 13. Effect of carboxyatractyloside (cATR, 2 μM) on ΔΨm of mouse liver mitochondria of WT mice compromised at complex I or III by rotenone (1 μM) or stigmatellin (1.2 μM), respectively, in the presence of different substrate combinations. ADP (2 mM) was added where indicated. Substrate concentrations were: glutamate (glut, 5 mM), malate (mal, 5 mM), β-hydroxybutyrate (bOH, 2 mM), acetoacetate, (AcAc, 0.5 mM), α-ketoglutarate (a-Kg, 5 mM), fumarate (5 mM). At the end of all experiments, 1 μM SF 6847 was added to achieve complete depolarization. Cyan traces: fumarate was added in addition to the substrate combination written in each panel. ↓

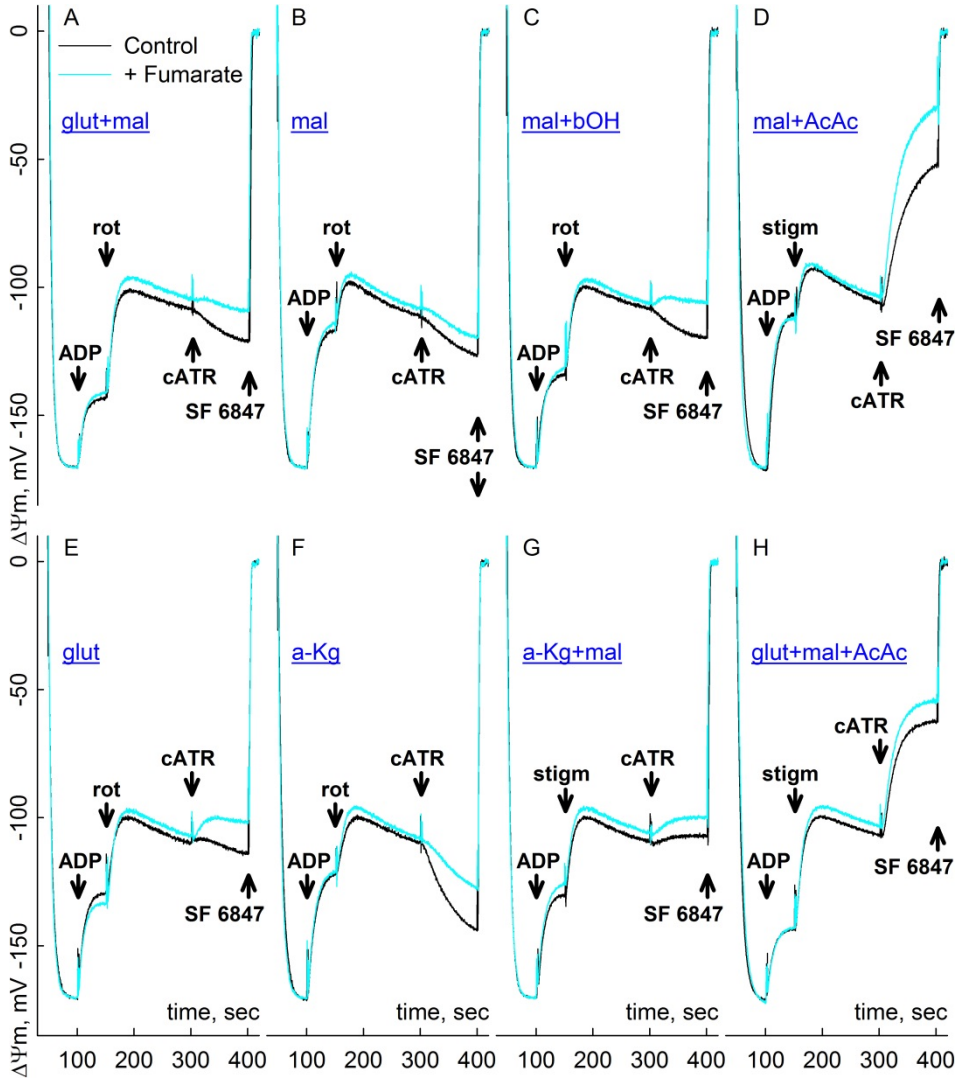

Figure 14. Effect of carboxyatractyloside (cATR, 2 μM) or oligomycin (olgm, 10 μg/ml, panels **E** and **F**, trace "o") on ΔΨm of mouse liver mitochondria of WT or DLST$^{+/-}$ transgenic mice compromised at complex I or III by rotenone (1 μM) or stigmatellin (1.2 μM), respectively, in the presence of different respiratory substrate combinations. ADP (2 mM) was added where indicated. Substrate concentrations were: glutamate (glut, 5 mM), malate (mal, 5 mM), acetoacetate, (AcAc, 0.5 mM), β-hydroxybutyrate (bOH, 2 mM), α-ketoglutarate (a-Kg, 5 mM), succinate (succ, 5 mM). At the end of all experiments, 1 μM SF 6847 was added to depolarize completely. ↓

DOI:10.14753/SE.2015.1713

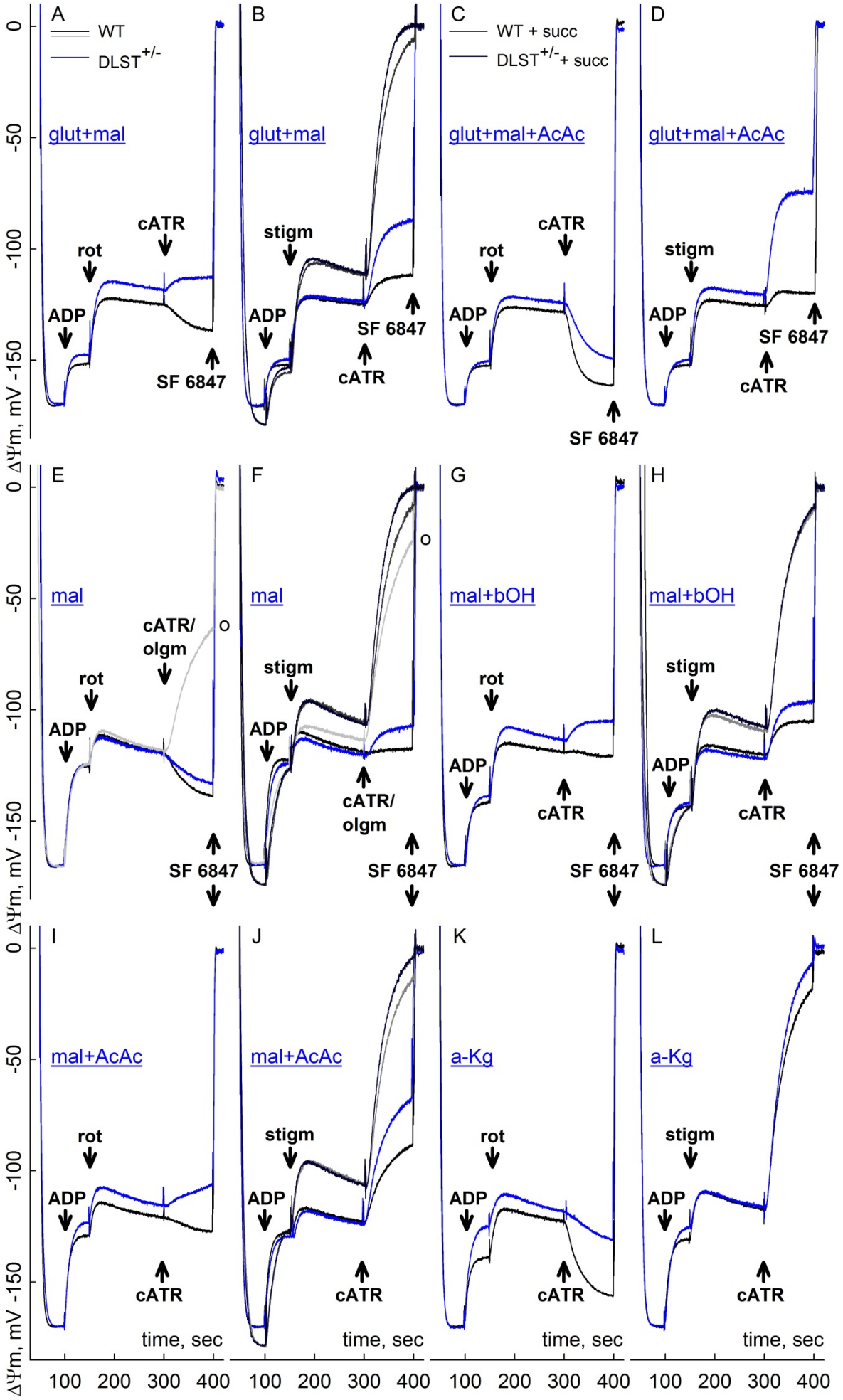

DOI:10.14753/SE.2015.1713

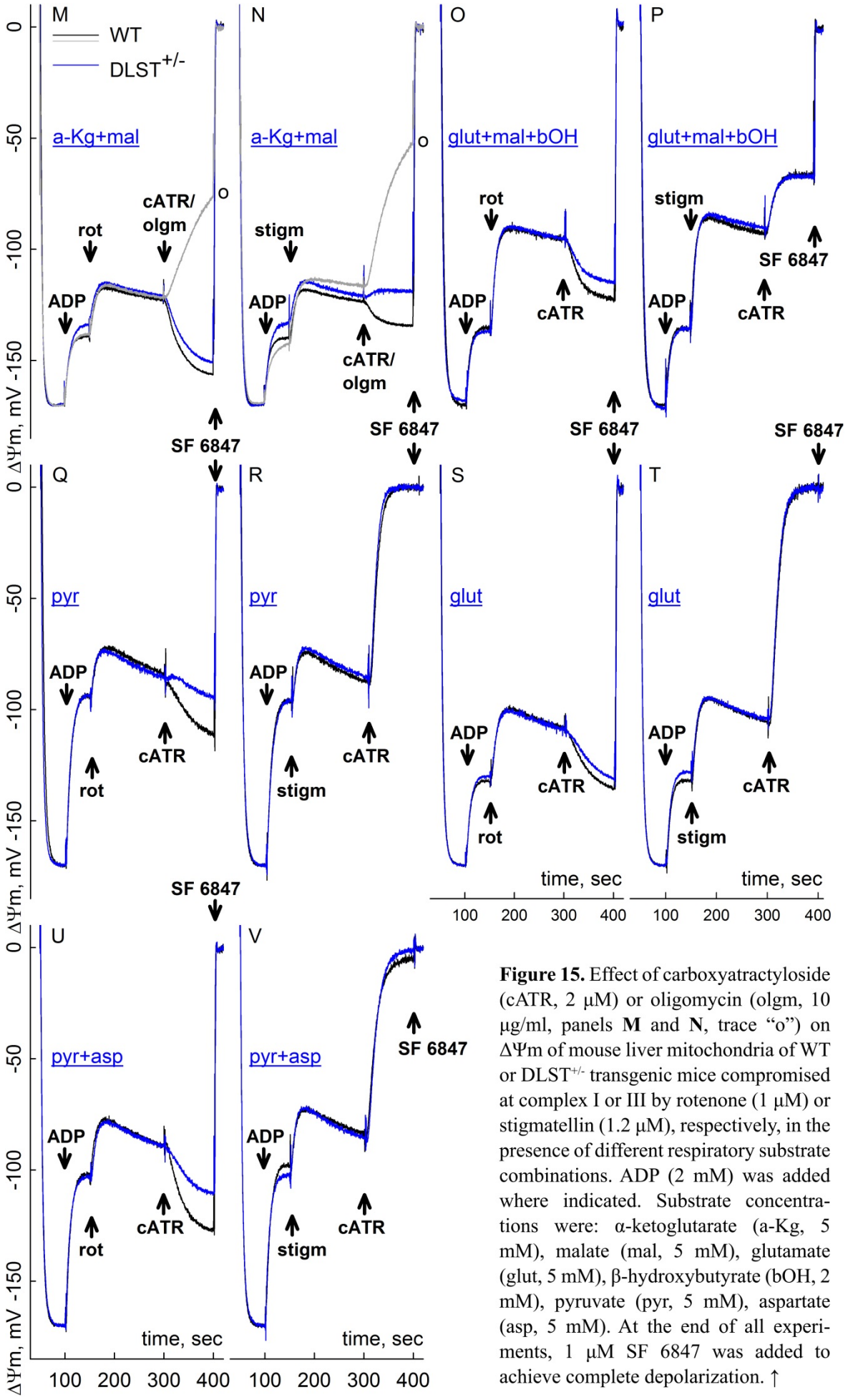

Figure 15. Effect of carboxyatractyloside (cATR, 2 μM) or oligomycin (olgm, 10 μg/ml, panels **M** and **N**, trace "o") on ΔΨm of mouse liver mitochondria of WT or DLST$^{+/-}$ transgenic mice compromised at complex I or III by rotenone (1 μM) or stigmatellin (1.2 μM), respectively, in the presence of different respiratory substrate combinations. ADP (2 mM) was added where indicated. Substrate concentrations were: α-ketoglutarate (a-Kg, 5 mM), malate (mal, 5 mM), glutamate (glut, 5 mM), β-hydroxybutyrate (bOH, 2 mM), pyruvate (pyr, 5 mM), aspartate (asp, 5 mM). At the end of all experiments, 1 μM SF 6847 was added to achieve complete depolarization. ↑

DOI:10.14753/SE.2015.1713

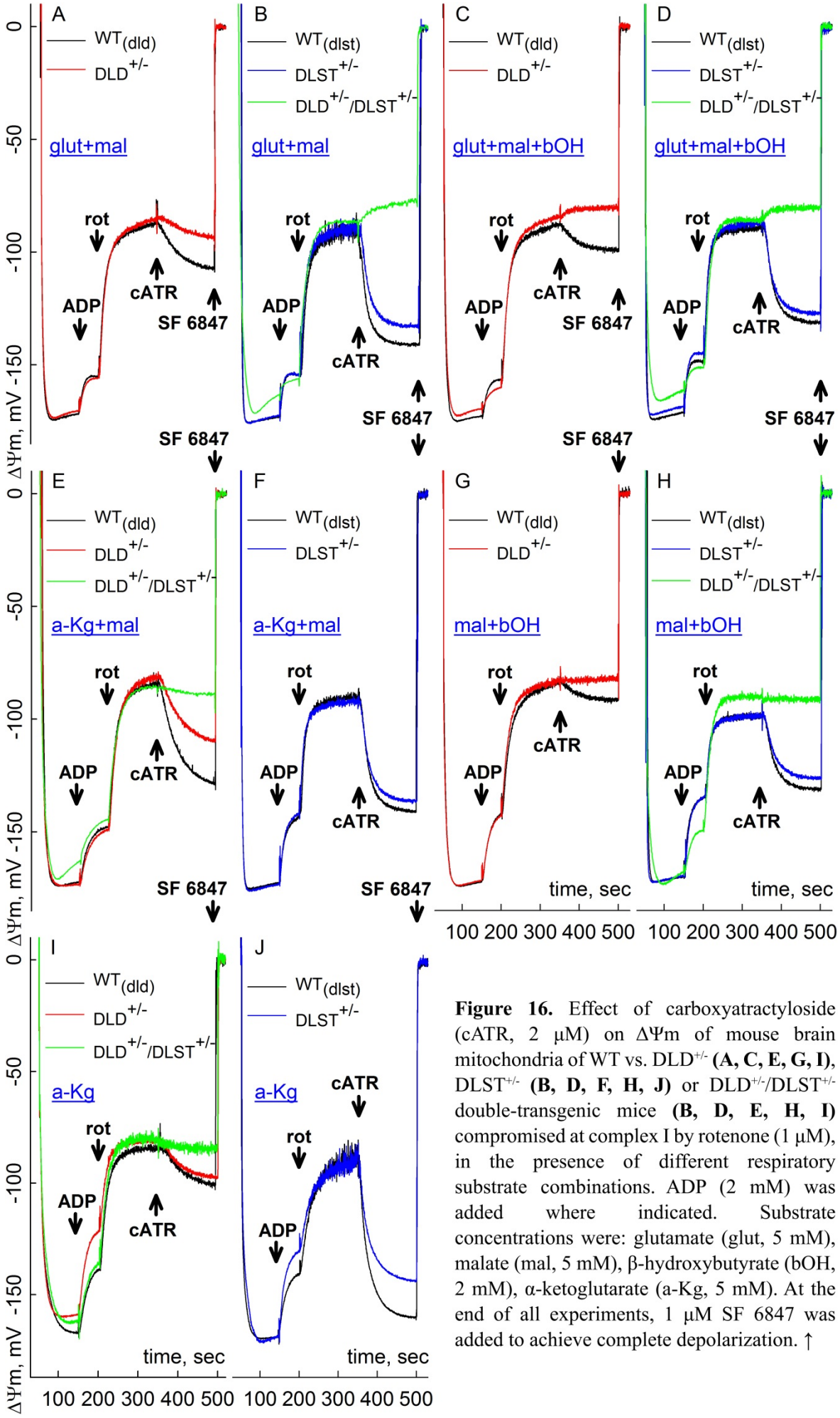

Figure 16. Effect of carboxyatractyloside (cATR, 2 μM) on ΔΨm of mouse brain mitochondria of WT vs. DLD$^{+/-}$ **(A, C, E, G, I)**, DLST$^{+/-}$ **(B, D, F, H, J)** or DLD$^{+/-}$/DLST$^{+/-}$ double-transgenic mice **(B, D, E, H, I)** compromised at complex I by rotenone (1 μM), in the presence of different respiratory substrate combinations. ADP (2 mM) was added where indicated. Substrate concentrations were: glutamate (glut, 5 mM), malate (mal, 5 mM), β-hydroxybutyrate (bOH, 2 mM), α-ketoglutarate (a-Kg, 5 mM). At the end of all experiments, 1 μM SF 6847 was added to achieve complete depolarization. ↑

In Fig. 16 and 17, the WT mice compared with the $DLD^{+/-}$ littermate mice are of C57BL/6 genetic background ($WT_{(dld)}$), while the WT mice compared with the $DLST^{+/-}$ littermate mice are of C57BL/6 and 129SV/EV hybrid genetic background ($WT_{(dlst)}$). $DLD^{+/-}/DLST^{+/-}$ double-transgenic mice are of either C57BL/6 only or C57BL/6 and 129SV/EV hybrid genetic background. Because of this background heterogeneity, the $\Delta\Psi m$ traces from $DLD^{+/-}/DLST^{+/-}$ double-transgenic mice are compared with either $WT_{(dld)}$ or $WT_{(dlst)}$ mice in order to match as littermates of the KGDHC-deficient mice.

5.2.4 ATP efflux rates in isolated mitochondria from WT, $DLD^{+/-}$, $DLST^{+/-}$ and $DLD^{+/-}/DLST^{+/-}$ mice

Fig. 17 shows ATP efflux rates of isolated liver (A, C) and Percoll-purified brain (B, D) mitochondria obtained from WT, $DLD^{+/-}$, $DLST^{+/-}$ and $DLD^{+/-}/DLST^{+/-}$ transgenic mice, calibrated as detailed in **Chapter 4.7**. While in $DLST^{+/-}$ liver and brain mitochondria all substrates and their combinations yielded lower ATP efflux rates than WT littermates – with the exception of malate plus β-hydroxybutyrate in brain mitochondria – (note the *p* values of j, k, l, m, n, o, p, q, r, s, t, u, v, w, x, y in the corresponding legend), in $DLD^{+/-}$ liver and brain mitochondria only some substrates and their combinations yielded lower ATP efflux rates than WT littermates (note the *p* values of a, b, c, d, e, f, g, h, i in the corresponding legend). Using some substrate combinations (note the *p* values of a, b, d, g, i in the corresponding legend) but not others mitochondria obtained from double-transgenic mice exhibited further reduced ATP efflux rates. From these results, the patern emerges that in KGDHC-deficient mitochondria, i) those substrates supporting substrate-level phosphorylation yielded lower ATP efflux rates than WT littermates; ii) for those substrates that support only weakly or not at all substrate-level phosphorylation, no statistically significant difference was found in the ATP efflux rates among WT and KGDHC-deficient mitochondria. However, α-ketoglutarate also did not show a statistically significant difference among WT and $DLD^{+/-}$, or not even among WT and $DLD^{+/-}/DLST^{+/-}$ liver mitochondria, nor for glutamate + malate + β-hydroxybutyrate for $DLD^{+/-}$ *vs.* WT brain mitochondria. The presence of acetoacetate or malate in most types of mitochondria was alleviating the differences conferred by the genetic manipulations on KGDHC subunits. Relevant to this, diseases characterized by deficiencies of KGDHC activity are associated by increases in malate dehydrogenase activity [153, 155, 231, 232].

DOI:10.14753/SE.2015.1713

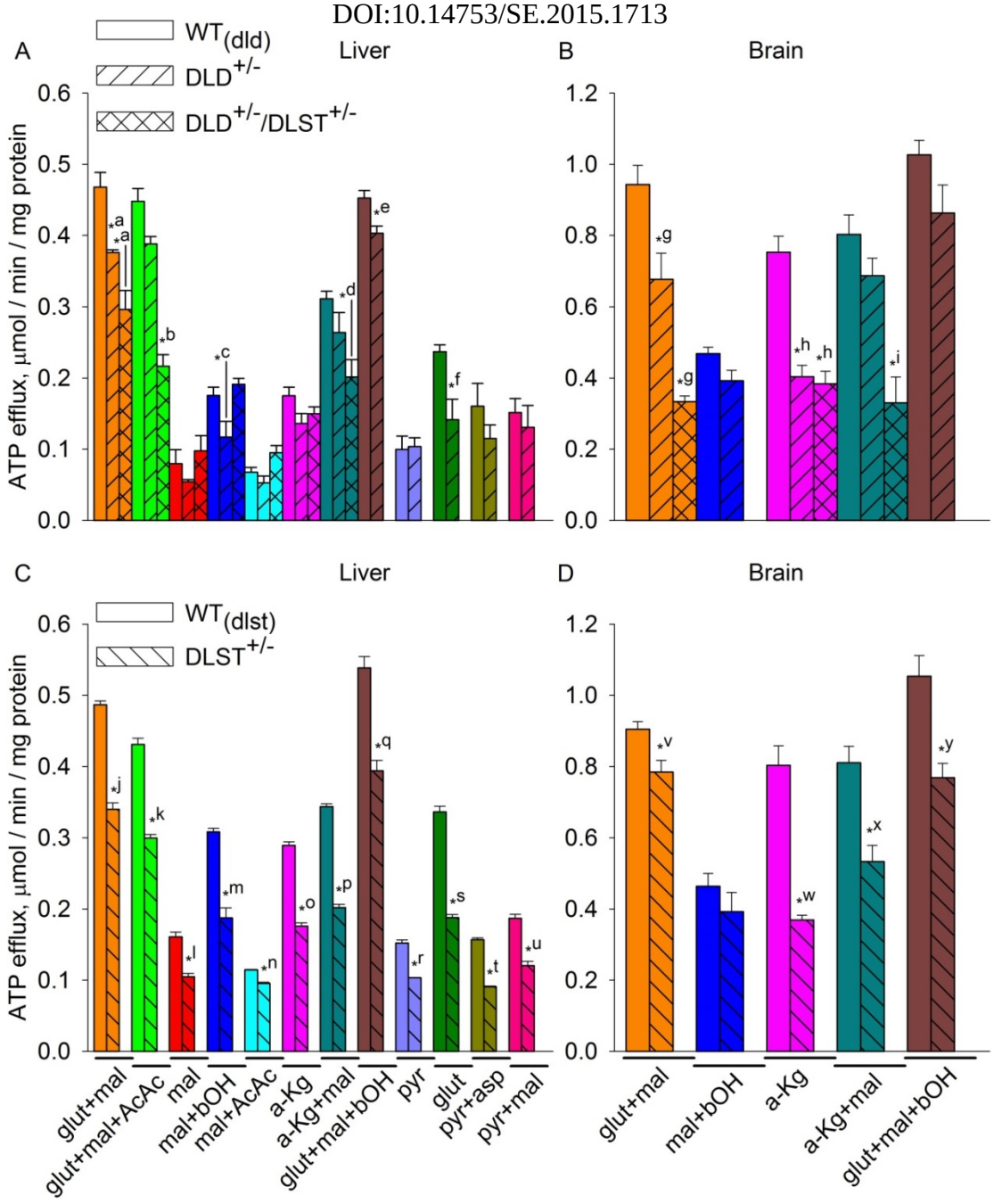

Figure 17. ATP efflux rates of isolated liver **(A, C)** and brain **(B, D)** mitochondria of WT, $DLD^{+/-}$, $DLST^{+/-}$ and $DLD^{+/-}$/ $DLST^{+/-}$ mice as a function of various substrate combinations. Panels **A** and **B** depict ATP efflux rates of WT *vs.* $DLD^{+/-}$ and $DLD^{+/-}$ /$DLST^{+/-}$ liver and brain mitochondria, respectively. Panels **C** and **D** depict ATP efflux rates of WT *vs.* $DLST^{+/-}$ liver and brain mitochondria, respectively. Substrate concentrations were: glutamate (glut, 5 mM), malate (mal, 5 mM), acetoacetate (AcAc, 0.5 mM), beta-hydroxybutyrate (bOH, 2 mM), α-ketoglutarate (a-Kg, 5 mM), pyruvate (pyr, 5 mM), aspartate (asp, 5 mM). *, statistically significant, $p < 0.05$ (Student's *t* test, if comparing two groups, 1-way ANOVA followed by Dunnett's test *post hoc* analysis if comparing three or more groups; control: results obtained from WT mice). *a $p = 0.001$; *b $p < 0.001$; *c $p = 0.015$; *d $p = 0.01$; *e $p = 0.022$; *f $p = 0.034$; *g $p < 0.001$; *h $p < 0.001$; *i $p = 0.001$; *j $p < 0.001$; *k $p < 0.001$; *l $p = 0.002$; *m $p = 0.001$; *n $p < 0.001$; *o $p < 0.001$; *p $p < 0.001$; *q $p = 0.003$; *r $p < 0.001$; *s $p < 0.001$; *t $p < 0.001$; *u $p = 0.001$; *v $p = 0.019$; *w $p = 0.001$; *x $p = 0.008$; *y $p = 0.014$. ↑

DOI:10.14753/SE.2015.1713

5.2.5 Respiration rates in isolated mitochondria from WT, $DLD^{+/-}$, $DLST^{+/-}$ and $DLD^{+/-}/DLST^{+/-}$ mice

To rule out the possibility that cATR-induced alterations in ΔΨm are due to membrane leaks, mitochondrial respiration (see **Chapter 2.2** for definitions of the respiratory steady states) were measured. Fig. 18 demonstrates such a representative measurement of mitochondrial oxigen consumption, performed and calibrated as detailed in **Chapter 4.8**. Respiration rates were measured during *State 2'*; *State 3* induced by a small bolus of ADP (0.1 mM); *State 4* (on phosphorylation of the entire amount of ADP); *State 3* reinduced by a large bolus of ADP (2 mM); *State 4* induced by cATR, and uncoupled respiration induced by SF 6847 (50 nM for brain and 170 nM for liver mitochondria). Experiments were performed for isolated liver and brain mitochondria from WT, $DLD^{+/-}$, $DLST^{+/-}$ and $DLD^{+/-}/DLST^{+/-}$ transgenic mice for all substrate combinations. Each substrate combination was repeated 4-6 times on independent occasions. Quantitative data in bar graph format are shown in Fig. 19 for liver and 20 for brain mitochondria. It is evident that in KGDHC-deficient mitochondria, several substrates and their combinations supporting substrate-level phosphorylation yielded lower respiration rates than WT littermates (glutamate + malate, glutamate + malate + acetoacetate, α-ketoglutarate, α-ketoglutarate + malate, glutamate + malate + β-hydroxybutyrate for liver and brain; glutamate for brain mitochondria only). From these results, the conclusion was drawn that mitochondria deficient in DLD and/or DLST subunit of KGDHC exhibited diminished respiration rates. For those substrates and their combinations that support only weakly substrate-level phosphorylation (malate, malate + β-hydroxybutyrate, malate + acetoacetate, pyruvate, pyruvate + aspartate), no difference was found in the respiration rates among WT and KGDHC-deficient mitochondria. These data are in congruence with the ATP efflux data shown in Fig. 17. Furthermore, *State 2'* respiration and *State 4* respiration (whether induced after phosphorylation of the entire bolus of ADP given or induced by cATR) was not statistically significantly different for any substrate combination among WT and KGDHC-deficient mice, arguing against a possible contribution from leaks to the changes in ΔΨm shown in Figs. 11-16.

DOI:10.14753/SE.2015.1713

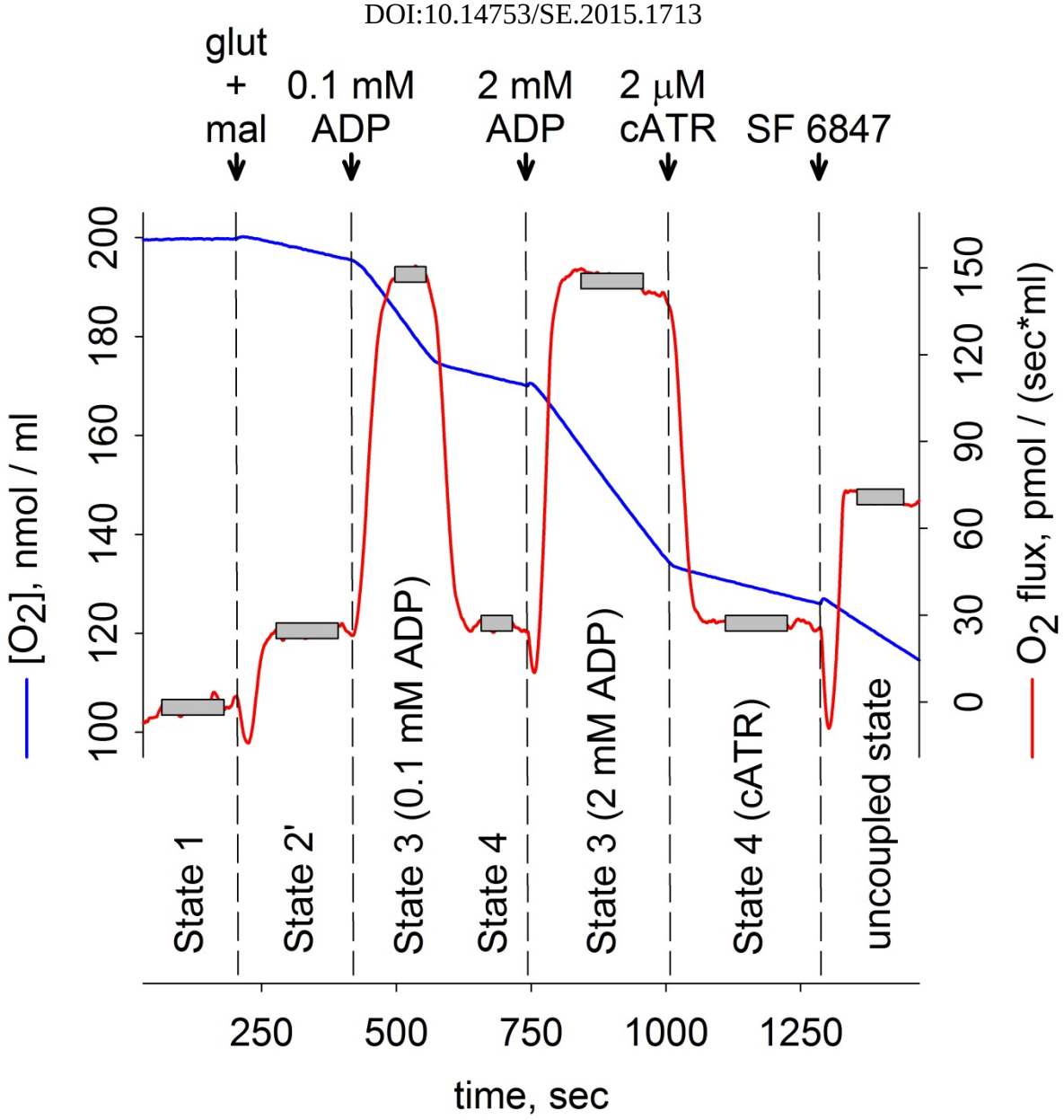

Figure 18. Representative graph of an oxygen consumption measurement in isolated brain mitochondria from WT mice respiring on glutamate (5 mM) plus malate (5 mM). Blue trace: oxygen concentration, in nmol/ml (μM). Red trace: oxygen flux (pmol/(sec*ml); negative time derivative of oxygen concentration). Gray boxes indicate the steady states of oxygen consumption rates. ↑

Figure 19. Respiration rates of isolated liver mitochondria from WT, $DLD^{+/-}$, $DLST^{+/-}$ and $DLD^{+/-}/DLST^{+/-}$ mice for various substrate combinations indicated in the panels. Substrate concentrations were: glutamate (glut, 5 mM), malate (mal, 5 mM), acetoacetate (AcAc, 0.5 mM), β-hydroxybutyrate (bOH, 2 mM), α-ketoglutarate (a-Kg, 5 mM), pyruvate (pyr, 5 mM), aspartate (asp, 5 mM). At the end of each experiment, 170 nM SF 6847 was administered. *, statistically significant, $p < 0.05$ one-way ANOVA followed by Dunnett's test *post hoc* analysis; control: results obtained from WT mice. *p* values were as follows: glut+mal: 0.1 mM ADP bolus: < 0.001, 2 mM ADP bolus: < 0.001; glut+mal+AcAc: 0.1 mM ADP bolus: 0.001, 2 mM ADP bolus: 0.016; α-Kg: 0.1 mM ADP bolus: 0.002, 2 mM ADP bolus: < 0.001; α-Kg+mal: 0.1 mM ADP bolus: < 0.001, 2 mM ADP bolus: < 0.001. *State 1* is not shown. ↓

DOI:10.14753/SE.2015.1713

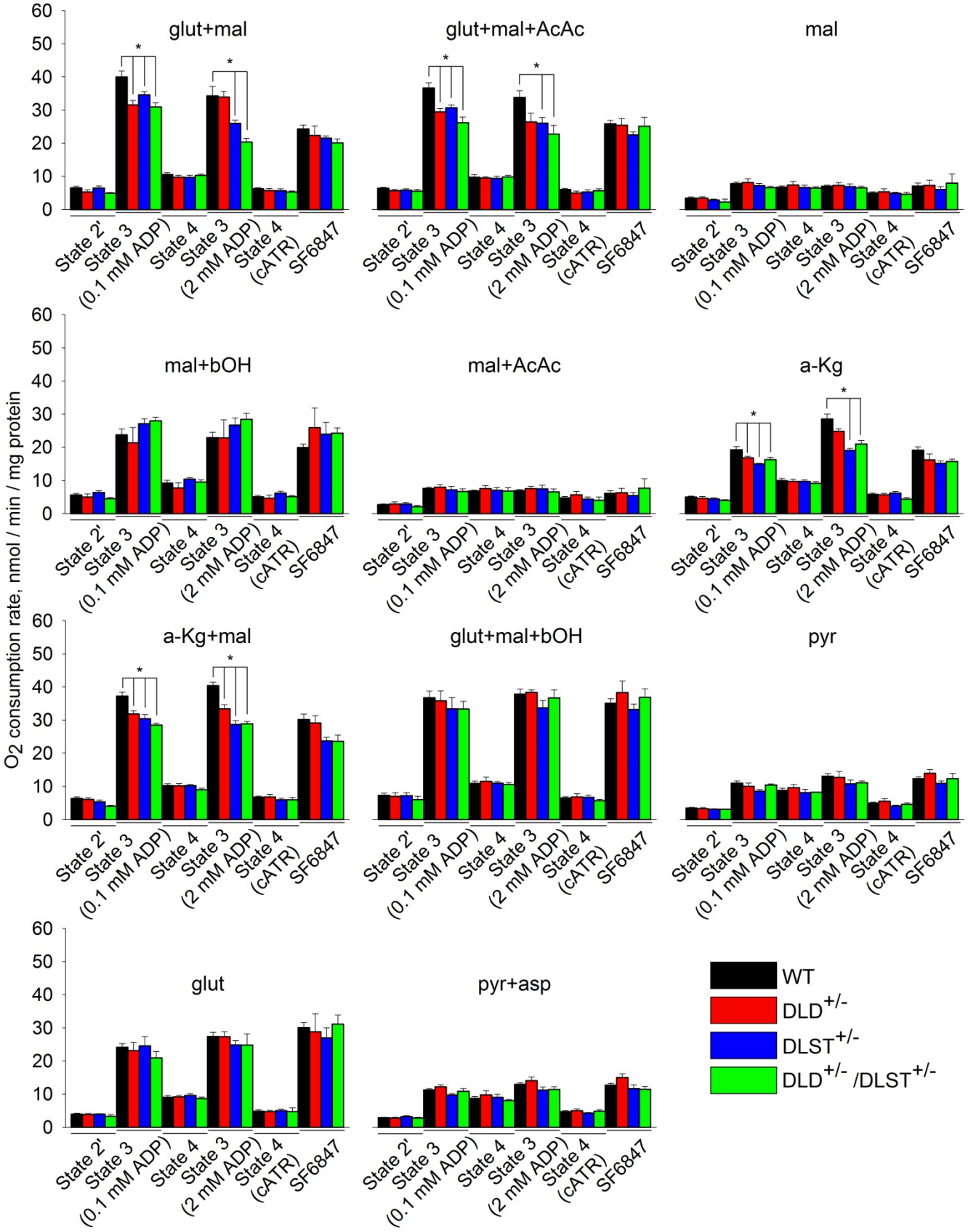

DOI:10.14753/SE.2015.1713

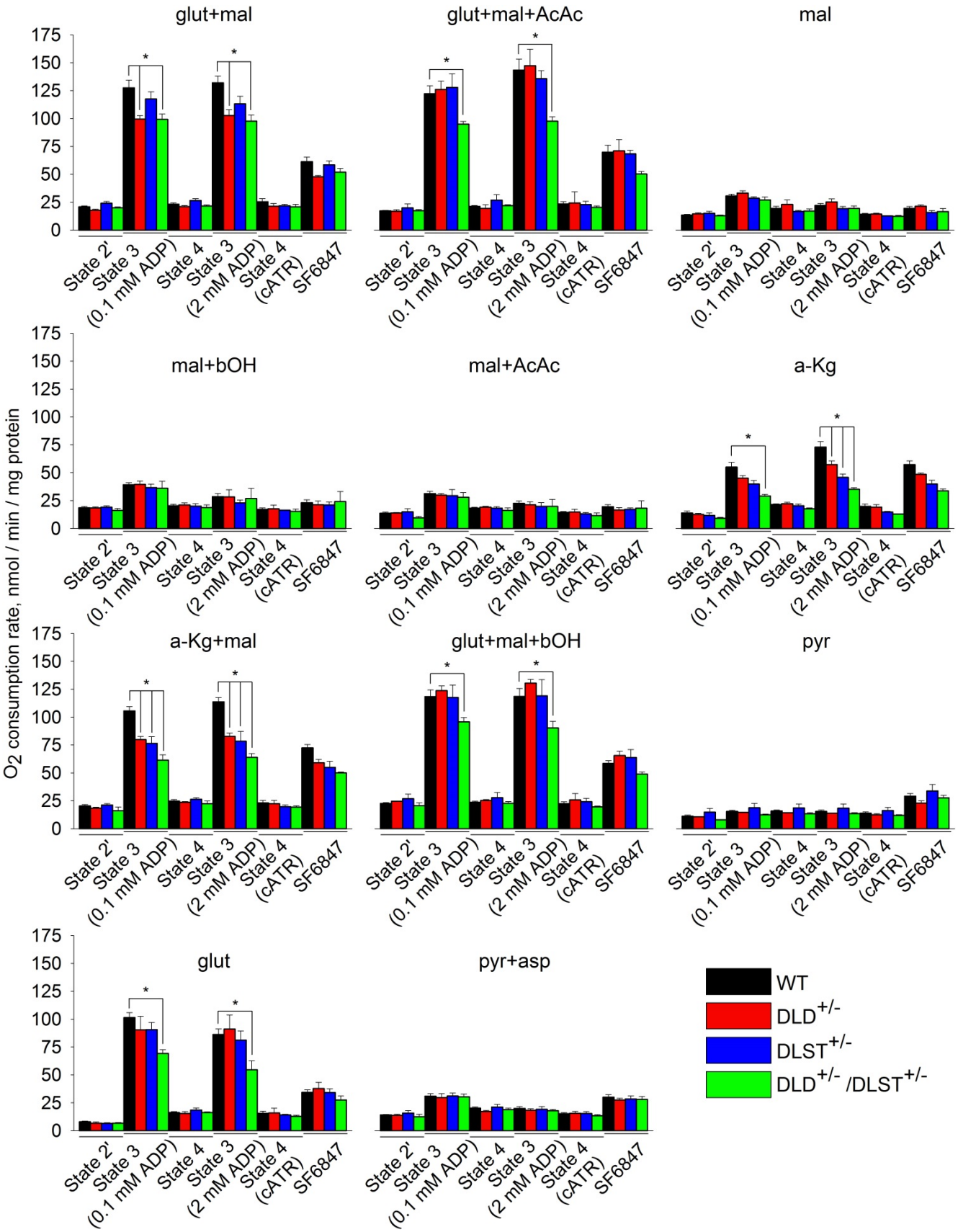

Figure 20. Respiration rates of isolated brain mitochondria from WT, $DLD^{+/-}$, $DLST^{+/-}$ and $DLD^{+/-}/DLST^{+/-}$ mice for various substrate combinations indicated in the panels. Substrate concentrations were: glutamate (glut, 5 mM), malate (mal, 5 mM), acetoacetate (AcAc, 0.5 mM), β-hydroxybutyrate (bOH, 2 mM), α-ketoglutarate (a-Kg, 5 mM), pyruvate (pyr, 5 mM), aspartate (asp, 5 mM). At the end of each experiment, 50 nM SF 6847 was administered. *, statistically significant, $p < 0.05$ one-way ANOVA followed by Dunnett's test *post hoc* analysis; control: results obtained from WT mice. *p* values were as follows: glut+mal: 0.1 mM ADP bolus, 0.002; glut+mal with 2 mM ADP bolus, 0.002; glut+mal+AcAc: 0.1 mM ADP bolus, 0.026; 2 mM ADP bolus, 0.006; α-Kg: 0.1 mM ADP bolus, 0.002; 2 mM ADP bolus, 0.001; α-Kg+mal: 0.1 mM ADP bolus, 0.001; 2 mM ADP bolus, 0.001; glut+mal+bOH: 0.1 mM ADP bolus, 0.021; 2 mM ADP bolus, 0.015; glut: 0.1 mM ADP bolus, 0.011; 2 mM ADP bolus, 0.022. *State 1* is not shown. ↑

5.2.6 Effect of BKA during respiratory inhibition of *in situ* synaptic and *in situ* neuronal somal mitochondria from WT and KGDHC-deficient mice

In the above experiments using isolated mitochondria, the choice of substrate was a controlled variable. It was therefore addressed whether the differences in ANT directionalities can be demonstrated among WT and KGDHC-deficient mice in *in situ* mitochondria, where substrate is an uncontrolled variable. For this purpose, isolated nerve terminals (synaptosomes) and cultured cortical neurons were prepared from the brains of WT, $DLD^{+/-}$, $DLST^{+/-}$ and $DLD^{+/-}/DLST^{+/-}$ mice. Also, BKA was used to inhibit the ANT instead of cATR, because the former can penetrate the plasma membrane, but the latter cannot. The same principles as detailed above apply here for identifying whether *in situ* synaptic mitochondria consume extramitochondrial ATP. The experimental protocol for the synaptosomes was the following (Fig. 21): synaptosomes were incubated in an extracellular-like buffer, supplemented with 15 mM glucose as the sole energy substrate, and ΔΨm was measured by TMRM fluorescence, as detailed in **Chapter 4.5**. Addition of SF 6847 at the end of each experiment, causing the complete collapse of ΔΨm, assisted in the normalization of the TMRM signal of all traces. In this *in situ* mitochondrial model, mitochondria respire, albeit submaximally [233]. Application of the complex I inhibitor, rotenone (1 μM; Fig. 21A, C) or the complex III inhibitor, stigmatellin (1.2 μM; Fig. 21B, D) caused a significant depolarization. Subsequent addition of oligomycin (10 μg/ml; Fig. 21; gray traces) caused a nearly complete collapse of ΔΨm, implying that *in situ* mitochondria relied on ATP hydrolysis by the F_O-F_1 ATP synthase. However, addition of BKA instead of oligomycin led to a robust repolarization in WT, $DLD^{+/-}$ and $DLST^{+/-}$ mice (Fig. 21A,

C; black, red and blue traces), implying that the ANT was still operating in the forward mode. Only in synaptosomes prepared from $DLD^{+/-}/DLST^{+/-}$ double-transgenic mice did BKA cause almost no repolarization (Fig. 21C; green trace), followed by a delayed minor depolarization. This implied that in double-transgenic animals, net adenine nucleotide flux through the ANT of rotenone-treated *in situ* synaptic mitochondria is near zero, and perhaps importing minor amounts of synaptoplasmic ATP into the matrix. Synaptosomes of WT mice inhibited by stigmatellin did not exhibit BKA-induced repolarization (Fig. 21B, D; black traces), and neither did those obtained from $DLD^{+/-}$, $DLST^{+/-}$ and $DLD^{+/-}/DLST^{+/-}$ mice (Fig. 21B, D; red, blue and green traces). It must be emphasized that KGDHC determinations from synaptosomal preparations (see Fig. 23) also involve enzymes from contaminating isolated mitochondria, the extent of which cannot be reliably estimated from the various transgenic mouse colonies. Therefore, the results obtained from the TMRM measurements of *in situ* mitochondria from the isolated nerve terminals cannot be reliably correlated to the extent of maximal KGDHC activity from the exact same mitochondria.

Results obtained from cultured cortical neurons are shown in Fig. 22. Neurons of $DLD^{+/-}$ *vs.* WT mice are compared in Fig. 22A, B; neurons of $DLST^{+/-}$ *vs.* WT mice in Fig. 22C, D. For all panels, the experimental paradigm was similar to that applied for synaptosomes. Cultures were bathed in an extracellular-like buffer, supplemented with 15 mM glucose as the sole substrate, and $\Delta\Psi m$ was measured by TMRM fluorescence (see **Chapters 4.5** and **4.6**). Addition of SF 6847 at the end of each experiment, causing the complete collapse of $\Delta\Psi m$, assisted in the normalization of the TMRM signal of all traces. Rotenone (1 μM) or stigmatellin (1.2 μM) was applied where indicated to inhibit *in situ* mitochondrial respiration, causing a significant depolarization. Subsequent addition of oligomycin (10 μg/ml) caused a nearly complete collapse of $\Delta\Psi m$ (Fig. 22; gray traces), implying that respiration-impaired *in situ* mitochondria relied on ATP hydrolysis by the F_O-F_1 ATP synthase. However, when *in situ* mitochondria were inhibited by rotenone, subsequent addition of BKA instead of oligomycin led to a repolarization in WT cultures (Fig. 22A, C; black traces), unlike in cultures obtained from $DLD^{+/-}$ and $DLST^{+/-}$ mice where a depolarization was observed (Fig. 22A, C; red and blue traces). This implied that respiration-impaired *in situ* neuronal somal mitochondria of $DLD^{+/-}$ and $DLST^{+/-}$ mice were consuming extramitochondrial ATP.

Application of stigmatellin (1.2 μM) instead of rotenone caused a large depolarization, and subsequent addition of BKA in either WT or transgenic mice neurons did not confer any repolarization (Fig. 22B, D; black, red and blue traces). The results obtained from *in situ* somal neuronal mitochondria using stigmatellin are supported by results obtained from Percoll-purified mitochondria (which consist of both somal neuronal and astrocytic mitochondria), where a very large depolarization was observed (not shown).

Figure 21. Effect of BKA and oligomycin on the rotenone- or stigmatellin-evoked depolarization of ΔΨm in isolated nerve terminals of WT *vs.* $DLD^{+/-}$ mice **(A, B)**, or WT *vs.* $DLST^{+/-}$ **(C, D)** or $DLD^{+/-}/DLST^{+/-}$ mice **(B, C)**. ΔΨm was followed using the potentiometric probe TMRM. Concentrations: BKA, 20 μM; oligomycin (olgm), 10 μg/ml; rotenone (rot), 1 μM; stigmatellin (stigm), 1.2 μM. At the end of each experiment, 1 μM SF 6847 was added to achieve complete depolarization. ↓

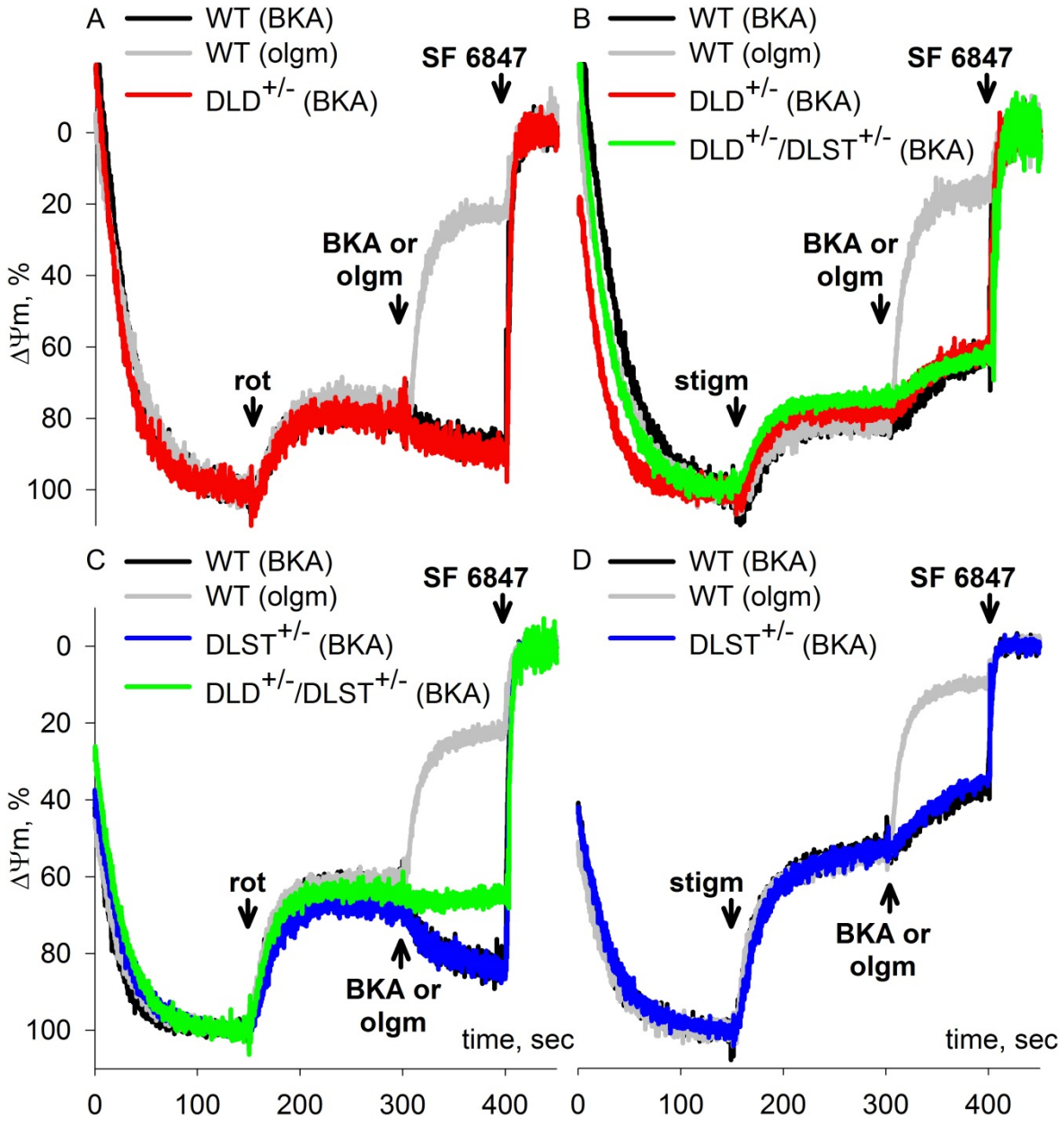

DOI:10.14753/SE.2015.1713

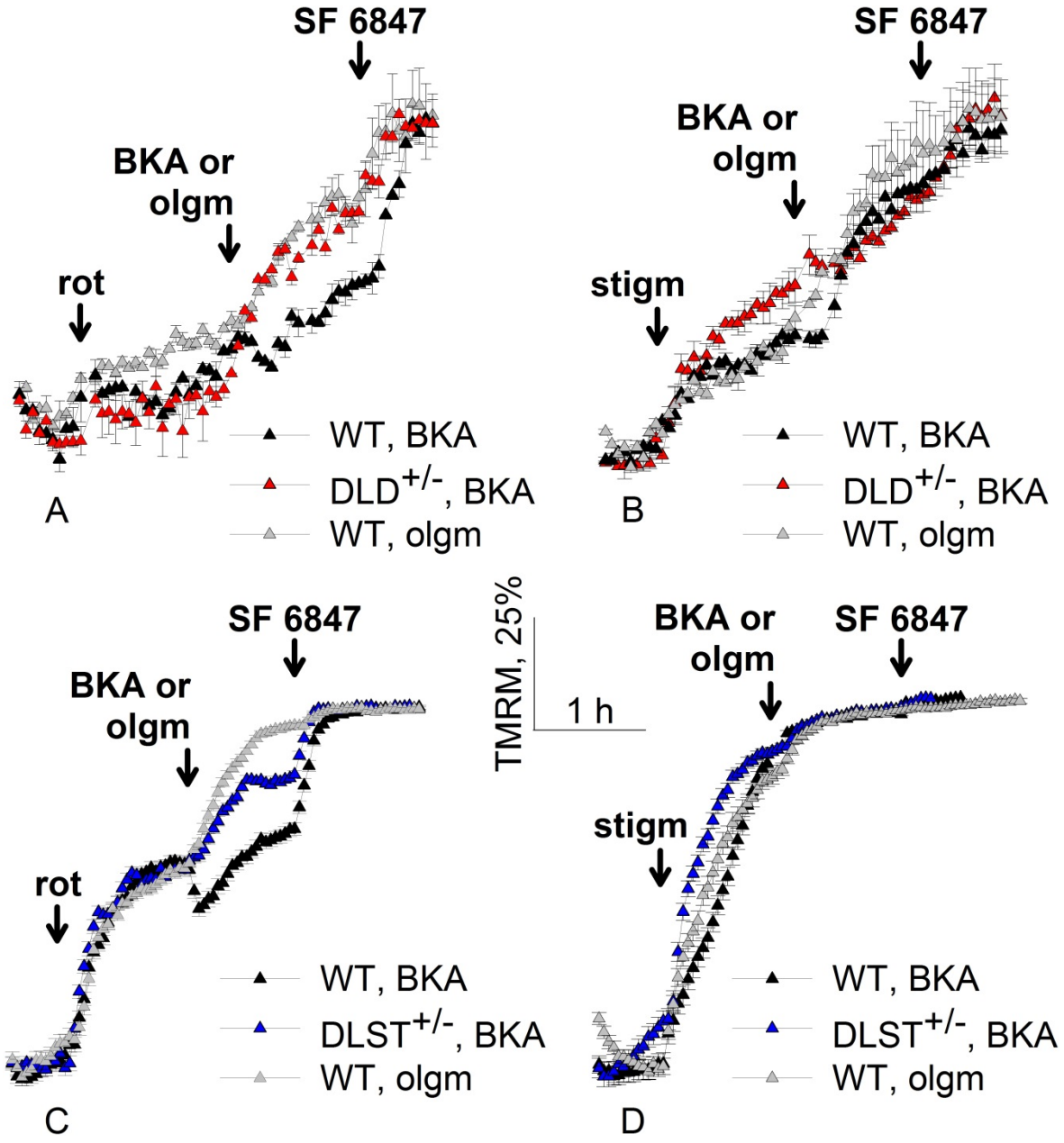

Figure 22. Effect of BKA and oligomycin (olgm, gray triangles) on the rotenone- or stigmatellin-evoked depolarization of ΔΨm in cultured mouse cortical neurons of WT (black triangles) *vs.* $DLD^{+/-}$ (red triangles) mice **(A, B)**, or WT *vs.* $DLST^{+/-}$ (blue triangles) mice **(C, D)**. ΔΨm was followed in intact cells with epifluorescence **(A, B)** or confocal **(C, D)** microscopy using the potentiometric probe TMRM. Concentrations: BKA, 20 μM; oligomycin (olgm), 10 μg/ml; rotenone (rot), 1 μM; stigmatellin (stigm), 1.2 μM. Data were pooled from 13 cell culture preparations. Data points obtained by epifluorescent imaging represent means ± SEM of 2 view fields/well containing 50-60 neurons/condition. Data points obtained by confocal imaging represent means ± SEM of 3 view fields/well containing 90-120 neurons/condition. At the end of each experiment, 5 μM SF 6847 was added to achieve complete depolarization. ↑

5.2.7 KGDHC and SUCL maximal activities in tissues from WT and KGDHC-deficient mice

SUCL has been reported to coprecipitate with KGDHC [234]; therefore, alterations in KGDHC due to genetic manipulations could have an effect also on SUCL (KGDHC and SUCL have been characterized in **Chapters 2.10** and **2.7**, respectively). To address this possibility, KGDHC activity and ATP- and GTP-forming activities of the two SUCL isoforms were measured in isolated liver and brain mitochondria and synaptosomes obtained from WT and transgenic mice, as well as immunoreactivities of all three subunits of SUCL. Due to limitations on the available tissue (*i.e.*, neurons from one pup brain were sufficient to cover a single Lab-Tek chamber), it was not possible to measure KGDHC and SUCL activities from cultured neurons. Results on KGDHC activities are shown in Fig. 23A (isolated brain mitochondria), C (synaptosomes), E (isolated liver mitochondria). Immunoreactivities of the subunits SUCLG1, SUCLG2, and SUCLA2 from the same tissues are shown in Fig. 23F, G. As shown in Fig. 23A and consistent with previous reports [156, 162], KGDHC activity of $DLD^{+/-}$ and $DLST^{+/-}$ brain and liver mitochondria was reduced by 20-48%, compared to WT littermates. KGDHC activity of double-transgenic $DLD^{+/-}/DLST^{+/-}$ brain and liver isolated mitochondria was reduced by 62 and 50%, respectively. On the contrary, ATP- and GTP-forming maximal activities of the two SUCL isoforms were not different between WT and transgenic mice (Fig. 23B, D). These data are in good agreement with the findings regarding immunoreactivities of the subunits of the SUCL enzyme, showing no differences between WT and any KGDHC-deficient mice (Fig. 23F, G). These results strongly suggest that the effect of genetic manipulations of KGDHC on matrix substrate-level phosphorylation is solely due to decreased provision of succinyl-CoA.

Figure 23. Enzymatic activities of KGDHC and SUCL and immuno-reactivities of the subunits of the latter enzyme in isolated liver and brain mitochondria and synaptosomes. **(A, C, E)** KGDHC activities of isolated brain mitochondria **(A)**, synaptosomes **(C)**, and isolated liver mitochondria **(E)** of WT, $DLST^{+/-}$, $DLD^{+/-}$ and $DLD^{+/-}/DLST^{+/-}$ transgenic mice. * $p < 0.05$; 1-way ANOVA followed by Dunnett's test *post hoc* analysis. **(B, D)** SUCL activities (ATP- and GTP-forming) of isolated liver and brain mitochondria of WT *vs.* $DLD^{+/-}$ **(B)** and WT *vs.* $DLST^{+/-}$ mice **(D)**. **(F, G)** Immunoreactivities of SUCLG1, SUCLG2, SUCLA2 subunits of succinate-CoA ligase; CYPD; and MnSOD of isolated brain and liver mitochondria **(F)** and synaptosomes **(G)** of WT, $DLD^{+/-}$, $DLST^{+/-}$ and $DLD^{+/-}/DLST^{+/-}$ mice. ↓

DOI:10.14753/SE.2015.1713

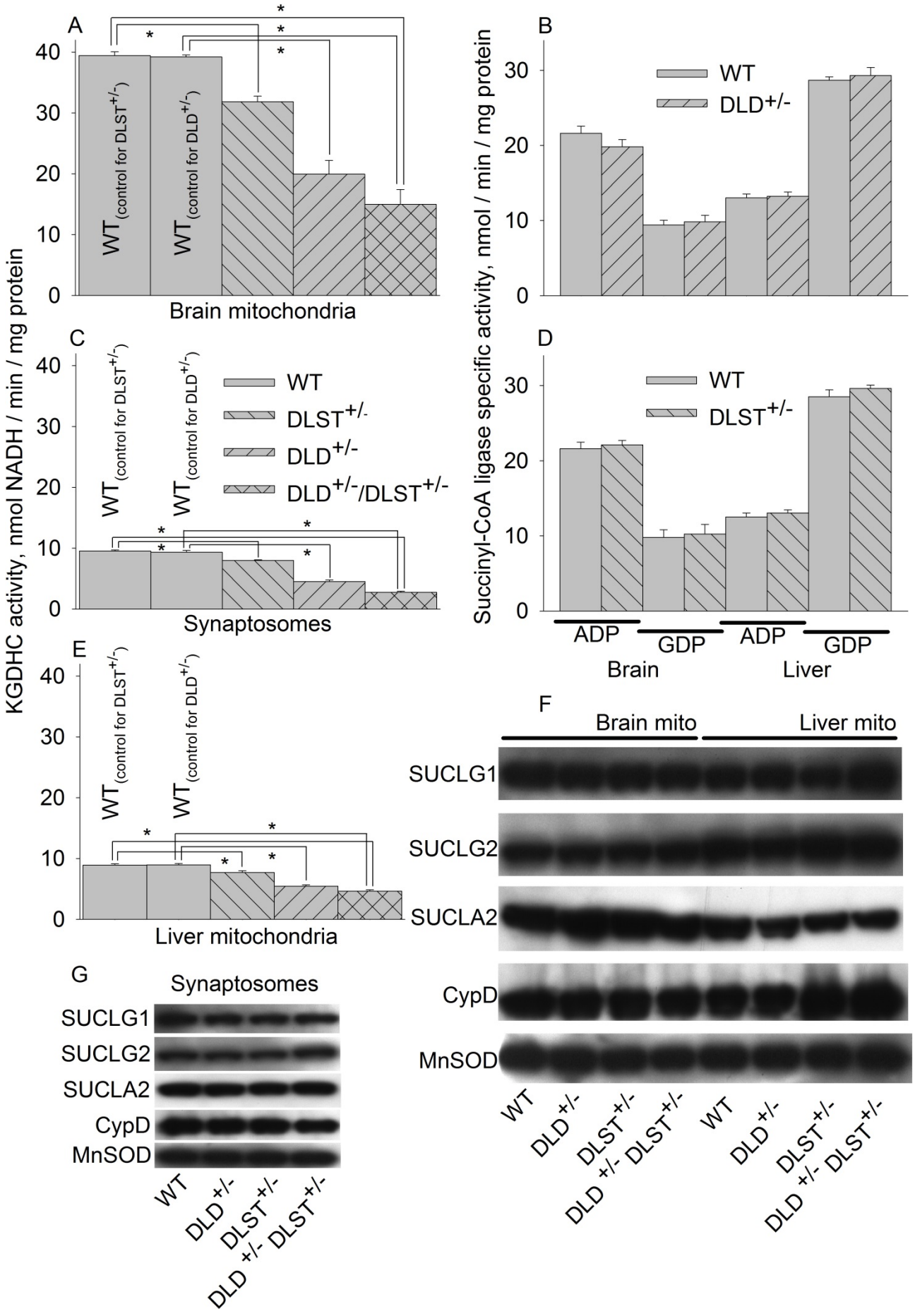

DOI:10.14753/SE.2015.1713

5.3 Mitochondrial diaphorases as NAD^+ donors to segments of the citric acid cycle that support substrate-level phosphorylation yielding ATP during respiratory arrest

Substrate-level phosphorylation mediated by succinate-CoA ligase (SUCL) in the mitochondrial matrix produces high-energy phosphates in the absence of oxidative phosphorylation. Furthermore, when the respiratory chain is dysfunctional, provision of succinyl-CoA by the α-ketoglutarate dehydrogenase complex (KGDHC) is crucial for maintained operation of SUCL yielding ATP, preventing the ANT from reversing. This chapter addresses the source of NAD^+ supply for KGDHC under anoxic conditions and inhibition of complex I. Using pharmacological tools, specific substrates and by examining tissues from pigeon liver exhibiting no diaphorase activity it is shown that mitochondrial diaphorases in the mouse liver contributed up to 81% to the NAD^+ pool during respiratory inhibition. Under these conditions, KGDHC function, essential for the provision of succinyl-CoA to SUCL, is supported by NAD^+ derived from diaphorases. By this, diaphorases contribute to the maintenance of substrate-level phosphorylation during respiratory inhibition, which is manifested in the forward operation of ANT. Finally, it is demonstrated here that re-oxidation of the reducible substrates for the diaphorases is mediated by complex III of the respiratory chain.

5.3.1 Identifying mitochondria as extramitochondrial ATP consumers during anoxia

As elaborated in **Chapter 5.2.1**, to label a mitochondrion as an extramitochondrial ATP consumer its ΔΨm, matrix ATP/ADP ratio and reversal potentials of F_O-F_1 ATP synthase and ANT must be determined, which is an extremely challenging experimental undertaking. It is simpler and equally informative to examine the effect of an ANT inhibitor on ΔΨm during ADP-induced respiration [5, 80], [Chinopoulos *et al.* 2010]. This *biosensor test*, *i.e.* the effect of cATR on safranin O fluorescence reflecting ΔΨm was successfully employed in addressing the directionality of ANT during respiratory inhibition in Chinopoulos *et al.* 2010; further on, it was employed in Kiss *et al.* 2013 using KGDHC-deficient mice for addressing the contribution of KGDHC as succinyl-CoA provider to the SUCL reaction during respiratory inhibition. In this chapter this method is used in isolated mitochondria subjected to true anoxic conditions and/or specific inhibitors of the respiratory chain, while sources of NAD^+ for KGDHC is being sought.

DOI:10.14753/SE.2015.1713

Using the recently developed O2k-Fluorescence LED2-Module of the OROBOROS Oxygraph-2k (Oroboros Instruments, Innsbruck, Austria), it became possible to achieve time-lapse recordings of safranin O fluorescence reflecting ΔΨm while measuring oxygen concentration in the same sample. Therefore, fundamental experiments establishing the basis of **Chapter 5.2** were repeated hence at the time they were performed such technology was not yet available. Mitochondria were allowed to deplete the oxygen dissolved in the air-sealed chamber and additions of chemicals through a tiny-bore hole did not allow reoxygenation of the buffer from the ambient atmosphere.

The results of a typical experiment is shown in Fig. 24. Mouse liver mitochondria (2 mg) were added in 4 ml buffer (see **Chapter 4.5**) containing substrates indicated in the panels, and allowed to fully polarize (solid traces). *State 3* respiration was initiated by ADP (2 mM) depolarizing mitochondria by ~25 mV; with a respiration rate of ~60 nmol × min^{-1} × mg^{-1} mitochondria run out of oxygen within 5-6 min as verified by recording "zero" levels of dissolved oxygen in the chamber at ~400 sec (dotted traces). Anoxia also coincided with the onset of an additional depolarization leading to a clamp of ΔΨm at ~-100 mV. In mitochondria respiring on glutamate plus malate, *i.e.* substrates that support substrate-level phosphorylation, subsequent addition of cATR (Fig. 24A, black solid trace) caused a moderate repolarization. This implied that at ~-100 mV, the ANT was still operating in the forward mode, in accordance with the ADP-ATP steady-state exchange activity/ΔΨm relationship shown in [42, 62]. In contrast, when the specific F_O-F_1 ATP synthase inhibitor oligomycin (Fig. 24A, orange solid trace) was added instead of cATR, an immediate depolarization was observed, implying that F_O-F_1 ATP synthase was working in reverse and generated the residual ΔΨm. This depolarization was complete, since further addition of SF 6847 (1 μM) yielded no further depolarization. Obviously, under the conditions shown in Fig. 24A, ATP was available in the matrix from sources other than ANT. As it was previously discussed, under this condition, ATP was supplied by matrix substrate-level phosphorylation mediated by SUCL. This was further validated by the experiments shown in panels 24B and C: in panel B, mitochondria respiring on succinate (black trace) or glutamate plus malate plus succinate (olive green trace), both conditions unfavoring substrate-level phosphorylation by SUCL (succinate shifts this reversible reaction towards ATP or GTP hydrolysis), reacted to cATR with an immediate and complete depolarization in anoxia.

DOI:10.14753/SE.2015.1713

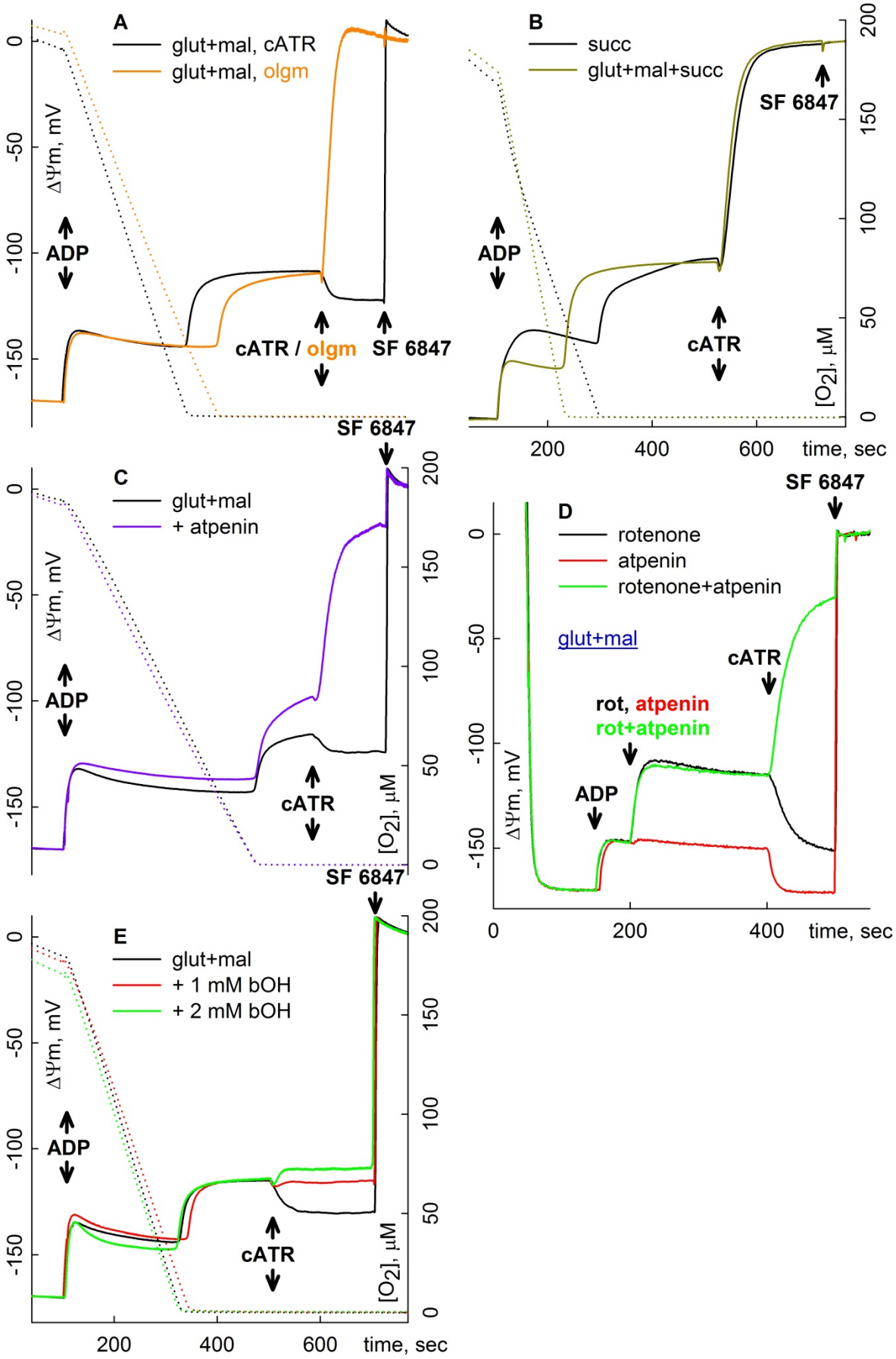

Figure 24. Reconstructed time courses of safranin O signal calibrated to ΔΨm (solid traces), and parallel measurements of oxygen concentration in the medium (dotted traces) in isolated mouse liver mitochondria. Effect of carboxyatractyloside (cATR, 2 μM) or oligomycin (olgm, 5 μM) on ΔΨm during anoxia **(A, B, C, E)** or during compromised respiratory chain by poisons **(D)**, in the presence of different substrate combinations. ADP (2 mM) was added where indicated. Substrate concentrations were: glutamate (glut, 5 mM), malate (mal, 5 mM), succinate (succ, 5 mM), β-hydroxybutyrate, (bOH, 1 or 2 mM as indicated). Substrate concentrations were the same for all subsequent experiments shown below. At the end of each experiment 1 μM SF 6847 was added to achieve complete depolarization. ↑

Likewise, in the presence of 2 μM atpenin A5 – a specific inhibitor of succinate dehydrogenase [235] causing accumulation of succinate in the matrix – cATR induced depolarization in mitochondria that had been previously respiring on glutamate plus malate and were subject to anoxia (Fig. 24C, lilac trace). In the presence of atpenin A5 though, onset of anoxia was associated with a greater depolarization prior to addition of cATR, thus it is possible that the value of ΔΨm exceeded the value of the reversal potential of the ANT (E_{rev_ANT}). However, when the respiratory chain was rendered inoperable by rotenone in lieu of anoxia, ΔΨm values were identical prior to addition of the ANT inhibitor (Fig. 24D, compare black with green trace), but loss of ΔΨm implying ANT reversal in the presence of atpenin A5 was verified by cATR.

From the above experiments the conclusion was drawn that in true anoxic conditions the ANT could be maintained in forward mode implying active matrix substrate-level phosphorylation in isolated mitochondria, similar to the paradigms with a poisoned respiratory chain described in **Chapter 5.2**. Furthermore, the results obtained in **Chapter 5.2** showing that provision of succinyl-CoA by KGDHC is critical for matrix substrate-level phosphorylation imply an emerging demand of NAD^+ for KGDHC, a concept that is at odds with the idea that in anoxia there is a shortage of NAD^+ in the mitochondrial matrix. Indeed, Fig. 24E shows that after elevating matrix NADH/NAD^+ ratio by 1 or 2 mM β-hydroxybutyrate cATR-induced a small depolarization, compare to near repolarization in panels 24E, A and C (black traces). The same effect with β-hydroxybutyrate was found in mitochondria with poisoned respiratory chain [Kiss *et al.* 2013]. These results underline the importance of NAD^+ for establishing the conditions for the forward operation of ANT during anoxia.

DOI:10.14753/SE.2015.1713

5.3.2 The importance of NAD^+ for a maintained operation of KGDHC during anoxia or respiratory chain inhibition

The negative impact of KGDHC deficiency on matrix substrate-level phosphorylation in mitochondria with a poisoned respiratory chain has been demonstrated in **Chapter 5.2**. Here the importance of a maintained operation of KGDHC was addressed requiring supply of NAD^+ in mitochondria during anoxia using arsenite, which enters intact mitochondria in an energy-dependent manner [236] and inhibits PDHC and KGDHC [237]. When mitochondria respire on glutamate plus malate, an effect of arsenite could be attributed to inhibition of KGDHC. Safranin O fluorescence and oxygen concentration in the medium where mitochondria underwent anoxia or drug-induced respiratory inhibition was recorded. As shown in Fig. 25A, the fully polarized mitochondria in the presence of glutamate plus malate were depolarized by ~25 mV by ADP (2 mM, solid black and green traces) consuming within ~6 min the total amount of oxygen present in the medium (dotted black and green traces) leading to an additional depolarization to ~-100 mV. Respiration rates are indicated in the panel, in nmol × min^{-1} × mg^{-1} protein. The transient repolarization upon addition of 2 mM sodium arsenite ($NaAsO_2$) at 700 sec was due to the high volume of the addition (0.08 ml), which contained a significant amount of dissolved oxygen. This is seen as a minor elevation in oxygen concentration (Fig. 25A, dotted green line near 700 sec) which quickly subsided as it was consumed by mitochondria and was also associated with a reestablishment of $\Delta\Psi m$ to ~-100 mV. Subsequent addition of cATR to mitochondria treated with $NaAsO_2$ (Fig. 25A, green solid trace) initiated a drop in $\Delta\Psi m$ as opposed to a moderate repolarization observed in the absence of arsenite (Fig. 25A, black solid trace). cATR also caused a depolarization when arsenite was present in the medium prior to addition of mitochondria (Fig. 25A, red solid trace), which as expected, was associated with a diminished rate of respiration (Fig. 25A, red dotted trace) leading to a prolongation until complete anoxia was achieved. cATR also caused a depolarization when arsenite was present in the medium prior to mitochondria (Fig. 25B, red trace), in which electron transport was halted by inhibiting complex I with rotenone (rot). Subsequent addition of succinate (succ, 5 mM) fully restored $\Delta\Psi m$ indicating that mitochondria were capable of electron transport from complex II when complex I was blocked, in the presence of arsenite.

DOI:10.14753/SE.2015.1713

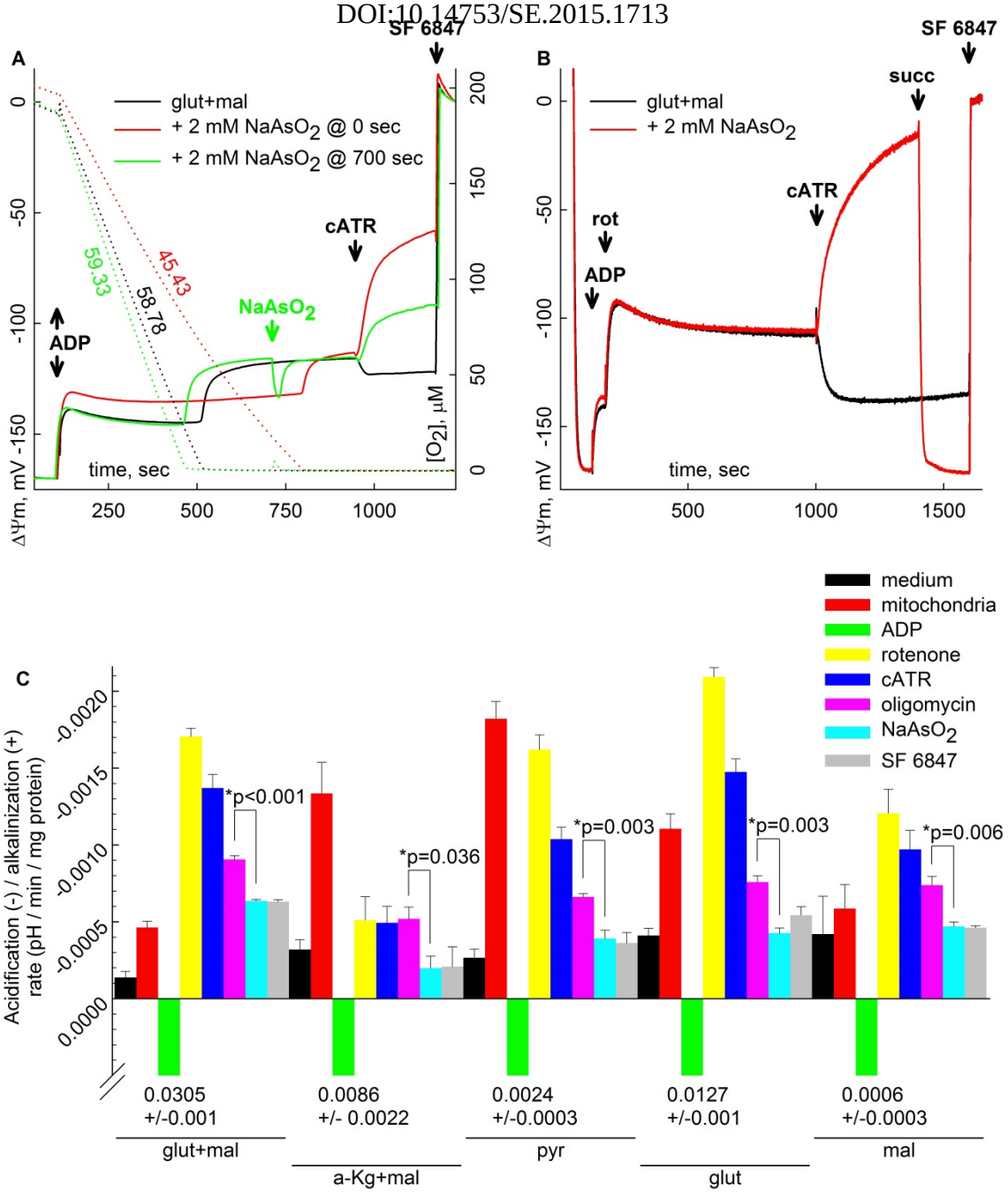

Figure 25. (A) Reconstructed time courses of safranin O signal calibrated to ΔΨm (solid traces), and parallel measurements of oxygen concentration in the medium (dotted traces) in isolated mouse liver mitochondria. The effect of carboxyatractyloside (cATR, 2 μM) on ΔΨm of mitochondria during anoxia in the presence or absence of 2 mM $NaAsO_2$ is shown. ADP (2 mM) was added where indicated. Respiration rates in nmol × min^{-1} × mg^{-1} protein are indicated on the dotted lines. **(B)** Reconstructed time courses of safranin O signal calibrated to ΔΨm in isolated mouse liver mitochondria in an open-chamber. The effect of carboxyatractyloside (cATR, 2 μM) on ΔΨm of mitochondria treated with rotenone (rot, 1 μM, where indicated) in the presence or absence of 2 mM $NaASO_2$ (2 mM, red trace) is shown. ADP (2 mM) was added where indicated. At the end of each experiment 1 μM SF 6847 was added to achieve complete depolarization. **(C)** Bar graph of rates of acidification in the suspending medium of mitochondria respiring on various substrate combinations (5 mM for all substrates indicated in the panel) upon addition of different bioenergetic poisons. *, statistically significant. ↑

Finally, the effect of arsenite was investigated on the rate of acidification in weakly buffered media, in which mitochondria were treated with a specific set of inhibitors. The concept of this experiment relies on the fact that mitochondria are net CO_2 producers acidifying the medium due to the following equilibria:

$$CO_2 + H_2O \leftrightarrow H_2CO_3 \leftrightarrow H^+ + HCO_3^- \quad (11)$$

Depending on the substrate(s) combined with targeted inhibition of bioenergetic entities, one may deduce the role of arsenite-inhibitable targets. Mitochondria were suspended in a weakly buffered medium (see **Chapter 4.9**) containing different substrates as indicated in Fig. 25C. Acidification is indicated as an upward-pointing bar, alkalinization as a downward-pointing bar. The sequence of additions were: medium (black), mitochondria (2 mg, red), ADP (2 mM, green) rotenone (1 μM, yellow), cATR (2 μM, blue), oligomycin (5 μM, magenta), $NaAsO_2$ (2 mM, cyan), and SF 6847 (1 μM, grey). With substrate combinations bypassing PDHC (glutamate plus malate, α-ketoglutarate plus malate or glutamate alone) arsenite caused a statistically significant – $p < 0.05$ (Student's *t* test) – decrease in acidification in mitochondria pretreated with rotenone, cATR and oligomycin. The assumption was made that in mitochondria in which complex I is blocked by rotenone, the ANT and the F_O-F_1 ATP synthase are blocked by cATR and oligomycin, respectively, the arsenite-inhibitable acidification may only stem from KGDHC generating CO_2. The CO_2 production by KGDHC in respiration-impaired mitochondria suggested the availability of NAD^+. Mindful of the above results, NAD^+ sources in mitochondria other than that produced by complex I were sought for and the possibility of NAD^+ provision by mitochondrial diaphorases were considered.

5.3.3 The effect of diaphorase inhibitors on bioenergetic parameters

As mentioned in **Chapter 2.11**, diaphorase activity is attributed to flavoproteins designated as NQOs [178]. Depending on the organism several isoforms and their polymorphisms have been identified, reviewed in [180] and [179]. Among these, NQO1 (EC 1.6.5.2) and NQO2 (EC 1.10.99.2) have been most extensively characterized [180]. Although NQO1 is not in the list of mouse or human mitochondrial proteins (*MitoCarta*) [238] and it was also suggested not to localize in mitochondria of certain human cancers [239], it has been found in mitochondria from different tissues [183-185]. To address the contribution of mitochondrial diaphorases to provision of NAD^+

for KGDHC reaction in anoxia, an array of pharmacological inhibitors were used; however, all of them exhibit uncoupling properties at high concentrations [240, 241]. The potential uncoupling effect of an inhibitor would be confounding, because in its presence ΔΨm could become less negative than E_{rev_ANT} leading to ANT reversal (see **Chapters 2.5** and **2.6**); in this case, its impact could not be distinguished from a genuine effect on the diaphorases. Therefore, the first step was to determine the concentration-range in which their uncoupling effects were negligible. As shown in Fig. 26, the dosedependent effect of four different NQO1 inhibitors: chrysin, 7,8-dihydroxyflavone hydrate (diOH-flavone), phenindione, and dicoumarol have been compared to a vehicle (black bars) on ΔΨm in mitochondria respiring on glutamate plus malate (panel A), after addition of 2 mM ADP (panel B), and after the addition of cATR (panel C), while simultaneously in the same samples rates of oxygen consumption were also recorded (panels D, E and F, for *State 2'*, *3* and *4c* (induced by cATR), respectively). Fig. 26 shows the effects of eight consecutive additions of chrysin, (2.5 μM each: red bars); diOH-flavone (5 μM each: green bars); phenindione (2.5 μM each: yellow bars) and dicoumarol (1.25 μM each: blue bars). From the bar graphs it is apparent that all diaphorase inhibitors exhibited a concentration range in which they had no significant uncoupling effect. That was for chrysin ≤ 5 μM, for phenindione ≤ 20 μM, and for dicoumarol ≤ 5 μM. diOH-flavone showed a significant quenching effect on the safranin O signal during *State 3* respiration, thus only its effect on oxygen consumption rate was evaluated to establish the safe use at a concentration below 20 μM. Finally, the effect of diaphorase inhibitors was compared to that of the uncoupler SF 6847 in decreasing NADH signals in intact isolated mitochondria. Such an experiment (for dicoumarol) is demonstrated in Fig. 26G and H. Mouse liver mitochondria (1 mg) were allowed to fully polarize in a medium (detailed in **Chapter 4.11**) containing glutamate plus malate, then either vehicle (control) or 1.25 μM dicoumarol or 10 nM SF 6847 were added where indicated. As shown in Fig. 26G, while SF 6847 dose-dependently decreased NADH fluorescence, dicoumarol 1.25-5 μM was without an effect. The changes in NADH fluorescence shown in panel G were largely controlled by complex I, because in the presence of rotenone (panel H), responses to dicoumarol and SF 6847 were almost completely dampened.

DOI:10.14753/SE.2015.1713

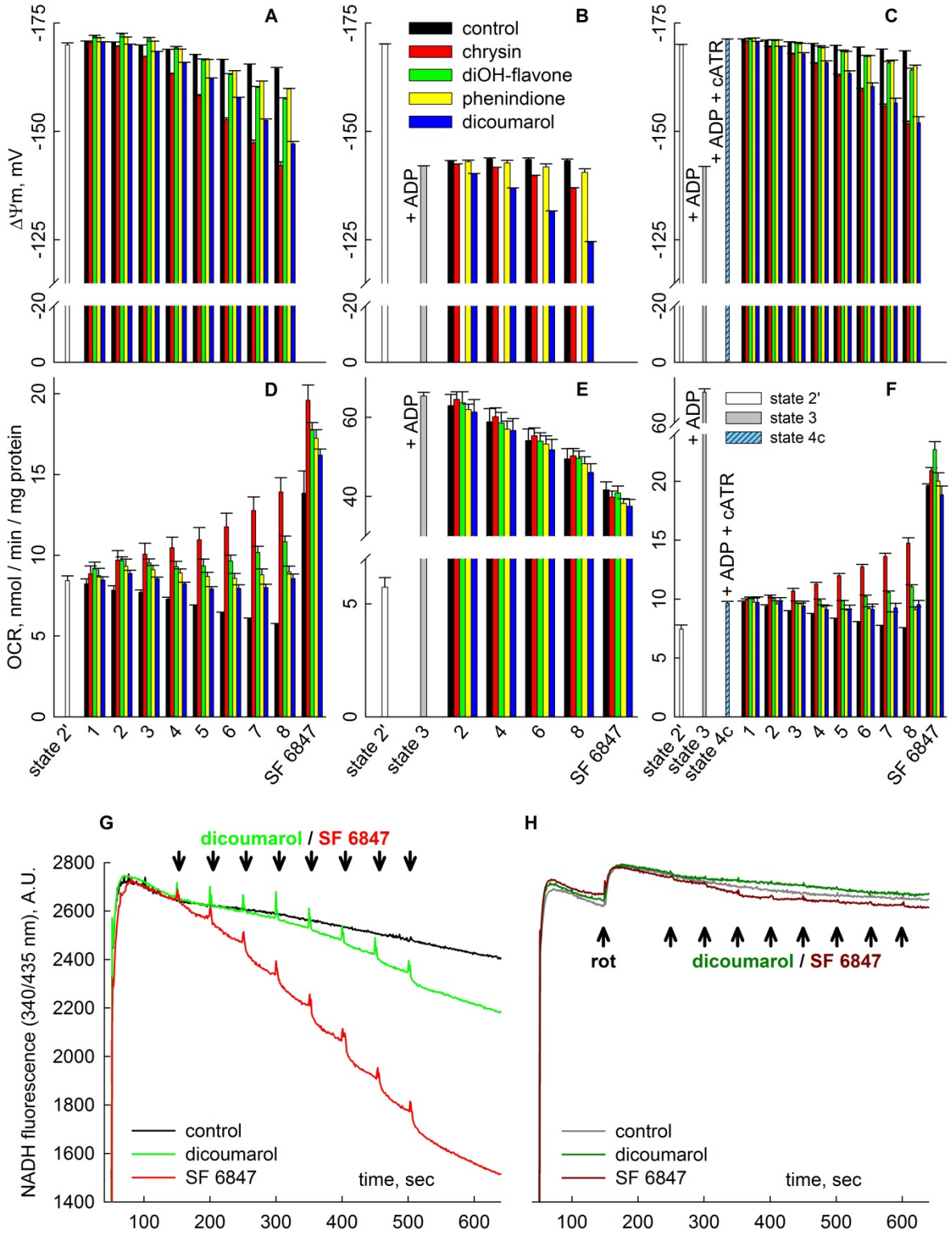

Figure 26. (A-F) Bar graphs of the effect of diaphorase inhibitors (color-coded within panel **B**) on ΔΨm (panels **A**, **B** and **C**) and oxygen consumption rates (OCR, panels **D**, **E** and **F**) under *State 2'* (panel **A**), *State 3* (+ 2mM ADP, panel **B**) or *State 4* (+ 2 mM ADP + 2 μM cATR, panel **C**) conditions. **(G, H)** Reconstructed time courses of NADH autofluorescence in isolated mouse liver mitochondria in the absence (panel **G**) and presence of 1 μM rotenone (panel **H**), and the effect of dicoumarol applied consecutively in 1.25 μM concentrations or that of SF 6847 in 10 nM concentrations, as indicated by the arrows. ↑

DOI:10.14753/SE.2015.1713

5.3.4 The effect of diaphorase inhibitors on ANT directionality in anoxic or rotenone-treated mitochondria

Having established the concentration range of the diaphorase inhibitors exhibiting no appreciable uncoupling activity, the next step was to determine their effects in the *biosensor test* addressing the direction of ANT operation by recording the effect of cATR on ΔΨm in respiration-impaired mitochondria, when they are exquisitely dependent on matrix substrate-level phosphorylation (see **Chapters 2.7** and **5.2.1**). The rationale behind these experiments was that diaphorases might be responsible for providing NAD^+ to KGDHC, which in turn is important for generating succinyl-CoA for substrate-level phosphorylation. The experimental conditions for Fig. 27A-D were essentially similar to those shown for Fig. 24, again demonstrating changes of ΔΨm in response to cATR. The anoxia also coincided with the onset of a depolarization leading to a clamp of ΔΨm to ~-100 mV. As shown in Fig. 27, panels A, B, C, and D black solid traces, addition of cATR in mitochondria made anoxic caused a repolarization, implying a forward operation of the ANT in spite of the lack of oxygen. However, in the presence of diaphorase inhibitors (concentration and color-coding detailed in panel A), cATR induced depolarization (solid traces) without affecting the rate of respiration (Fig. 27, panels A, B, C, and D, dotted traces), implying ANT reversal. Likewise, in the presence of diaphorase inhibitors (concentration and colorcoding detailed in panels E-H) rotenone-treated mitochondria (Fig. 27, panels E, F, G and H, red and orange traces) responded with depolarization to cATR, as compared to control or their vehicles showing cATR-induced repolarizations (black and grey traces, respectively). These results led to the conclusion that diaphorases were likely to provide NAD^+ to KGDHC that in turn supported substrate-level phosphorylation via generating succinyl-CoA during anoxia or inhibition of complex I by rotenone.

In order to quasi-quantify the extent of contribution of NAD^+ emanating from the mitochondrial diaphorases that can be utilized by KGDHC during anoxia, the rates of cATR-induced depolarizations (mV/sec) in the presence of diaphorase inhibitors were compared to the rate of cATR-induced depolarization in the presence of 2 mM $NaAsO_2$. From the data obtained with 20 μM diOH-flavone, 5 μM dicoumarol, 5 μM chrysin and 20 μM phenindione, it was inferred that mitochondrial diaphorases contributed 26, 41, 37 and 81% to the matrix NAD^+ pool during anoxia, respectively.

DOI:10.14753/SE.2015.1713

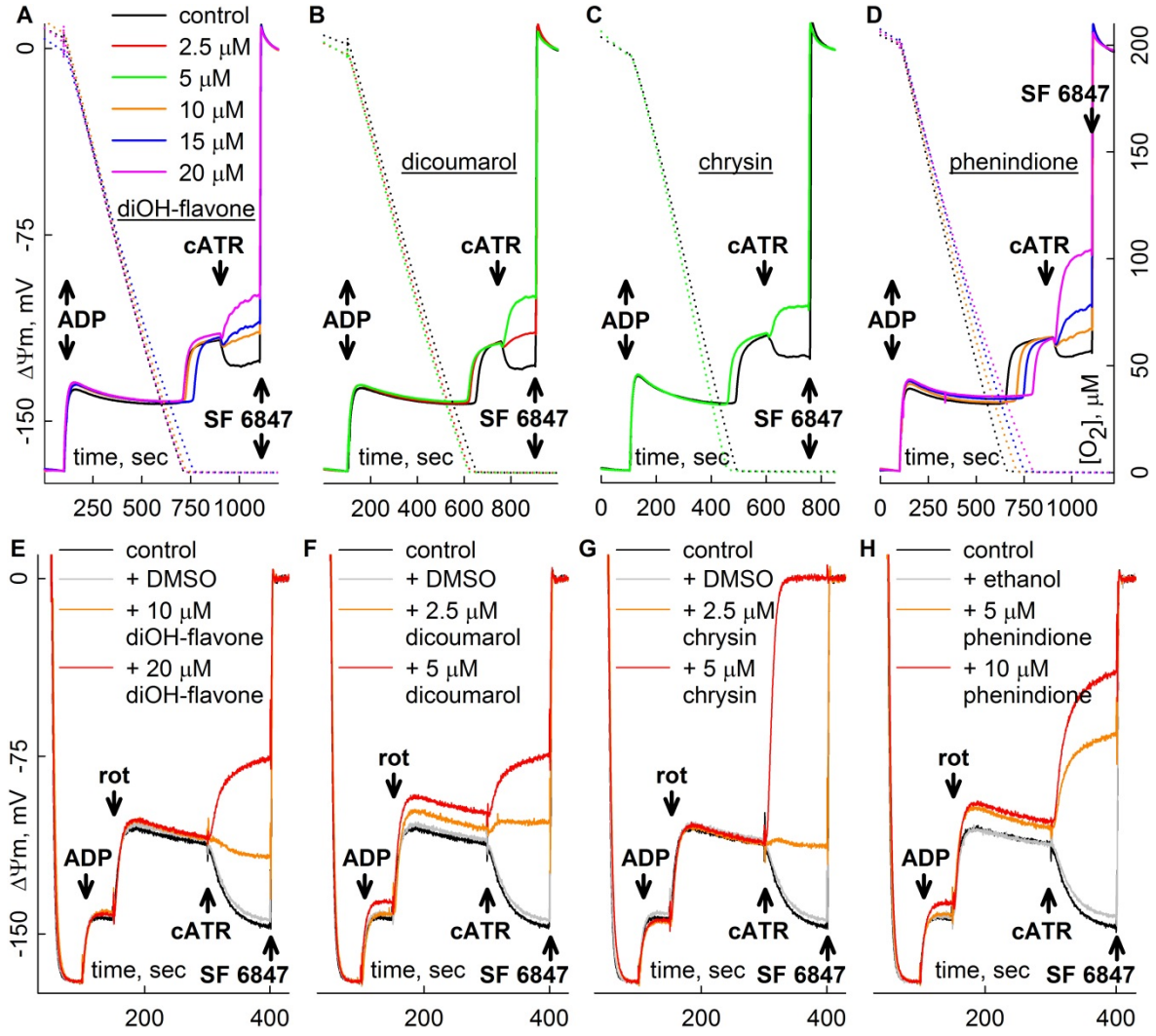

Figure 27. Reconstructed time courses of safranin O signal calibrated to ΔΨm (solid traces), and parallel measurements of oxygen concentration in the medium (dotted traces) in isolated mouse liver mitochondria supported by glutamate plus malate. The effect of diaphorase inhibitors (doses are color-coded within panel **A**) on cATR-induced changes of ΔΨm during anoxia (**A-D**) or under complex I inhibition by rotenone (**E-H**). Grey traces in panels **E-H** show the effect of vehicles (either DMSO or ethanol). At the end of each experiment 1 μM SF 6847 was added to achieve complete depolarization. ↑

5.3.5 The effect of diaphorase substrates on ANT directionality of respiration-impaired mitochondria due to anoxia or rotenone

To strengthen the above conclusion, next the *biosensor test* was performed in the presence of known diaphorase substrates in mitochondria undergoing respiratory inhibition by anoxia or rotenone. Diaphorase activity mediated by NQO1 exhibits lack of substrate- and electron donor specificity because its active site can accommodate molecules of varying size and structure [242, 243] therefore, various types of quinoid compounds and their derivatives can be processed by the isolated enzyme [244]. Furthermore, it is also able to react with different dyes, nitro compounds and some

inorganic substances [244]. The mitochondrial matrix is a quinone-rich environment, containing several coenzyme Qs with variable side-chains. Of course, NQO1 exhibits unequal affinities for them, but it is reasonable to assume that some coenzyme Qs are in the millimolar concentration range and could be substrates for NQO1. The following 14 diaphorase substrates were tested: phylloquinone (vitamin K_1, 10 μM), menaquinone (vitamin K_2, 10 μM), menadione (vitamin K_3, 10 μM), duroquinone (DQ, 10-100 μM), mitoquinone mesylate (mitoQ, 0.5 μM), *p*-benzoquinone (BQ, 10 μM), methyl-*p*-benzoquinone (MBQ, 10 μM), 2,6-dimethylbenzoquinone (DMBQ, 10-50 μM), 2-chloro-1,4-benzoquinone (CBQ, 10 μM), 2,6-dichloro-1,4-benzoquinone (DCBQ, 10 μM), 1,2-naphthoquinone (1,2-NQ 10 μM), 1,4-naphthoquinone (1,4-NQ 10 μM), 2,6-dichloroindophenol (DCIP, 50 μM) and 2-(3,4-dihydroxyphenyl)-3,5,7-trihydroxy-4H-chromen-4-one (quercetin, 10 μM). In concentrations exhibiting no uncoupling or other side-effects on ΔΨm or rate of respiration (not shown), mouse liver mitochondria were treated with ADP and cATR similarly to that demonstrated in Fig. 24. As shown in Fig. 28A-C and demonstrated in supplementary material of Kiss *et al.* 2014, when using different substrate combinations supporting respiration, addition of cATR caused repolarization except when glutamate plus malate plus β-hydroxybutyrate were used (panel C, black solid trace), a substrate combination that – as discussed in **Chapter 5.2.2** – limits the availability of NAD^+ during anoxic conditions. In this paradigm, dose-dependent addition of duroquinone during anoxia led to cATR-induced repolarization (panel C, colored solid traces). Addition of menadione had no effect (panel A, solid orange trace), while mitoQ even abolished the cATR-induced repolarization (panel B, solid green trace). By contrast, when respiratory inhibition was achieved by rotenone instead of anoxia, duroquinone, menadione and mitoQ resulted in a strong cATR-induced repolarization (Fig. 28D-H). This effect of menadione (vitamin K_3) was not shared by vitamins K_1 (phylloquinone) and K_2 (menaquinone), as shown in panels G and H, respectively. The variable effects of a host of other quinones in this paradigm are shown in supplementary material of Kiss *et al.* 2014. Furthermore, since safranin O may also be a substrate for diaphorases due to its structural similarity to Janus Green B, which is a genuine diaphorase substrate [241], redistribution of tetraphenylphosphonium (TPP) as an index of ΔΨm was also measured as an alternative, using a TPP electrode, (Fig. 28I). Mitochondria were allowed to polarize by glutamate plus malate then ADP

(2 mM) was added, followed by rotenone that led to a depolarization. Addition of cATR induced a repolarization, like in the above experiment indicating that safranin O is unlikely to be a diaphorase substrate. From these results the conclusion was drawn that mitochondrial diaphorases were not saturated by endogenous quinones and were likely providing NAD^+ to KGDHC that in turn yielded succinyl-CoA supporting substrate-level phosphorylation during anoxia or inhibition of complex I by rotenone. Furthermore, there appeared to be a clear distinction between true anoxia and rotenone-induced respiratory inhibition; in anoxia, menadione and mitoQ were not effective in conferring cATR-induced repolarization. The reason(s) for this were investigated further, in the experiments outlined below.

Figure 28. Reconstructed time courses of safranin O signal calibrated to ΔΨm (solid traces), and parallel measurements of oxygen concentration in the medium (dotted traces) in isolated mouse liver mitochondria demonstrating the effect of diaphorase substrates on cATR-induced ΔΨm changes during anoxia (**A-C**) or complex I inhibition by rotenone (**D-H**). Substrate combinations are indicated in the panels; concentrations were the same as in experiments shown above. (**I**) Reconstructed time course of TPP signal (in volts) in isolated mouse liver mitochondria supported by glutamate plus malate. Additions were as indicated by the arrows. At the end of each experiment 1 μM SF 6847 was added to achieve complete depolarization. ↓

DOI:10.14753/SE.2015.1713

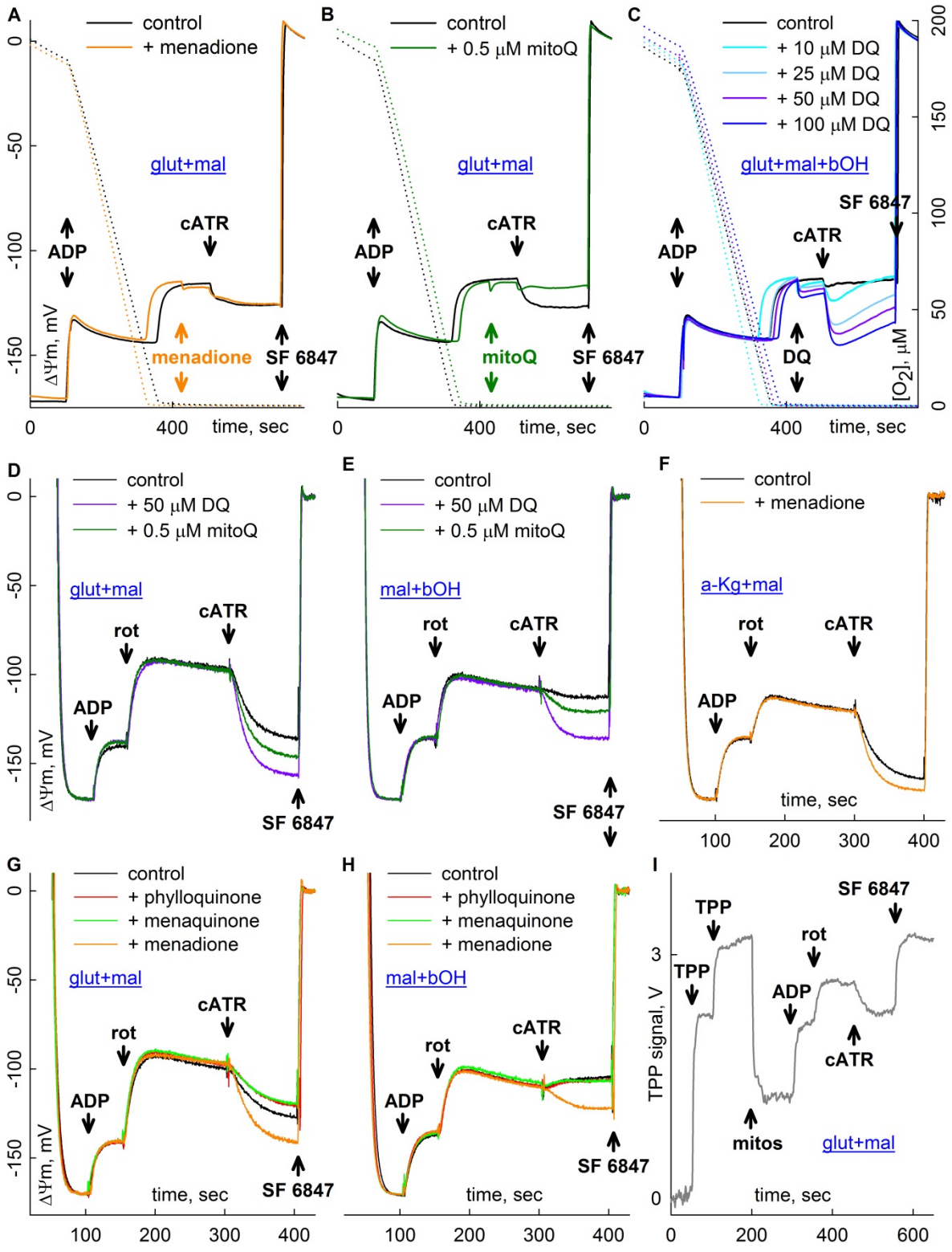

5.3.6 The role of complex III in re-oxidizing diaphorase substrates

To address the discrepancy that emerged from the results obtained with rotenone-treated *vs.* anoxia-treated mitochondria in respect to the effect of diaphorase substrates, we inhibited mitochondrial respiration with stigmatellin, a specific inhibitor of complex III (see **Chapter 5.2.3**). The rationale behind this relies on several reports pointing to

complex *b* of complex III as being capable of re-oxidizing substrates that are reduced by mitochondrial diaphorases [186, 187, 245-248]. As shown in Fig. 29A-D, in mouse liver mitochondria respiring on different substrate combinations indicated in the panels, *State 3* respiration initiated by ADP (2 mM) was arrested by 1.2 μM stigmatellin (stigm), leading to a clamp of ΔΨm to ~-100 mV. Subsequent addition of cATR (Fig. 29, panels A, B and C, black solid traces) conferred a depolarization to variable extent, depending on the substrates used, indicating that functional complex III was required for the forward operation of ANT when it relied on ATP generated by substrate-level phosphorylation. The lack of re-oxidation of the reduced diaphorase substrate by complex III is likely to reflect in the result (see below) showing that the presence of menadione (panels A, B and C, red traces) or mitoQ (panel D, lilac trace), but not duroquinone (panel D, green trace), conferred a more robust cATR-induced depolarization. In mitochondria undergoing respiratory arrest by anoxia (panel E), addition of stigmatellin (olive green trace) did not result in cATR-induced depolarization. However, while respiratory arrest of mitochondria achieved by inhibiting complex IV with KCN (1 mM) yielded a very small change in ΔΨm by cATR (panel F, green trace), co-presence of ferricyanide ($K_3[Fe(CN)_6]$ abbreviated to FerrCyan, 1 mM) – which can oxidize cytochrome *c* due to its higher redox potential (~400 mV *vs.* 247-264 mV for cytochrome *c*, depending on various factors [249, 250]) led to a cATR-induced repolarization (panel F, grey trace). This effect was abolished by stigmatellin (panel F, orange trace). When ferricyanide was used, it was necessary to titrate ΔΨm back to the same levels as in its absence, hence SF 6847 boluses (5 nM) were added where indicated (panel F, grey trace). From the above experiments we concluded that stigmatellin was negating the beneficial effect of diaphorase substrates assisting in cATR-induced repolarization emphasizing the involvement of complex III in mitochondria with respiratory inhibition by rotenone or anoxia. Evidently not all diaphorase substrates assisted in preventing mitochondria from being extramitochondrial ATP consumers, which meant that not all of them could be processed by either the diaphorases, and/or re-oxidized by complex III. Relevant to this, it is well known that vitamins K_1, K_2 and CoQ_{10} do not react with the isolated diaphorase [170, 251, 252]; furthermore, while numerous compounds have been shown to react readily with purified diaphorase [170, 188, 244], there is specificity in the

DOI:10.14753/SE.2015.1713

oxidation of the reduced quinone by the respiratory chain, discussed in [186]. Indeed, menadione and duroquinone were previously shown to be processed by the mitochondrial diaphorases and re-oxidized by complex III [186, 246].

Figure 29. The effect of diaphorase substrates on cATR-induced changes of ΔΨm after complex III inhibition by stigmatellin (stigm) or complex IV by KCN. Reconstructed time courses of safranin O signal calibrated to ΔΨm in isolated mouse liver mitochondria and oxygen consumption (panel **E**, dotted lines) are shown. Mitochondria respired by different substrates as shown in the panels. Additions were as indicated by the arrows. At the end of each experiment 1 μM SF 6847 was added to achieve complete depolarization. FerrCyan: ferricyanide. ↓

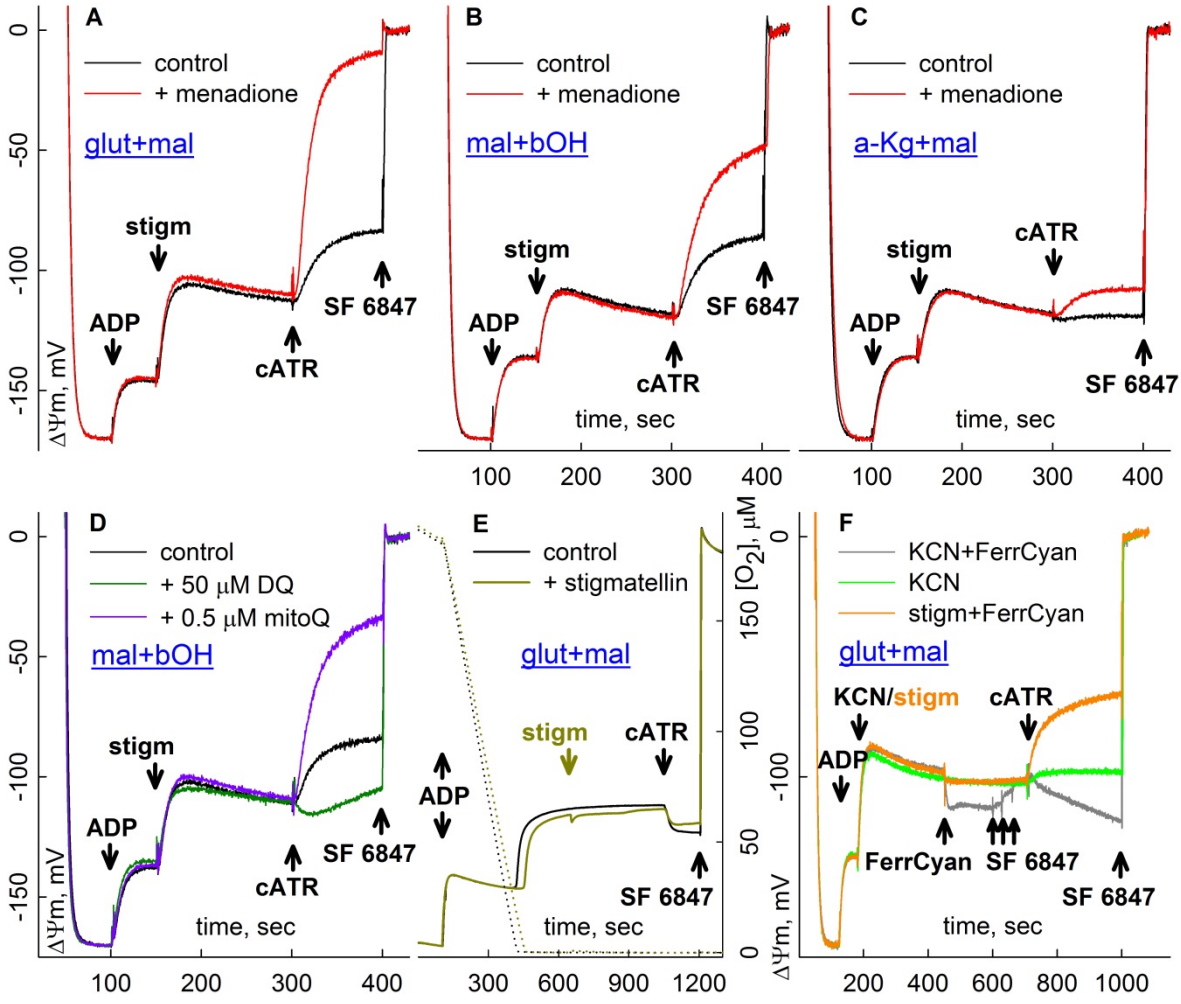

5.3.7 Lack of the role of diaphorase in the regeneration of NAD^+ during anoxia in mitochondria from pigeon liver

The diaphorase activity described for rodent and human tissues has been reported to be absent in the liver and breast muscle of pigeons (*Columba livia domestica*) [253, 254]. Therefore, it was reasoned that in mitochondria obtained from pigeon tissues, the diaphorase inhibitors and substrates would exhibit no effect. As shown in Fig. 30A-C (black traces), pigeon liver mitochondria respiring on different substrates were repolarized by cATR (2 μM) added after ADP (2 mM) and rotenone (1 μM) indicating ATP generation for the forward operation of ANT. The lack of diaphorase involvement in this effect was confirmed by the results that menadione (10 μM) failed to cause a more robust cATR-induced repolarization (panels A-C, red traces), and none of the diaphorase inhibitors caused cATR-induced depolarization (Fig. 30D). Accordingly, duroquinone (DQ, 50 μM) was without an effect on cATR-induced changes in ΔΨm of mitochondria during anoxia (Fig. 30E). These results support the conclusion that the effects of diaphorase substrates and inhibitors observed in mouse liver mitochondria were likely mediated through genuine diaphorase activity. Furthermore, it is also apparent that in the absence of a diaphorase, pigeon liver mitochondria were still able to maintain the KGDHC-SUCL axis sustaining substrate-level phosphorylation. Indeed, in Fig. 30F it is shown that the addition of succinate to pigeon mitochondria reverted the cATR-induced changes in ΔΨm during anoxia from a repolarization to a depolarization, in accordance to the schemes described in **Chapter 2.6** and thesis-related publications No. 1 and 3. The validity of this scheme is further supported in pigeon liver mitochondria from the results shown in Fig. 30G, where the addition of atpenin A5, which is expected to lead to a built-up of succinate in the mitochondrial matrix, also led to a cATR-induced depolarization during anoxia (red trace).

Figure 30. (**A-C, E**) Reconstructed time courses of safranin O signal calibrated to percentage reflecting ΔΨm in isolated pigeon liver mitochondria, demonstrating the effect of various respiratory and diaphorase substrates as indicated in the panels, on cATR-induced changes of ΔΨm after complex I inhibition by rotenone. (**D**) Diaphorase inhibitors were present as indicated (dicoumarol: 5 μM, chrysin: 5 μM, diOH-flavone: 20 μM, phenindione: 10 μM), and mitochondria were supported by glutamate plus malate. (**E-G**) Oxygen concentration in the medium (dotted traces) was also measured: (**E**) the effect of duroquinone (DQ, 50 μM) is shown; (**F**) that of various substrates, and (**G**) that of the inhibitors atpenin A5 (2 μM) and KCN (1 mM). At the end of each experiment 1 μM SF 6847 was added to achieve complete depolarization. ↓

DOI:10.14753/SE.2015.1713

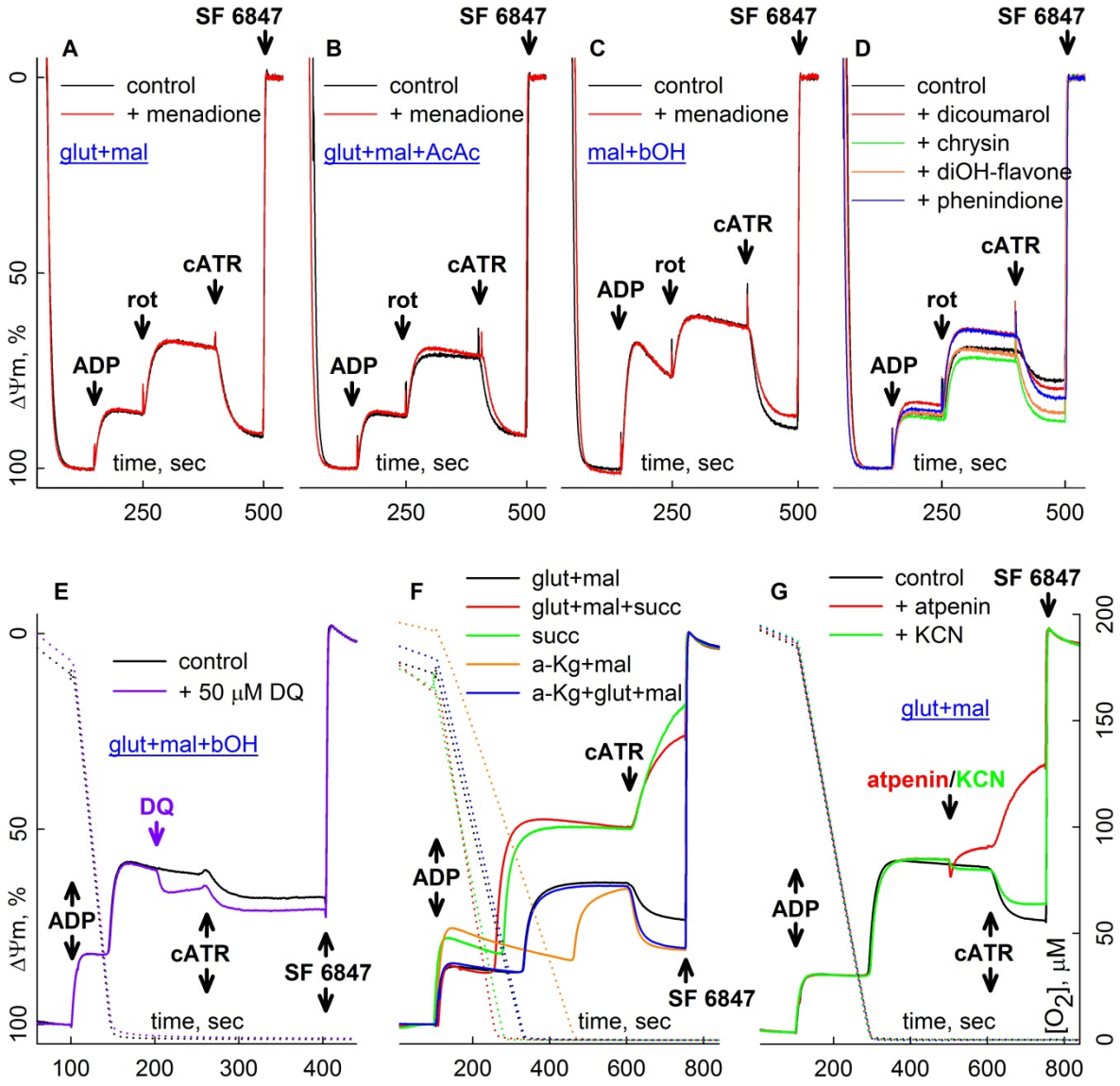

5.3.8 Alternative sources for NAD^+ provision in mitochondria during respiratory arrest

From the above data it is apparent that mitochondrial diaphorases are not the sole providers for NAD^+ during anoxia or respiratory inhibition by poisons. Therefore, the following alternative sources for NAD^+ were considered: i) isocitrate dehydrogenase (in reverse, see below), ii) nicotinamide nucleotide transhydrogenase, iii) malate dehydrogenase, iv) ROS-mediated direct and/or indirect NADH oxidation to NAD^+.

As it was already mentioned in the legend of Fig. 10, in mitochondria, there are two IDH isoforms: a reversible, $NADP^+$-dependent IDH2, [164, 165, 220-222], and an irreversible NAD^+-dependent IDH3 [223-226]. The reversibility of this reaction is well established [202, 221, 225, 255-260]. Mindful of the reactions catalyzed by the two

isoforms that co-exist in the mitochondrial matrix, it is possible that IDH2 converts α-ketoglutarate plus NADPH to isocitrate plus $NADP^+$ and then IDH3 oxidatively decarboxylates isocitrate plus NAD^+ back to α-ketoglutarate plus NADH (the transhydrogenase interconverts $NAD(P)^+$ and NAD(P)H [166, 229]). To address the extent of contribution of this IDH-mediated futility to mitochondrial NAD^+ provision it was attempted to shift the reaction towards NADH formation by manipulating the concentration of its substrates, *i.e.*, by causing isocitrate overload. Unlike citrate, isocitrate is not transported readily to mitochondria while citrate and isocitrate are in equilibrium in the matrix due to the reversibility of the aconitase reaction [230]; it was therefore reasoned that the presence of citrate in excess would negate the beneficial effect of other substrates supporting substrate-level phosphorylation in terms of cATR-induced changes in $\Delta\Psi m$ during respiratory arrest. Indeed, as shown in Fig. 31A, addition of 5 mM citrate to glutamate or α-ketoglutarate (magenta and brown traces, respectively) reverted the cATR-induced repolarization to a depolarization. However, addition of citrate to glutamate plus malate failed to revert the cATR-induced repolarization to a depolarization (green trace), probably because malate is known to assist in the entry of several mitochondrial substrates leading to a higher flux.

To address the extent of contribution of a proton-translocating transhydrogenase reversibly exchanging $NADP^+$ and NAD^+ to NADH and NADPH, respectively [229] – which is in congruence with the above concept involving IDH –, mitochondria obtained from C57Bl/6N *vs.* C57BL/6J mice were compared. The reason behind the comparison was that in the latter strain the gene coding for the transhydrogenase is absent [261]. Although the catalytic site of the transhydrogenase for oxidation and reduction of the nicotinamide nucleotides is facing the matrix, extramitochondrial pyridine nucleotides are also required; however, those released from broken mitochondria in our samples may have been sufficient for the exchange to materialize. As shown in Fig. 31B, cATR-induced repolarization after anoxia in mitochondria from C57Bl/6N mice (black trace) was virtually indistinguishable from mitochondria obtained from C57BL/6J mice (pink trace). This result led to the conclusion that NAD^+ provision by the transhydrogenase is not a viable possibility, at least in our isolated mitochondria preparations.

An obvious possibility for NAD^+ generation would be the malate dehydrogenase (MDH) reaction favoring malate formation from oxaloacetate [202], however, this is very difficult to address. WT C57BL/6J mice were compared with another strain expressing an isoform of MDH which yielded insignificantly smaller activity ($MDH2^b$), but no differences were observed (not shown). A "transgenic" or "silencing" approach for MDH inherently suffers from the pitfall that this enzyme exhibits an extremely high activity compared to the other enzymes of the citric acid cycle; therefore, one would expect to require very substantial decreases in activity in order to observe an impact on NAD^+ provision. The fact that there are no MDH specific inhibitors hinders the ability of studying the extent of contribution of MDH in these protocols.

Finally, the possibility was considered that ROS may shift redox equilibrium towards NAD^+, either through enzyme-mediated antioxidant mechanisms [262], or through non-enzymatic scavenging by keto-acids, themselves being in equilibrium with $NADH/NAD^+$ [263]. To address this, the effect of cATR-induced changes on $\Delta\Psi m$ after rotenone in heart mitochondria obtained from WT *vs.* heart-specific superoxide dismutase 2 overexpressing mice (MnSOD HO) were compared [264]. These mice exhibit very low levels of ROS emanation in cardiac mitochondria, primarily due to a 20-fold higher activity of MnSOD which scavenges superoxide (and a two-fold higher expression of catalase) than WT littermates in the matrix. As shown in Fig. 31C-E, in heart mitochondria of MnSOD HO mice (light blue traces), cATR-induced a much smaller repolarization (panels C and E) or even a depolarization (panel D), albeit the latter starting from a lower $\Delta\Psi m$ level, compared to WT mitochondria. From these results one can conclude that in the presence of rotenone, ROS may assist in the regeneration of NAD^+ in the mitochondrial matrix that in turn may be utilized by the KGDHC reaction yielding succinyl-CoA supporting substrate-level phosphorylation.

DOI:10.14753/SE.2015.1713

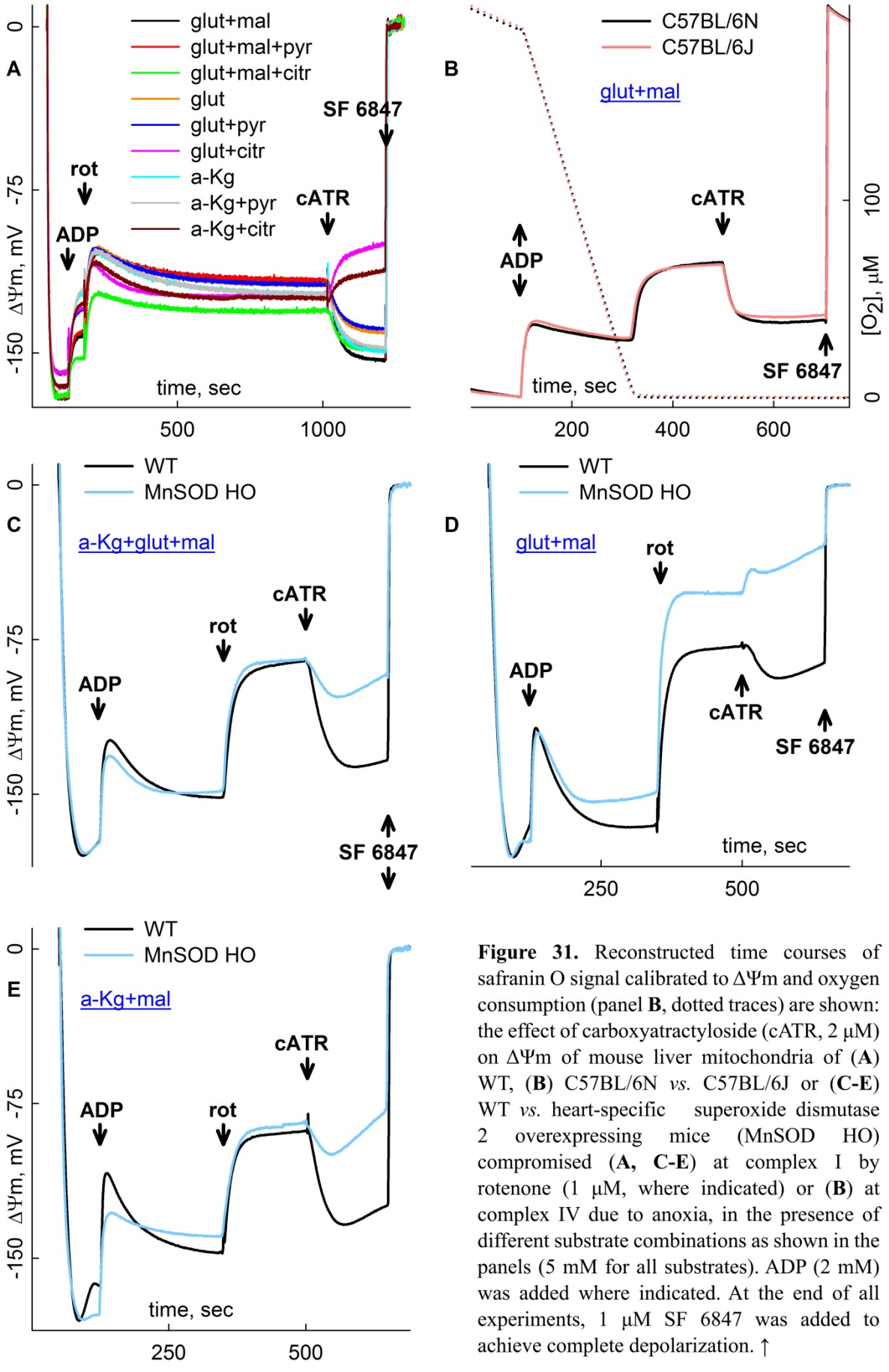

Figure 31. Reconstructed time courses of safranin O signal calibrated to ΔΨm and oxygen consumption (panel **B**, dotted traces) are shown: the effect of carboxyatractyloside (cATR, 2 μM) on ΔΨm of mouse liver mitochondria of (**A**) WT, (**B**) C57BL/6N *vs.* C57BL/6J or (**C-E**) WT *vs.* heart-specific superoxide dismutase 2 overexpressing mice (MnSOD HO) compromised (**A, C-E**) at complex I by rotenone (1 μM, where indicated) or (**B**) at complex IV due to anoxia, in the presence of different substrate combinations as shown in the panels (5 mM for all substrates). ADP (2 mM) was added where indicated. At the end of all experiments, 1 μM SF 6847 was added to achieve complete depolarization. ↑

DOI:10.14753/SE.2015.1713

6. DISCUSSION

6.1 Implications of CYPD-F_O-F_1 ATP synthase interaction in intact mitochondria

Experimental data outlined in **Chapter 5.1** extends the results obtained by Giorgio *et al.* [59] demonstrating that changes in ATP synthesis or hydrolysis rates of the F_O-F_1 ATP synthase as a result of CYPD binding do not translate to changes in ADP-ATP flux rates, even though CYPD binding on the F_O-F_1 ATP synthase and unbinding by cyclosporin A was demonstrated in this thesis in intact mitochondria. This is the result of an imposing role of the ANT. Apparently, ANT-mediated ADP-ATP exchange rates are slower than F_O-F_1 ATP synthase-mediated ADP-ATP interconversions; an assumption that is afforded by early findings from pioneers in the field, showing that the ANT is the step with the highest flux-control coefficient (for definition, see **Chapter 2.10**) in the phosphorylation of externally added ADP to energized mitochondria [265]. However, it could be argued that a 30% change in F_O-F_1 ATP synthase activity exhibiting a flux-control coefficient of ~0.3 would alter adenine nucleotide exchange rates in intact mitochondria by $0.3 \times 0.3 = 0.09$ (*i.e.* 9%). It should be emphasized that the flux-control coefficient applies for infinitesimally small changes in the percentage change in the steady-state rate of the pathway; if changes are large (*e.g.* 30%), the flux-control coefficient decreases by a factor of ~5, or more [266, 267]. Thereby, a 30% change in F_O-F_1 ATP synthase activity translates to a $0.3 \times 0.3 \times 0.2 = 0.018$ (*i.e.* 1.8%) or less difference in adenine nucleotide exchange rates in intact mitochondria. This is in accordance with the predictions of the kinetic modeling deduced in **Chapter 5.1.2**, suggesting that a 30% increase in F_O-F_1 ATP synthase activity yields a 1.38–1.7% increase in ANT-mediated ADP-ATP exchange rate in fully polarized or fully depolarized mitochondria. Yet, in ATP-energized mitochondria with a nonfunctional respiratory chain, abolition of CYPD or its inhibition by cyclosporin A resulted in an accelerated ATP hydrolysis rate, allowing intact mitochondria to maintain a higher $\Delta\Psi m$.

The present findings imply that the modulation of F_O-F_1 ATP synthase activity by CYPD comprises an “in-house” mechanism of regulating matrix adenine nucleotide levels, which does not transduce outside mitochondria, without evoking a functional correlation between CYPD and ANT as a result of a possible direct link [268]. This is

the first published example of an intramitochondrial mechanism of adenine nucleotide level regulation that is not reflected in the extramitochondrial compartment. Furthermore, the speculation can be made that the abolition of CYPD by genetic ablation or by cyclosporin A from the lateral stalk of the F_O-F_1 ATP synthase allows sufficiently depolarized mitochondria to hydrolyze ATP at a higher rate opposing a further drop in $\Delta\Psi m$, as well as releasing P_i with a higher rate in the matrix. In turn, elevated [P_i] not only shifts E_{rev_ATPase} toward more depolarizing $\Delta\Psi m$ values, but also activates the SUCL, thus matrix substrate-level phosphorylation to compensate for the increased ATP consumption by the F_O-F_1 ATP synthase (see **Chapter 2.7**). The overall outcome would be the expansion of the B space (see Fig. 3), implying that for progressively depolarizing mitochondria without a functional CYPD, it is less likely to consume cytosolic ATP. But if the genetic ablation or pharmacological inhibition of CYPD happens to be beneficial – as it clearly appears to be in Fig. 8A –, it seems reasonable to ask: why is it in mitochondria after all?

CYPD KO mice do not exhibit a severe phenotype; however, they exhibit enhanced anxiety, facilitation of avoidance behavior, occurrence of adult-onset obesity [269] and a defect in platelet activation and thrombosis [270]. These mice also show limited metabolic flexibilities in the heart [271], in line with the original report describing the effect of cyclosporin A on isolated mitochondria [272]. On the other hand, CYPD KO mice score better compared than WT littermates in mouse models of Alzheimer's disease [273], muscular dystrophy [274], and acute tissue damage induced by stroke or toxins gene [203, 275-277]. Furthermore, genetic ablation of CYPD or its inhibition by cyclosporin A or Debio 025[3] rescues mitochondrial defects and prevents muscle apoptosis in mice suffering from collagen VI myopathy [278-280]. The beneficial effects of cyclosporin A have also been demonstrated in patients suffering from this type of myopathy [281]. But even so the implication of CYPD in diverse pathologies is clear; the physiological function of this protein is still unknown.

The binding of CYPD to F_O-F_1 ATP synthase is phosphate-dependent; in the absence of P_i the interaction is negligible. Accordingly, inhibition of the F_O-F_1 ATP synthase activity by CYPD may only become pronounced when the enzyme operates in

[3] *Alisporivir (also known as Debio 025, DEB025 or UNIL-025) is a cyclophilin inhibitor without an immunosuppressive effect. Its structure is reminiscent of and synthesized from cyclosporin A.*

reverse mode: hydrolyzing ATP and generating high [P_i] microdomains in its vicinity. This is the case in anoxia and ischemia-reperfusion injury. Along this line, inhibition by CYPD may synergize with IF1 to reduce energy dissipation (see **Chapter 2.3**). The regulation of CYPD-F_O-F_1 ATP synthase interaction is poorly understood. Still, based upon the results of Giorgio *et al.* [59], modulation by CYPD seems to be independent of IF1 release. An important difference between the two proteins is that while CYPD binding to the oligomycin sensitivity-conferring protein subunit affects both forward and reverse modes of F_O-F_1 ATP synthase, IF1 binding to one of the β subunits inhibits ATP hydrolysis only [282]. In submitochondrial particles, cyclosporin A increases ATP synthesis more than ATP hydrolysis [59]; a finding probably related to IF1. Namely, the modulatory effect of cyclosporin A may be partially masked by IF1 binding during ATP hydrolysis, but not during synthesis when there is no interaction between IF1 and F_O-F_1 ATP synthase [282].

6.2 The role of IF1 in the preservation of the cytosolic ATP pool in anoxia

The IF1, evolved to limit the extent of ATP consumption by a reversed F_O-F_1 ATP synthase by blocking the F_1 subcomplex [48], ironically leads to robust depolarization [50, 54]. This loss of ΔΨm should allow the ANT to reverse with a high rate and bring cytosolic ATP into the matrix, even though F_O-F_1 ATP synthase is rendered inoperable by IF1. The question emerges though: how does the seemingly contradictory purpose of IF1 fit into the fail safe mechanism – proposed throughout this thesis – dedicated to hinder mitochondrial consumption of cytosolic ATP in case of a respiratory chain failure? As discussed in **Chapter 2.3**, inhibition of F_1-ATPase by IF1 is not necessarily complete, and even if the amount of ATP brought into the matrix due to a strongly reversed ANT is partially consumed by mitochondria, it will remain unavailable for cytosolic ATP-dissipating reactions. Considering that the action of IF1 on a reverse-operating F_O-F_1 ATP synthase leads to a decrease in ΔΨm, the reverse operation of the ANT is augmented. As a consequence, cytosolic ATP is exchanged for matrix ADP at an accelerated rate, opposing the decrease in matrix [ATP] by the reversed F_1-ATPase, stemming from whatever remaining activity is left due to the incomplete inhibitory action of IF1. This increase in matrix [ATP] will not only inhibit the unbinding of IF1 from the F_1 subcomplex [56], but also disfavor the reverse-operating mode of the ANT. Therefore, cytosolic ATP allocated into the matrix is spared from intramitochondrial

hydrolysis, and upon the rescission of the reasons conferring membrane depolarization in the first place, the only issue remaining is the return of matrix ATP to the cytosol. This is ensured by the dissociation of IF1 from F_1-ATPase upon generation of sufficient $\Delta\Psi m$ [55-57] and because E_{rev_ANT} is always less negative than E_{rev_ATPase}, during mitochondrial repolarization matrix ATP will first be transported into the cytosol due to ANT reverting towards forward mode of operation, prior to subject to hydrolysis from an F_1-ATPase about to unbind IF1.

6.3 KGDHC-deficiency jeopardizes adequate SUCL operation during respiratory inhibition

KGDHC is at a crossroad of biochemical pathways, and as such, greatly affects the overall cell metabolism. It is therefore not surprising that diminished KGDHC activity of transgenic mice results in alterations of glucose utilization, a hallmark of metabolic abnormality, albeit depending on the model [231, 232]. Yet, extensive work on transgenic mice for two of the three subunits of KGDHC failed to pinpoint the exact mechanisms responsible. In view of this gap of information, an aim of this thesis was to address the effect of a decreased KGDHC activity on matrix substrate-level phosphorylation in isolated and *in situ* mitochondria with diminished $\Delta\Psi m$ values achieved by respiratory inhibition.

The rationale of this aim is manifold: i) provision of succinyl-CoA through KGDHC is much higher than that originating from propionyl-CoA metabolism [13]; ii) matrix substrate-level phosphorylation provides ATP in the matrix parallel to that by oxidative phosphorylation [96, 97, 283]; iii) SUCL does not require oxygen to produce ATP, and it is even activated during hypoxia [102]; iv) in ischemia and/or hypoxia, there is mounting evidence of pronounced conversion of α-ketoglutarate to succinate, implying that KGDHC is operational [104, 105, 109, 202, 284-296], [Kiss *et al.* 2014]; v) brains from patients with autopsy-confirmed Alzheimer's disease exhibited significant decreases in the activities of the enzymes in the first part of the citric acid cycle (PDHC, -41%; IDH, -27%; and KGDHC, -57%), while enzyme activities of the second half of the cycle were increased (SDH, +44%; and MDH, +54%) [153, 154]. It is as though reactions after the SUCL step were upregulated in order to remove succinate and shift the equilibrium toward ATP formation, given the diminished succinyl-CoA provision.

ΔΨm values in neurons are far from being static; in physiological conditions, ΔΨm is regulated between -108 and -158 mV by concerted increases in ATP demand and Ca^{2+}-dependent metabolic activation [297], a range that would assign mitochondrial phosphorylation within the A, B, or C space of Fig. 3 (no conditions have been described that are suitable for the D space; see **Chapter 2.6**); the implications of the latter statement is that even under physiological conditions, mitochondria are not only ATP producers, but could also be consumers of ATP arising from the cytosol and/or the matrix, depending on their ΔΨm and matrix ATP/ADP ratio pair of values.

A potential drawback of the work described in **Chapter 5.2** is that succinyl-CoA flux could not be explicitly measured. This is technically extremely challenging; current state-of-the-art isotopomeric analysis would fall short in measuring fluxes of succinyl-CoA [298, 299], but more important, such information would be insufficient unless coupled to another measured parameter with a more profound effect, such as ATP flux across the inner mitochondrial membrane. Therefore, we relied on a biosensor approach, measuring the effect of ANT inhibition of respiration-impaired mitochondria on ΔΨm, during which the organelles are exquisitely dependent on matrix substrate-level phosphorylation [Chinopoulos *et al.* 2010]. It is a great strength of this work that transgenic animals exhibiting 20-62% decrease in KGDHC activity were used, a condition that does not evoke severe metabolic aberrations.

Mindful of the above considerations and the results presented in **Chapter 5.2**, the scenario that could be unfolding in the presence of diminished KGDHC activity is the following: KGDHC exhibits a high flux control coefficient for producing reducing equivalents in the citric acid cycle, also implying that provision of succinyl-CoA would be diminished when the enzyme complex is partially inhibited (especially because metabolism of propionyl-CoA yields only small amounts of succinyl-CoA); in turn, this would lead to a decreased production of ATP in the mitochondrial matrix from substrate-level phosphorylation. This was reflected in the smaller ATP efflux rates in isolated mitochondria from $DLD^{+/-}$, $DLST^{+/-}$ and $DLD^{+/-}/DLST^{+/-}$ double-transgenic mice compared to WT littermates, in the absence of respiratory inhibitors. The diminished production of ATP in the mitochondrial matrix from substrate-level phosphorylation results in a decrease in matrix ATP/ADP ratio, which is also a term in Eq. (6) defining E_{rev_ANT}, thereby shifting its values to the left in the computed graph of

Fig. 3. Since ΔΨm of mitochondria varies within a wide range even under physiological conditions, the likelihood of the organelles becoming extramitochondrial ATP consumers increases with shifting E_{rev_ANT} values toward more negative potentials. The consumption of extramitochondrial ATP by mitochondria of $DLD^{+/-}$, $DLST^{+/-}$ and $DLD^{+/-}/DLST^{+/-}$ double-transgenic mice have been demonstrated; mitochondria were provided with substrates supporting substrate-level phosphorylation, by clamping ΔΨm in a depolarized range due to targeted respiratory inhibition. Using the same substrates and their combinations, consumption of extramitochondrial ATP was not observed in isolated mitochondria of WT mice; likewise, cytosolic ATP was consumed by *in situ* neuronal somal mitochondria of $DLD^{+/-}$ and $DLST^{+/-}$, but not WT mice. In addition to the fact that KGDHC-deficient mitochondria exhibit diminished ATP output when fully polarized, excessive reliance of submaximally polarized mitochondria on extramitochondrial ATP poses an overall metabolic stress. This renders the cell less capable of dealing with unrelated circumstantial challenges predisposing to neurodegenerative diseases, as is already shown to occur *in situ* [63, 300], or *in vivo* [156, 158, 159].

6.4 The oxidation of matrix NADH in view of impaired mitochondrial respiration

The generation of high-energy phosphates independently from respiratory chain operation through matrix substrate-level phosphorylation is attributed almost entirely to SUCL. As it is a reversible reaction, formation of ATP or GTP will happen only if the equilibrium favors succinate production and succinyl-CoA is readily available. Succinyl-CoA may arise from either propionyl-CoA metabolism or KGDHC; provision of succinyl-CoA through KGDHC is much higher than that from propionyl-CoA metabolism [13]. According to Fig. 10, for KGDHC to operate, the inputs of CoASH, α-ketoglutarate, and NAD^+ are necessary. α-ketoglutarate may arise from either isocitrate – by the IDH reaction – or from glutamate, an amino acid that is abundant in at least two pools in the central nervous system [301]. CoASH will re-emerge from SUCL if the equilibrium favors ATP or GTP production [302]. Therefore, the key ingredient is NAD^+. Whatever the source of NAD^+ is, the continuous operation of KGDHC will supply SUCL with succinyl-CoA, which will generate high-energy phosphates and succinate. The reaction proceeds even in the absence of oxygen and perhaps under these

conditions with a higher rate, because hypoxia activates the enzyme [102]. Relevant to this, considerable body of evidence points out that conversion of α-ketoglutarate to succinate indeed occurs in hypoxia, implying SUCL and therefore, KGDHC operability (for references, see **Chapter 6.3**). The high-energy phosphates emerging for the SUCL reaction will support the hydrolytic function of the reverse operating F_O-F_1 ATP synthase during anoxic conditions, which thus will be able to maintain a suboptimal ΔΨm [303, 304]. Succinyl-CoA provision by KGDHC will shift the SUCL reaction equilibrium in the direction of ATP (or GTP) generation in the mitochondrial matrix; and will eventually lead to an increase of their local concentration, thereby maintaining E_{rev_ANT} in the B space (see Fig. 3), where it will prevent ANT from reversing, sparing the extramitochondrial ATP pools from mitochondrial consumption when the respiratory chain becomes inoperable (see **Chapters 2.6**-**2.8** and **2.10**).

From considerations above as well as in **Chapters 5.2** and **6.3** the question arises as to which metabolic pathway(s) could provide NAD^+ for KGDHC during impaired respiration, when the respiratory chain is dysfunctional and complex I cannot oxidize NADH. Of course, a rotenone-mediated block in complex I can be bypassed by succinate or α-glycerophosphate [305], substrates that generate $FADH_2$; however, succinate disfavors substrate-level phosphorylation by the reversible SUCL due to mass action, while α-glycerophosphate (provided that the mitochondrial α-glycerophosphate dehydrogenase activity is sufficiently high [306]) steals endogenous ubiquinones from the diaphorases. Mitochondrial diaphorases and a finite pool of oxidizable quinones were considered in this thesis as potential sources of NAD^+ generated within the mitochondrial matrix during ceased respiration caused by anoxia or poisons of the respiratory chain (Fig. 32).

The results presented in **Chapter 5.3** support the notion that a mitochondrial diaphorase, likely encoded by the *NQO1* gene [170, 307], mediates NAD^+ regeneration in the mitochondrial matrix during respiratory arrest by anoxia or inhibition of complex I by rotenone. Inexorably, the classic diaphorase inhibitor dicoumarol [170, 188, 191] suffers from potential specificity problems, in that it acts as a mitochondrial uncoupler [240] in addition to inhibiting other enzymes, such as NADH:cytochrome *b*5 reductase [308]. The cATR-induced effects on ΔΨm have been compared in mitochondria during respiratory arrest by rotenone or anoxia from WT *vs.* Cyb5r2$^{-/-}$ KO mice (**Chapter 4.1**),

and the results were indistinguishable (not shown). Furthermore, dicoumarol and other diaphorase inhibitors were titrated and used at concentrations at which their uncoupling activity was negligible. Finally, none of the diaphorase inhibitors nor any of the diaphorase substrates had an effect on pigeon liver mitochondria, where DT-diaphorase activity was absent [253, 254]. On the other hand, pigeon liver mitochondria did show robust cATR-induced repolarizations during respiratory arrest, pointing to alternative mechanisms for providing NAD^+ in the matrix. The absence of diaphorase activity in pigeon liver is not surprising; 1-4% of the human population exhibit a polymorphic version of NQO1 that deprives them of NAD(P)H:quinone oxidoreductase activity [309]. It may well be that pigeons exhibit the same or a similar polymorphic version of NQO in a much higher percentage of their population.

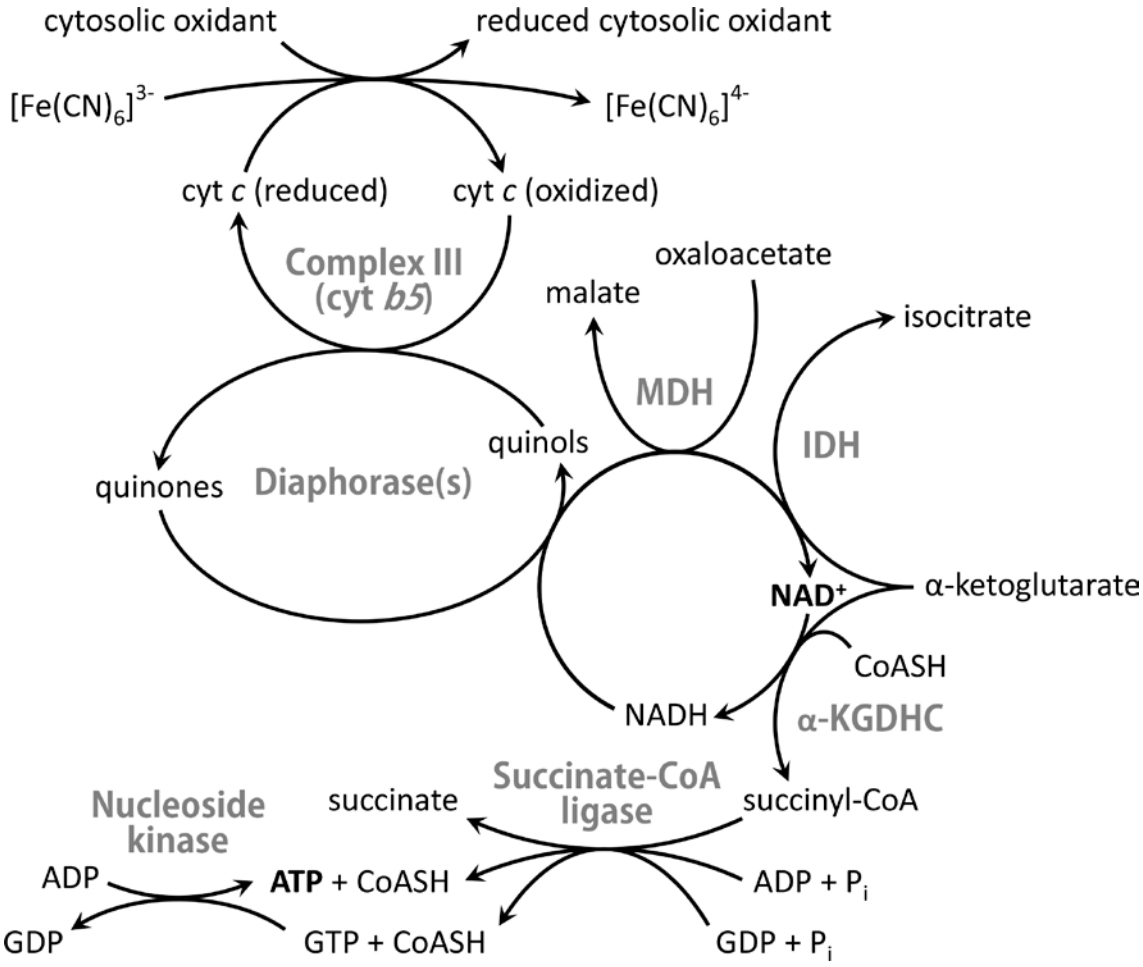

Figure 32. Illustration of the pathway linking ATP production by the SUCL reaction to KGDHC activity, reversed IDH and MDH activity, diaphorase activity, re-oxidation of diaphorase substrates by complex III, re-oxidation of cytochrome *c*, and re-reduction of a cytosolic oxidant. ↑

The pathways responsible for providing oxidized substrates to the diaphorases were also sought. Although various CoQ analogues are maintained in reduced form by the DT-diaphorase [310], their availability is finite [311] and is likely to require a means of re-oxidation. Such a pathway has been demonstrated in the mitochondrial matrix; even in the earlier publication by Conover and Ernster [186], it was noted that electrons provided by diaphorase substrates enter the respiratory chain at the level of cytochrome *b*, which belongs to complex III. Later on, this concept was entertained by the group of Iaguzhinskii [246, 247, 312, 313], which examined the stimulatory effect of various diaphorase substrates during cyanide-resistant respiration of isolated mitochondria. Consistent with this, protection in an ischemia model by menadione was abolished by the complex III inhibitor myxothiazol [314]. In the same line of investigation, the cytotoxicity caused by complex I inhibition by rotenone, but not that caused by complex III inhibition by antimycin, was prevented by CoQ_1 or menadione [315]. Furthermore, also consistent with the substrate selectivity of NQOs in HepG2 cells where NQO1 expression is very high [316], both idebenone and CoQ_1, but not CoQ_{10}, partially restored cellular ATP levels under conditions of impaired complex I function, in an antimycin-sensitive manner [252]. Cytoprotection by rotenone but not antimycin by CoQ_1, mediated by NQO1, has also been shown in primary hepatocytes [315] and lymphocytes [245]. Menadione has even been shown to support mitochondrial respiration with an inhibited complex I but not complex III before DT-diaphorase was identified [187]. This was later confirmed to occur through oxidation of NADH by the intramitochondrial DT-diaphorase [186]. The experimental results in **Chapter 5.3** clearly show that the re-oxidation of substrates being used by the diaphorases for generation of NAD^+ during respiratory arrest by rotenone or anoxia is mediated by complex III. In the process, complex III oxidizes cytochrome *c* (Fig. 32). Therefore, the finiteness of the reducible amount of cytochrome *c* would contribute to the finiteness of the oxidizable pool of diaphorase substrates. Indeed, addition of ferricyanide led to cATR-induced repolarization in the presence of complex IV inhibition by cyanide, but not in the presence of complex III inhibition by stigmatellin. However, the question arises, as to what could oxidize cytochrome *c* naturally, when oxygen is not available. An attractive candidate is p66Shc, a protein residing in the intermembrane space of mitochondria [317, 318], which is known to oxidize cytochrome *c* [317].

In summary, the results described in **Chapter 5.3** point to the importance of mitochondrial diaphorases in providing NAD^+ for the KGDHC during anoxia, yielding succinyl-CoA, which in turn supports ATP production through substrate-level phosphorylation. In addition, the realization of diaphorases as NAD^+ providers renders them a likely target for cancer prevention, as they may be the means of energy harnessing in solid tumors with anoxic/hypoxic centers. Finally, since diaphorases are upregulated by dietary nutrients such as sulforaphane [319] through the Nrf2 pathway [320] and a gamut of dietary elements, mainly quinones of plant origin, are substrates for this enzyme [321], this may be a convenient way to increase the matrix NAD^+/NADH ratios that play a role in the activation of the mitochondrial NAD^+-dependent deacetylase sirtuin-3 [322], a major metabolic sensor.

6.5 On which ATP pool do depolarized *in situ* mitochondria rely?

From the considerations proposed throughout this thesis the hypothesis is tendered that respiration-impaired depolarized mitochondria cannot deplete cytosolic ATP levels, based on the fact that upon reversal of F_O-F_1 ATP synthase, $\Delta\Psi m$ is generated to a level similar to that of E_{rev_ANT}, thereby preventing the ANT from maintaining a forceful import of cytosolic ATP to mitochondria (see **Chapter 2.8**). A feasible way for yielding appreciable ANT reversal rates is to depolarize mitochondria further. Paradoxically, in tissues where the endogenous inhibitor, IF1 is expressed, further depolarization can be achieved by blocking the reverse function of the $\Delta\Psi m$-generating F_O-F_1 ATP synthase. But in this case, F_1-ATPase activity is decreased by IF1 and the extent of this block increases with increasing matrix [ATP] and decreasing $\Delta\Psi m$ (see **Chapter 2.3**). ATP imported from the cytosol is spared from hydrolysis by the F_1-ATPase and it is ensured to return to the cytosol because during repolarization (whenever possible), E_{rev_ANT} is less negative than E_{rev_ATPase}. Therefore, the ANT would expel matrix ATP before the uninhibited F_1-ATPase seizes the opportunity to hydrolyze it (see **Chapter 6.2**).

In line with the theoretical considerations above accompanied with supporting results presented in my thesis, earlier findings showing that inhibition of the respiratory chain of *in situ* mitochondria failed to induce a drop in cytosolic [ATP] levels can now be explained [323-326]. Subsequent application of uncouplers led to unquestionable decreases in cytosolic [ATP], as this is expected to induce high reversal rates of the ANT [323]. Limited consumption of cytosolic ATP by *in situ* mitochondria is also

assisted by the fact that when mitochondrial respiration becomes impaired, cells maintain cellular ATP by relying on glycolysis, leading to a buildup of lactate that decreases intracellular pH. This drop in pH impairs the activity of the ANT [42] and F_O-F_1 ATP synthase [327] in addition to affecting the concentrations of deprotonated ATP and ADP [62]. All of these effects decrease the ability of mitochondria to consume ATP. Furthermore, in human cells lacking mitochondrial DNA, therefore being unable to carry out oxidative phosphorylation [328], the maximum ΔΨm value attainable *in situ* was found to be in the range of -110 to -67 mV [329], in agreement to the E_{rev_ANT} value predicted in **Chapter 2.6**. In the same cells it was also deduced that only 13% of the ATP produced by glycolysis was sufficient to maintain ΔΨm [329]. Still, for *in situ* mitochondria of other cell types or even whole organs there is plenty of evidence for cytosolic ATP consumption in various pathologic paradigms [2, 6, 7, 54, 213, 330]. Apparently, there must be conditions pertaining *in situ* that counter the principles elaborated in this thesis; future efforts should be directed towards their identification.

6.6 Closing remarks

Before the publication of Chinopoulos *et al.* 2010, mitochondria had been unanimously convicted as ATP consumers in diverse pathologies. It is beyond question that if these conditions involve i) robust uncoupling, ii) abolishment of the inner mitochondrial membrane integrity or iii) any other circumstances characterized by dissipated *pmf*, F_1-ATPase will indiscriminately hydrolyze all ATP pools in the cell as those become readily accessible to the enzyme. However, in respiration-impaired mitochondria with intact inner mitochondrial membranes, if ATP hydrolysis by F_1-ATPase is supplied by matrix substrate-level phosphorylation, the situation becomes different in a way that ΔΨm will be sustained at a value more negative than that of E_{rev_ANT}. This ensures that only matrical ATP reserves are available for F_1-ATPase to hydrolyze and those outside mitochondria are spared. On the contrary, in order to access the cytosolic ATP reserves as well, the conditions must allow the ΔΨm value to exceed that of E_{rev_ANT}. Yet, even in this case, potential-generating actions of reversed F_O-F_1 ATP synthase and ANT will allow only limited ATP influx rates through the translocase. In the end, ΔΨm seems to be the dominant factor in determining whether a mitochondrion with intact membranes will produce or consume ATP: eventually deciding the fate of the harboring cell.

DOI:10.14753/SE.2015.1713

7. CONCLUSION

The results elaborated throughout my thesis clearly indicate that in case of impaired mitochondrial respiration or submaximal uncoupling, mitochondria not only withstand to consume extramitochondrial ATP, but may even continue to export it. This is possible because the F_O-F_1 ATP synthase is able to operate in reverse mode without the concomitant reversal of the ANT. Under these circumstances matrix substrate-level phosphorylation – almost exclusively attributed to SUCL – plays a critical role in supplying ATP for the reversed F_O-F_1 ATP synthase, therefore it can be interpreted as an endogenous fail safe mechanism, with the benefit of clamping $\Delta\Psi m$ at a level just enough to prevent ANT reversal. The resultant prevention of cytosolic ATP consumption by dysfunctional mitochondria may mean the difference between life and death for the harboring cell.

SUCL does not require oxygen for ATP production and it is even activated during hypoxia, providing ATP parallel to that by oxidative phosphorylation. Adequate succinyl-CoA provision through KGDHC thus dissociates mitochondria with a dysfunctional respiratory chain from extramitochondrial ATP dependence. Relevant to this, in anoxia there is pronounced conversion of α-ketoglutarate to succinate, implying KGDHC operability. However, the question arises as to which metabolic pathway(s) could provide NAD^+ for KGDHC during impaired respiration, when complex I cannot oxidize NADH. Potential sources of NAD^+ generated within the mitochondrial matrix during respiratory arrest are considered in my thesis and the final conclusion is drawn that mitochondrial diaphorases are the major contributors.

CYPD binds to the F_O-F_1 ATP synthase decreasing both ATP synthesis and hydrolysis rates. However, as a result of the imposing role of the ANT, this is not reflected in the extramitochondrial compartment. The modulation of F_O-F_1 ATP synthase activity by CYPD rather represents a means of regulating the matrix ATP/ADP ratio, influencing the reversal potentials of both ANT and F_O-F_1 ATP synthase.

DOI:10.14753/SE.2015.1713

8.1 SUMMARY

Substrate-level phosphorylation in the mitochondrial matrix is the only means for production of high-energy phosphates when the respiratory chain is impaired or in the absence of oxygen. Mitochondrial substrate-level phosphorylation is almost exclusively attributed to succinate-CoA ligase, an enzyme of the citric acid cycle which catalyzes the reversible conversion of succinyl-CoA and ADP (or GDP) to CoASH, succinate and ATP (or GTP). This thesis is based upon the concept that when the respiratory chain is compromised and F_O-F_1 ATP synthase reverses, pumping protons out of the matrix at the expense of ATP hydrolysis, the mitochondrial membrane potential is maintained – albeit at decreased levels – for as long as matrix substrate-level phosphorylation is operational, without a concomitant reversal of the adenine nucleotide translocase (ANT). This prevents mitochondria from becoming cytosolic ATP consumers. One of our recent publications show that cyclophilin D (CYPD) – a ubiquitous protein in the matrix – interacts with and regulates the F_O-F_1 ATP synthase in intact mitochondria: CYPD binding results in decelerated ATP synthesis and hydrolysis rates. The CYPD-F_O-F_1 ATP synthase interaction represents an "in-house" mechanism of regulating matrix adenine nucleotide levels, which is not reflected in the extramitochondrial compartment due to the presence of the ANT. It has been reported by our group that provision of succinyl-CoA by the α-ketoglutarate dehydrogenase complex (KGDHC) in respiration-impaired mitochondria is critical for sustained operation of the succinate-CoA ligase reaction. Mindful of the reaction catalyzed by KGDHC converting α-ketoglutarate, CoASH and NAD^+ to succinyl-CoA, NADH and CO_2, the question arises as to the source of NAD^+, under conditions of dysfunctional respiratory chain. It is a textbook definition that NADH generated in the citric acid cycle is oxidized by complex I, resupplying NAD^+ to the cycle. In the absence of oxygen or when complexes are not functional, an excess of NADH in the matrix is expected. Yet, our previous reports demonstrated that without NADH oxidation by complex I of the respiratory chain, substrate-level phosphorylation was operational and supported by succinyl-CoA, implying KGDHC activity. Our latest results support the notion that during anoxia or pharmacological blockade of complex I, mitochondrial diaphorases oxidized matrix NADH supplying NAD^+ to KGDHC, which in turn yielded succinyl-CoA supporting substrate-level phosphorylation catalyzed by succinate-CoA ligase.

DOI:10.14753/SE.2015.1713

8.2 ÖSSZEFOGLALÁS

A légzési lánc működési hibája vagy oxigénhiány esetén a “magas energiájú” foszfátvegyületek előállításának egyetlen módja a szubsztrátszintű foszforiláció a mitokondriális mátrixban. Itt a szubsztrátszintű foszforiláció szinte kizárólagosan a citrátköri szukcinát-KoA ligáznak tulajdonítható, mely enzim a szukcinil-KoA és ADP (vagy GDP) átalakulását katalizálja koenzim A-vá, szukcináttá és ATP-vé (vagy GTP-vé). Tézisem azon az elképzelésen alapszik, hogy mikor a légzési lánc leáll és az F_O-F_1 ATP szintáz megfordulva protonokat pumpál ki a mátrixból ATP hidrolízis terhére, a mitokondriális membránpotenciált ezzel csökkent mértékben ugyan, de mindaddig fenntartja, amíg szubsztrátszintű foszforiláció zajlik a mátrixban; így megakadályozza az adenin nukleotid transzlokáz (ANT) megfordulását és a mitokondriumok nem válnak ATP fogyasztókká. Korábbi közleményünk szerint a mitokondriális mátrixban jelen lévő ciklofilin D (CYPD) kölcsönhat az F_O-F_1 ATP szintázzal és szabályozza annak működését ép mitokondriumokban: a CYPD kötődése az ATP szintézis és hidrolízis sebességét egyaránt csökkenti. A CYPD-F_O-F_1 ATP szintáz kölcsönhatás a mátrixbeli adenin nukleotidok szintjének egy olyan belső szabályozó mechanizmusát képviseli, mely az ANT jelenléte miatt nem realizálódik az extramitokondriális közegben. A közelmúltban arról számoltunk be, hogy az α-ketoglutarát dehidrogenáz komplex (KGDHC) szukcinil-KoA termelése légzésükben gátolt mitokondriumokban alapvető fontosságú a szukcinát-KoA ligáz katalizálta reakció fenntartása szempontjából. Mivel az KGDHC reakció során az α-ketoglutarátból, koenzim A-ból és NAD^+-ból szukcinil-KoA, NADH és CO_2 keletkezik, felvetődik a kérdés: vajon mi a NAD^+ forrása abban az esetben, ha a légzési lánc nem működik? Tankönyvi definíció szerint a citrátkörben keletkező NADH-t a komplex I oxidálja, így látva el NAD^+-dal a ciklust. Oxigén hiányában, vagy ha a légzési komplexek működésképtelenek, a mátrixban NADH többlet várható. Mégis, korábban közölt eredményeink azt mutatták, hogy az első légzési komplex NADH oxidációja nélkül is folyik szubsztrátszintű foszforiláció, és szukcinil-KoA ellátása zavartalan marad, igazolva az KGDHC működését. Legutóbbi kísérleti eredményeink alátámasztják azon feltevésünket, miszerint oxigén hiányában vagy a komplex I gátlása során mitokondriális diaforázok oxidálják a NADH-t NAD^+-dá a mátrixban az KGDHC számára, mely így szukcinil-KoA-t képes előállítani a szukcinát-KoA ligáz katalizálta szubsztrátszintű foszforilációhoz.

9. REFERENCES

1. Siekevitz P. (1957) Powerhouse of the cell. Scientific American, 197: 131-144.

2. Chinopoulos C, Adam-Vizi V. (2010) Mitochondria as ATP consumers in cellular pathology. Biochim Biophys Acta, 1802: 221-227.

3. Brookes PS, Yoon Y, Robotham JL, Anders MW, Sheu SS. (2004) Calcium, ATP, and ROS: a mitochondrial love-hate triangle. Am J Physiol Cell Physiol, 287: C817-833.

4. Jacobson J, Duchen MR. (2001) 'What nourishes me, destroys me': towards a new mitochondrial biology. Cell Death Differ, 8: 963-966.

5. Chinopoulos C. (2011) Mitochondrial consumption of cytosolic ATP: not so fast. FEBS Lett, 585: 1255-1259.

6. Grover GJ, Atwal KS, Sleph PG, Wang FL, Monshizadegan H, Monticello T, Green DW. (2004) Excessive ATP hydrolysis in ischemic myocardium by mitochondrial F1F0-ATPase: effect of selective pharmacological inhibition of mitochondrial ATPase hydrolase activity. Am J Physiol Heart Circ Physiol, 287: H1747-1755.

7. McKenzie M, Liolitsa D, Akinshina N, Campanella M, Sisodiya S, Hargreaves I, Nirmalananthan N, Sweeney MG, Abou-Sleiman PM, Wood NW, Hanna MG, Duchen MR. (2007) Mitochondrial ND5 gene variation associated with encephalomyopathy and mitochondrial ATP consumption. J Biol Chem, 282: 36845-36852.

8. Krieger C, Duchen MR. (2002) Mitochondria, Ca2+ and neurodegenerative disease. Eur J Pharmacol, 447: 177-188.

9. Nicholls DG, Budd SL. (2000) Mitochondria and neuronal survival. Physiol Rev, 80: 315-360.

10. Duchen MR. (2004) Mitochondria in health and disease: perspectives on a new mitochondrial biology. Mol Aspects Med, 25: 365-451.

11. Nicholls DG, Ferguson SSJ. Bioenergetics 3. Academic Press, London, 2002: 57-88.

12. Ebbing DD, Gammon SD. General chemistry. Houghton Mifflin Company, Boston, 2009: 144-153.

13. Nelson DL, Cox MM. Lehninger Principles of Biochemistry. W. H. Freeman and Company, New York, 2008: 647-772.

14. Brand MD, Nicholls DG. (2011) Assessing mitochondrial dysfunction in cells. Biochem J, 435: 297-312.

15. Veech RL, Gitomer WL, King MT, Balaban RS, Costa JL, Eanes ED. (1986) The effect of short chain fatty acid administration on hepatic glucose, phosphate, magnesium and calcium metabolism. Adv Exp Med Biol, 194: 617-646.

16. Klingenberg M, Rottenberg H. (1977) Relation between the gradient of the ATP/ADP ratio and the membrane potential across the mitochondrial membrane. Eur J Biochem, 73: 125-130.

17. Brand MD. (1990) The proton leak across the mitochondrial inner membrane. Biochim Biophys Acta, 1018: 128-133.

18. Krauss S, Zhang CY, Lowell BB. (2005) The mitochondrial uncoupling-protein homologues. Nat Rev Mol Cell Biol, 6: 248-261.

19. Rolfe DF, Brand MD. (1997) The physiological significance of mitochondrial proton leak in animal cells and tissues. Biosci Rep, 17: 9-16.

20. Jastroch M, Divakaruni AS, Mookerjee S, Treberg JR, Brand MD. (2010) Mitochondrial proton and electron leaks. Essays Biochem, 47: 53-67.

21. Murphy MP. (1989) Slip and leak in mitochondrial oxidative phosphorylation. Biochim Biophys Acta, 977: 123-141.

22. Brown GC. (1992) The leaks and slips of bioenergetic membranes. FASEB J, 6: 2961-2965.

23. Nicholls DG, Rial E. (1999) A history of the first uncoupling protein, UCP1. J Bioenerg Biomembr, 31: 399-406.

24. Brand MD, Esteves TC. (2005) Physiological functions of the mitochondrial uncoupling proteins UCP2 and UCP3. Cell Metab, 2: 85-93.

25. Nedergaard J, Ricquier D, Kozak LP. (2005) Uncoupling proteins: current status and therapeutic prospects. EMBO Rep, 6: 917-921.

26. Kim-Han JS, Dugan LL. (2005) Mitochondrial uncoupling proteins in the central nervous system. Antioxid Redox Signal, 7: 1173-1181.

27. Terada H. (1990) Uncouplers of oxidative phosphorylation. Environ Health Perspect, 87: 213-218.

28. Gnaiger E. (2009) Capacity of oxidative phosphorylation in human skeletal muscle: new perspectives of mitochondrial physiology. Int J Biochem Cell Biol, 41: 1837-1845.

29. Brand MD, Murphy MP. (1987) Control of electron flux through the respiratory chain in mitochondria and cells. Biol Rev Camb Philos Soc, 62: 141-193.

30. Chance B, Williams GR, Holmes WF, Higgins J. (1955) Respiratory enzymes in oxidative phosphorylation. V. A mechanism for oxidative phosphorylation. J Biol Chem, 217: 439-451.

31. Chance B, Williams GR. (1955) A method for the localization of sites for oxidative phosphorylation. Nature, 176: 250-254.

32. Chance B, Williams GR. (1955) Respiratory enzymes in oxidative phosphorylation. IV. The respiratory chain. J Biol Chem, 217: 429-438.

33. Chance B, Williams GR. (1955) Respiratory enzymes in oxidative phosphorylation. III. The steady state. J Biol Chem, 217: 409-427.

34. Chance B, Williams GR. (1955) Respiratory enzymes in oxidative phosphorylation. II. Difference spectra. J Biol Chem, 217: 395-407.

35. Chance B, Williams GR. (1955) Respiratory enzymes in oxidative phosphorylation. I. Kinetics of oxygen utilization. J Biol Chem, 217: 383-393.

36. Chance B, Williams GR. (1956) The respiratory chain and oxidative phosphorylation. Adv Enzymol Relat Subj Biochem, 17: 65-134.

37. Chance B, Williams GR. (1956) Respiratory enzymes in oxidative phosphorylation. VI. The effects of adenosine diphosphate on azide-treated mitochondria. J Biol Chem, 221: 477-489.

38. Estabrook RW. Mitochondrial respiratory control and the polarographic measurement of ADP : O ratios. In: Estabrook RW, Pullman ME. (ed.), Methods in Enzymology Vol. 10. Oxidation and Phosphorylation. Academic Press, Burlington, 1967: 41-47.

39. Scandurra FM, Gnaiger E. (2010) Cell respiration under hypoxia: facts and artefacts in mitochondrial oxygen kinetics. Adv Exp Med Biol, 662: 7-25.

40. Chance B, Williams GR. (1955) A simple and rapid assay of oxidative phosphorylation. Nature, 175: 1120-1121.

41. Slater EC, Rosing J, Mol A. (1973) The phosphorylation potential generated by respiring mitochondria. Biochim Biophys Acta, 292: 534-553.

42. Chinopoulos C, Vajda S, Csanady L, Mandi M, Mathe K, Adam-Vizi V. (2009) A novel kinetic assay of mitochondrial ATP-ADP exchange rate mediated by the ANT. Biophys J, 96: 2490-2504.

43. Boyer PD, Cross RL, Momsen W. (1973) A new concept for energy coupling in oxidative phosphorylation based on a molecular explanation of the oxygen exchange reactions. Proc Natl Acad Sci U S A, 70: 2837-2839.

44. Feniouk BA, Yoshida M. (2008) Regulatory mechanisms of proton-translocating F(O)F (1)-ATP synthase. Results Probl Cell Differ, 45: 279-308.

45. Acin-Perez R, Salazar E, Kamenetsky M, Buck J, Levin LR, Manfredi G. (2009) Cyclic AMP produced inside mitochondria regulates oxidative phosphorylation. Cell Metab, 9: 265-276.

46. Acin-Perez R, Hoyos B, Gong J, Vinogradov V, Fischman DA, Leitges M, Borhan B, Starkov A, Manfredi G, Hammerling U. (2010) Regulation of intermediary metabolism by the PKCdelta signalosome in mitochondria. FASEB J, 24: 5033-5042.

47. Belogrudov GI. (2009) Recent advances in structure-functional studies of mitochondrial factor B. J Bioenerg Biomembr, 41: 137-143.

48. Pullman ME, Monroy GC. (1963) A naturally occurring inhibitor of mitochondrial adenosine triphosphatase. J Biol Chem, 238: 3762-3769.

49. Strauss M, Hofhaus G, Schroder RR, Kuhlbrandt W. (2008) Dimer ribbons of ATP synthase shape the inner mitochondrial membrane. EMBO J, 27: 1154-1160.

50. Campanella M, Casswell E, Chong S, Farah Z, Wieckowski MR, Abramov AY, Tinker A, Duchen MR. (2008) Regulation of mitochondrial structure and function by the F1Fo-ATPase inhibitor protein, IF1. Cell Metab, 8: 13-25.

51. Bisetto E, Di Pancrazio F, Simula MP, Mavelli I, Lippe G. (2007) Mammalian ATPsynthase monomer versus dimer profiled by blue native PAGE and activity stain. Electrophoresis, 28: 3178-3185.

52. Rouslin W, Frank GD, Broge CW. (1995) Content and binding characteristics of the mitochondrial ATPase inhibitor, IF1, in the tissues of several slow and fast heart-rate homeothermic species and in two poikilotherms. J Bioenerg Biomembr, 27: 117-125.

53. Rouslin W, Broge CW. (1996) IF1 function in situ in uncoupler-challenged ischemic rabbit, rat, and pigeon hearts. J Biol Chem, 271: 23638-23641.

54. Campanella M, Parker N, Tan CH, Hall AM, Duchen MR. (2009) IF(1): setting the pace of the F(1)F(o)-ATP synthase. Trends Biochem Sci, 34: 343-350.

55. Schwerzmann K, Pedersen PL. (1981) Proton-adenosinetriphosphatase complex of rat liver mitochondria: effect of energy state on its interaction with the adenosinetriphosphatase inhibitory peptide. Biochemistry, 20: 6305-6311.

56. Lippe G, Sorgato MC, Harris DA. (1988) The binding and release of the inhibitor protein are governed independently by ATP and membrane potential in ox-heart submitochondrial vesicles. Biochim Biophys Acta, 933: 12-21.

57. Lippe G, Sorgato MC, Harris DA. (1988) Kinetics of the release of the mitochondrial inhibitor protein. Correlation with synthesis and hydrolysis of ATP. Biochim Biophys Acta, 933: 1-11.

58. Rouslin W, Broge CW. (1993) Factors affecting the species-homologous and species-heterologous binding of mitochondrial ATPase inhibitor, IF1, to the mitochondrial ATPase of slow and fast heart-rate hearts. Arch Biochem Biophys, 303: 443-450.

59. Giorgio V, Bisetto E, Soriano ME, Dabbeni-Sala F, Basso E, Petronilli V, Forte MA, Bernardi P, Lippe G. (2009) Cyclophilin D modulates mitochondrial F0F1-ATP synthase by interacting with the lateral stalk of the complex. J Biol Chem, 284: 33982-33988.

60. Giorgio V, von Stockum S, Antoniel M, Fabbro A, Fogolari F, Forte M, Glick GD, Petronilli V, Zoratti M, Szabo I, Lippe G, Bernardi P. (2013) Dimers of mitochondrial ATP synthase form the permeability transition pore. Proc Natl Acad Sci U S A, 110: 5887-5892.

61. Wang P, Heitman J. (2005) The cyclophilins. Genome Biol, 6: 226.

62. Metelkin E, Demin O, Kovacs Z, Chinopoulos C. (2009) Modeling of ATP-ADP steady-state exchange rate mediated by the adenine nucleotide translocase in isolated mitochondria. FEBS J, 276: 6942-6955.

63. Chinopoulos C, Tretter L, Adam-Vizi V. (1999) Depolarization of in situ mitochondria due to hydrogen peroxide-induced oxidative stress in nerve terminals: inhibition of alpha-ketoglutarate dehydrogenase. J Neurochem, 73: 220-228.

64. Nury H, Dahout-Gonzalez C, Trezeguet V, Lauquin GJ, Brandolin G, Pebay-Peyroula E. (2006) Relations between structure and function of the mitochondrial ADP/ATP carrier. Annu Rev Biochem, 75: 713-741.

65. Pebay-Peyroula E, Brandolin G. (2004) Nucleotide exchange in mitochondria: insight at a molecular level. Curr Opin Struct Biol, 14: 420-425.

66. Palmieri F. (2004) The mitochondrial transporter family (SLC25): physiological and pathological implications. Pflugers Arch, 447: 689-709.

67. Dolce V, Scarcia P, Iacopetta D, Palmieri F. (2005) A fourth ADP/ATP carrier isoform in man: identification, bacterial expression, functional characterization and tissue distribution. FEBS Lett, 579: 633-637.

68. Dahout-Gonzalez C, Nury H, Trezeguet V, Lauquin GJ, Pebay-Peyroula E, Brandolin G. (2006) Molecular, functional, and pathological aspects of the mitochondrial ADP/ATP carrier. Physiology (Bethesda), 21: 242-249.

69. Faustin B, Rossignol R, Rocher C, Benard G, Malgat M, Letellier T. (2004) Mobilization of adenine nucleotide translocators as molecular bases of the biochemical threshold effect observed in mitochondrial diseases. J Biol Chem, 279: 20411-20421.

70. Klingenberg M. (2008) The ADP and ATP transport in mitochondria and its carrier. Biochim Biophys Acta, 1778: 1978-2021.

71. Brand MD, Pakay JL, Ocloo A, Kokoszka J, Wallace DC, Brookes PS, Cornwall EJ. (2005) The basal proton conductance of mitochondria depends on adenine nucleotide translocase content. Biochem J, 392: 353-362.

72. Zoratti M, Szabo I. (1995) The mitochondrial permeability transition. Biochim Biophys Acta, 1241: 139-176.

73. Kokoszka JE, Waymire KG, Levy SE, Sligh JE, Cai J, Jones DP, MacGregor GR, Wallace DC. (2004) The ADP/ATP translocator is not essential for the mitochondrial permeability transition pore. Nature, 427: 461-465.

74. Marzo I, Brenner C, Zamzami N, Jurgensmeier JM, Susin SA, Vieira HL, Prevost MC, Xie Z, Matsuyama S, Reed JC, Kroemer G. (1998) Bax and adenine nucleotide translocator cooperate in the mitochondrial control of apoptosis. Science, 281: 2027-2031.

75. Watt IN, Montgomery MG, Runswick MJ, Leslie AG, Walker JE. (2010) Bioenergetic cost of making an adenosine triphosphate molecule in animal mitochondria. Proc Natl Acad Sci U S A, 107: 16823-16827.

76. Senior AE, Nadanaciva S, Weber J. (2002) The molecular mechanism of ATP synthesis by F1F0-ATP synthase. Biochim Biophys Acta, 1553: 188-211.

77. Van Dop C, Hutson SM, Lardy HA. (1977) Pyruvate metabolism in bovine epididymal spermatozoa. J Biol Chem, 252: 1303-1308.

78. Hutson SM, Van Dop C, Lardy HA. (1977) Mitochondrial metabolism of pyruvate in bovine spermatozoa. J Biol Chem, 252: 1309-1315.

79. Aprille JR. (1993) Mechanism and regulation of the mitochondrial ATP-Mg/P(i) carrier. J Bioenerg Biomembr, 25: 473-481.

80. Chinopoulos C. (2011) The “B space” of mitochondrial phosphorylation. J Neurosci Res, 89: 1897-1904.

81. Wu F, Zhang EY, Zhang J, Bache RJ, Beard DA. (2008) Phosphate metabolite concentrations and ATP hydrolysis potential in normal and ischaemic hearts. J Physiol, 586: 4193-4208.

82. Tomashek JJ, Brusilow WS. (2000) Stoichiometry of energy coupling by proton-translocating ATPases: a history of variability. J Bioenerg Biomembr, 32: 493-500.

83. Cross RL, Muller V. (2004) The evolution of A-, F-, and V-type ATP synthases and ATPases: reversals in function and changes in the H+/ATP coupling ratio. FEBS Lett, 576: 1-4.

84. Duchen MR, Leyssens A, Crompton M. (1998) Transient mitochondrial depolarizations reflect focal sarcoplasmic reticular calcium release in single rat cardiomyocytes. J Cell Biol, 142: 975-988.

85. O’Reilly CM, Fogarty KE, Drummond RM, Tuft RA, Walsh JV, Jr. (2003) Quantitative analysis of spontaneous mitochondrial depolarizations. Biophys J, 85: 3350-3357.

86. Gerencser AA, Adam-Vizi V. (2005) Mitochondrial Ca2+ dynamics reveals limited intramitochondrial Ca2+ diffusion. Biophys J, 88: 698-714.

87. Mannella CA, Pfeiffer DR, Bradshaw PC, Moraru, II, Slepchenko B, Loew LM, Hsieh CE, Buttle K, Marko M. (2001) Topology of the mitochondrial inner membrane: dynamics and bioenergetic implications. IUBMB Life, 52: 93-100.

88. Demin OV, Westerhoff HV, Kholodenko BN. (1998) Mathematical modelling of superoxide generation with the bc1 complex of mitochondria. Biochemistry (Mosc), 63: 634-649.

89. Demin OV, Gorianin, II, Kholodenko BN, Westerhoff HV. (2001) [Kinetic modeling of energy metabolism and generation of active forms of oxygen in hepatocyte mitochondria]. Mol Biol (Mosk), 35: 1095-1104.

90. Chinopoulos C, Adam-Vizi V. (2010) Mitochondrial Ca2+ sequestration and precipitation revisited. FEBS J, 277: 3637-3651.

91. Kawamata H, Starkov AA, Manfredi G, Chinopoulos C. (2010) A kinetic assay of mitochondrial ADP-ATP exchange rate in permeabilized cells. Anal Biochem, 407: 52-57.

92. Metelkin E, Goryanin I, Demin O. (2006) Mathematical modeling of mitochondrial adenine nucleotide translocase. Biophys J, 90: 423-432.

93. Ottaway JH, McClellan JA, Saunderson CL. (1981) Succinic thiokinase and metabolic control. Int J Biochem, 13: 401-410.

94. Wilson DF, Erecinska M, Schramm VL. (1983) Evaluation of the relationship between the intra- and extramitochondrial [ATP]/[ADP] ratios using phosphoenolpyruvate carboxykinase. J Biol Chem, 258: 10464-10473.

95. Lambeth DO. (2002) What is the function of GTP produced in the Krebs citric acid cycle? IUBMB Life, 54: 143-144.

96. Lambeth DO, Tews KN, Adkins S, Frohlich D, Milavetz BI. (2004) Expression of two succinyl-CoA synthetases with different nucleotide specificities in mammalian tissues. J Biol Chem, 279: 36621-36624.

97. Johnson JD, Mehus JG, Tews K, Milavetz BI, Lambeth DO. (1998) Genetic evidence for the expression of ATP- and GTP-specific succinyl-CoA synthetases in multicellular eucaryotes. J Biol Chem, 273: 27580-27586.

98. Li X, Wu F, Beard DA. (2013) Identification of the kinetic mechanism of succinyl-CoA synthetase. Biosci Rep, 33: 145-163.

99. Kaufman S, Gilvarg C, Cori O, Ochoa S. (1953) Enzymatic oxidation of alpha-ketoglutarate and coupled phosphorylation. J Biol Chem, 203: 869-888.

100. Hamilton ML, Ottaway JH. (1981) An ATP-dependent succinic thiokinase in birds and its relation to ketone-body utilization. FEBS Lett, 123: 252-254.

101. Labbe RF, Kurumada T, Onisawa J. (1965) The role of succinyl-CoA synthetase in the control of heme biosynthesis. Biochim Biophys Acta, 111: 403-415.

102. Phillips D, Aponte AM, French SA, Chess DJ, Balaban RS. (2009) Succinyl-CoA synthetase is a phosphate target for the activation of mitochondrial metabolism. Biochemistry, 48: 7140-7149.

103. Dobolyi A, Ostergaard E, Bago AG, Doczi T, Palkovits M, Gal A, Molnar MJ, Adam-Vizi V, Chinopoulos C. (2013) Exclusive neuronal expression of SUCLA2 in the human brain. Brain Struct Funct, 2013. Oct. 2. [Epub ahead of print].

104. Pisarenko OI, Solomatina ES, Ivanov VE, Studneva IM, Kapelko VI, Smirnov VN. (1985) On the mechanism of enhanced ATP formation in hypoxic myocardium caused by glutamic acid. Basic Res Cardiol, 80: 126-134.

105. Weinberg JM, Venkatachalam MA, Roeser NF, Nissim I. (2000) Mitochondrial dysfunction during hypoxia/reoxygenation and its correction by anaerobic metabolism of citric acid cycle intermediates. Proc Natl Acad Sci U S A, 97: 2826-2831.

106. Holt SJ, Riddle DL. (2003) SAGE surveys C. elegans carbohydrate metabolism: evidence for an anaerobic shift in the long-lived dauer larva. Mech Ageing Dev, 124: 779-800.

107. Kadrmas EF, Ray PD, Lambeth DO. (1991) Apparent ATP-linked succinate thiokinase activity and its relation to nucleoside diphosphate kinase in mitochondrial matrix preparations from rabbit. Biochim Biophys Acta, 1074: 339-346.

108. Kowluru A, Tannous M, Chen HQ. (2002) Localization and characterization of the mitochondrial isoform of the nucleoside diphosphate kinase in the pancreatic beta cell: evidence for its complexation with mitochondrial succinyl-CoA synthetase. Arch Biochem Biophys, 398: 160-169.

109. Sanadi DR, Fluharty AL. (1963) On the mechanism of oxidative phosphorylation. VII. The energy-requiring reduction of pyridine nucleotide by succinate and the energy-yielding oxidation of reduced pyridinenucleotide by fumarate. Biochemistry, 2: 523-528.

110. Chinnery PF. (2007) Mutations in SUCLA2: a tandem ride back to the Krebs cycle. Brain, 130: 606-609.

111. Neely JR, Grotyohann LW. (1984) Role of glycolytic products in damage to ischemic myocardium. Dissociation of adenosine triphosphate levels and recovery of function of reperfused ischemic hearts. Circ Res, 55: 816-824.

112. Ostergaard E. (2008) Disorders caused by deficiency of succinate-CoA ligase. J Inherit Metab Dis, 31: 226-229.

113. Siess EA, Kientsch-Engel RI, Fahimi FM, Wieland OH. (1984) Possible role of Pi supply in mitochondrial actions of glucagon. Eur J Biochem, 141: 543-548.

114. Pisarenko OI. (1996) Mechanisms of myocardial protection by amino acids: facts and hypotheses. Clin Exp Pharmacol Physiol, 23: 627-633.

115. Kushnareva YE, Sokolove PM. (2000) Prooxidants open both the mitochondrial permeability transition pore and a low-conductance channel in the inner mitochondrial membrane. Arch Biochem Biophys, 376: 377-388.

116. Kinnally KW, Antonenko YN, Zorov DB. (1992) Modulation of inner mitochondrial membrane channel activity. J Bioenerg Biomembr, 24: 99-110.

117. Heldt HW. (1970) Differences between the phosphorylation potentials of adenosine triphosphate inside and outside the mitochondria. Biochem J, 116: 15P.

118. Heldt HW, Klingenberg M, Milovancev M. (1972) Differences between the ATP-ADP ratios in the mitochondrial matrix and in the extramitochondrial space. Eur J Biochem, 30: 434-440.

119. Davis EJ, Lumeng L, Bottoms D. (1974) On the relationships between the stoichiometry of oxidative phosphorylation and the phosphorylation potential of rat liver mitochondria as functions of respiratory state. FEBS Lett, 39: 9-12.

120. Davis EJ, Lumeng L. (1974) The effects of palmityl-coenzyme A and atractyloside on the steady-state intra- and extra-mitochondrial phosphorylation potentials generated during ADP-controlled respiration. FEBS Lett, 48: 250-252.

121. Walajtys EI, Gottesman DP, Williamson JR. (1974) Regulation of pyruvate dehydrogenase in rat liver mitochondria by phosphorylation-dephosphorylation. J Biol Chem, 249: 1857-1865.

122. Wieland OH, Portenhauser R. (1974) Regulation of pyruvate-dehydrogenase interconversion in rat-liver mitochondria as related to the phosphorylation state of intramitochondrial adenine nucleotides. Eur J Biochem, 45: 577-588.

123. Vignais PV, Vignais PM, Doussiere J. (1975) Functional relationship between the ADP/ATP-carrier and the F1-ATPase in mitochondria. Biochim Biophys Acta, 376: 219-230.

124. Siess EA, Wieland OH. (1976) Phosphorylation state of cytosolic and mitochondrial adenine nucleotides and of pyruvate dehydrogenase in isolated rat liver cells. Biochem J, 156: 91-102.

125. Shrago E, Ball M, Sul HS, Baquer NZ, McLean P. (1977) Interrelationship in the regulation of pyruvate dehydrogenase and adenine-nucleotide translocase by palmitoyl-CoA in isolated mitochondria. Eur J Biochem, 75: 83-89.

126. Soboll S, Scholz R, Heldt HW. (1978) Subcellular metabolite concentrations. Dependence of mitochondrial and cytosolic ATP systems on the metabolic state of perfused rat liver. Eur J Biochem, 87: 377-390.

127. Letko G, Kuster U, Duszynski J, Kunz W. (1980) Investigation of the dependence of the intramitochondrial [ATP]/[ADP] ratio on the respiration rate. Biochim Biophys Acta, 593: 196-203.

128. Brawand F, Folly G, Walter P. (1980) Relation between extra- and intramitochondrial ATP/ADP ratios in rat liver mitochondria. Biochim Biophys Acta, 590: 285-289.

129. Wanders RJ, Van Woerkom GM, Nooteboom RF, Meijer AJ, Tager JM. (1981) Relationship between the rate of citrulline synthesis and bulk changes in the intramitochondrial ATP/ADP ratio in rat-liver mitochondria. Eur J Biochem, 113: 295-302.

130. Wilson DF, Nelson D, Erecinska M. (1982) Binding of the intramitochondrial ADP and its relationship to adenine nucleotide translocation. FEBS Lett, 143: 228-232.

131. Soboll S, Akerboom TP, Schwenke WD, Haase R, Sies H. (1980) Mitochondrial and cytosolic ATP/ADP ratios in isolated hepatocytes. A comparison of the digitonin method and the non-aqueous fractionation procedure. Biochem J, 192: 951-954.

132. Soboll S, Seitz HJ, Sies H, Ziegler B, Scholz R. (1984) Effect of long-chain fatty acyl-CoA on mitochondrial and cytosolic ATP/ADP ratios in the intact liver cell. Biochem J, 220: 371-376.

133. Schwenke WD, Soboll S, Seitz HJ, Sies H. (1981) Mitochondrial and cytosolic ATP/ADP ratios in rat liver in vivo. Biochem J, 200: 405-408.

134. Pfaff E, Klingenberg M. (1968) Adenine nucleotide translocation of mitochondria. 1. Specificity and control. Eur J Biochem, 6: 66-79.

135. Lusty CJ. (1978) Carbamoylphosphate synthetase I of rat-liver mitochondria. Purification, properties, and polypeptide molecular weight. Eur J Biochem, 85: 373-383.

136. Matlib MA, Shannon WA, Jr., Srere PA. (1977) Measurement of matrix enzyme activity in isolated mitochondria made permeable with toluene. Arch Biochem Biophys, 178: 396-407.

137. Harris DA, Rosing J, van de Stadt RJ, Slater EC. (1973) Tight binding of adenine nucleotides to beef-heart mitochondrial ATPase. Biochim Biophys Acta, 314: 149-153.

138. Jault JM, Allison WS. (1994) Hysteretic inhibition of the bovine heart mitochondrial F1-ATPase is due to saturation of noncatalytic sites with ADP which blocks activation of the enzyme by ATP. J Biol Chem, 269: 319-325.

139. Senior AE, Nadanaciva S, Weber J. (2000) Rate acceleration of ATP hydrolysis by F(1)F(o)-ATP synthase. J Exp Biol, 203: 35-40.

140. Boyer PD. (2001) Toward an adequate scheme for the ATP synthase catalysis. Biochemistry (Mosc), 66: 1058-1066.

141. Out TA, Valeton E, Kemp A, Jr. (1976) Role of the intramitochondrial adenine nucleotides as intermediates in the uncoupler-induced hydrolysis of extramitochondrial ATP. Biochim Biophys Acta, 440: 697-710.

142. Vignais PV. (1976) Molecular and physiological aspects of adenine nucleotide transport in mitochondria. Biochim Biophys Acta, 456: 1-38.

143. Hamman HC, Haynes RC, Jr. (1983) Elevated intramitochondrial adenine nucleotides and mitochondrial function. Arch Biochem Biophys, 223: 85-94.

144. Murthy MS, Pande SV. (1985) Microcompartmentation of transported carnitine, acetylcarnitine and ADP occurs in the mitochondrial matrix. Implications for transport measurements and metabolism. Biochem J, 230: 657-663.

145. Heldt HW, Pfaff E. (1969) Adenine nucleotide translocation in mitochondria. Quantitative evaluation of the correlation between the phosphorylation of endogenous and exogenous ADP in mitochondria. Eur J Biochem, 10: 494-500.

146. Hartung KJ, Bohme G, Kunz W. (1983) Involvement of intramitochondrial adenine nucleotides and inorganic phosphate in oxidative phosphorylation of

extramitochondrially added adenosine-5'-diphosphate. Biomed Biochim Acta, 42: 15-26.

147. Sheu KF, Blass JP. (1999) The alpha-ketoglutarate dehydrogenase complex. Ann N Y Acad Sci, 893: 61-78.

148. Gibson GE, Park LC, Sheu KF, Blass JP, Calingasan NY. (2000) The alpha-ketoglutarate dehydrogenase complex in neurodegeneration. Neurochem Int, 36: 97-112.

149. Cooper AJ. (2012) The role of glutamine synthetase and glutamate dehydrogenase in cerebral ammonia homeostasis. Neurochem Res, 37: 2439-2455.

150. Atamna H, Frey WH, 2nd. (2004) A role for heme in Alzheimer's disease: heme binds amyloid beta and has altered metabolism. Proc Natl Acad Sci U S A, 101: 11153-11158.

151. Atamna H, Liu J, Ames BN. (2001) Heme deficiency selectively interrupts assembly of mitochondrial complex IV in human fibroblasts: revelance to aging. J Biol Chem, 276: 48410-48416.

152. Kanamori T, Nishimaki K, Asoh S, Ishibashi Y, Takata I, Kuwabara T, Taira K, Yamaguchi H, Sugihara S, Yamazaki T, Ihara Y, Nakano K, Matuda S, Ohta S. (2003) Truncated product of the bifunctional DLST gene involved in biogenesis of the respiratory chain. EMBO J, 22: 2913-2923.

153. Bubber P, Haroutunian V, Fisch G, Blass JP, Gibson GE. (2005) Mitochondrial abnormalities in Alzheimer brain: mechanistic implications. Ann Neurol, 57: 695-703.

154. Gibson GE, Starkov A, Blass JP, Ratan RR, Beal MF. (2010) Cause and consequence: mitochondrial dysfunction initiates and propagates neuronal dysfunction, neuronal death and behavioral abnormalities in age-associated neurodegenerative diseases. Biochim Biophys Acta, 1802: 122-134.

155. Bubber P, Hartounian V, Gibson GE, Blass JP. (2011) Abnormalities in the tricarboxylic acid (TCA) cycle in the brains of schizophrenia patients. Eur Neuropsychopharmacol, 21: 254-260.

156. Yang L, Shi Q, Ho DJ, Starkov AA, Wille EJ, Xu H, Chen HL, Zhang S, Stack CM, Calingasan NY, Gibson GE, Beal MF. (2009) Mice deficient in dihydrolipoyl succinyl transferase show increased vulnerability to mitochondrial toxins. Neurobiol Dis, 36: 320-330.

157. Johnson MT, Yang HS, Magnuson T, Patel MS. (1997) Targeted disruption of the murine dihydrolipoamide dehydrogenase gene (Dld) results in perigastrulation lethality. Proc Natl Acad Sci U S A, 94: 14512-14517.

158. Klivenyi P, Starkov AA, Calingasan NY, Gardian G, Browne SE, Yang L, Bubber P, Gibson GE, Patel MS, Beal MF. (2004) Mice deficient in dihydrolipoamide dehydrogenase show increased vulnerability to MPTP, malonate and 3-nitropropionic acid neurotoxicity. J Neurochem, 88: 1352-1360.

159. Browne SE, Beal MF. (2002) Toxin-induced mitochondrial dysfunction. Int Rev Neurobiol, 53: 243-279.

160. Calingasan NY, Ho DJ, Wille EJ, Campagna MV, Ruan J, Dumont M, Yang L, Shi Q, Gibson GE, Beal MF. (2008) Influence of mitochondrial enzyme deficiency on adult neurogenesis in mouse models of neurodegenerative diseases. Neuroscience, 153: 986-996.

161. Dumont M, Ho DJ, Calingasan NY, Xu H, Gibson G, Beal MF. (2009) Mitochondrial dihydrolipoyl succinyltransferase deficiency accelerates amyloid pathology and memory deficit in a transgenic mouse model of amyloid deposition. Free Radic Biol Med, 47: 1019-1027.

162. Starkov AA, Fiskum G, Chinopoulos C, Lorenzo BJ, Browne SE, Patel MS, Beal MF. (2004) Mitochondrial alpha-ketoglutarate dehydrogenase complex generates reactive oxygen species. J Neurosci, 24: 7779-7788.

163. Tretter L, Adam-Vizi V. (2004) Generation of reactive oxygen species in the reaction catalyzed by alpha-ketoglutarate dehydrogenase. J Neurosci, 24: 7771-7778.

164. Lemons JM, Feng XJ, Bennett BD, Legesse-Miller A, Johnson EL, Raitman I, Pollina EA, Rabitz HA, Rabinowitz JD, Coller HA. (2010) Quiescent fibroblasts exhibit high metabolic activity. PLoS Biol, 8: e1000514.

165. Metallo CM, Walther JL, Stephanopoulos G. (2009) Evaluation of 13C isotopic tracers for metabolic flux analysis in mammalian cells. J Biotechnol, 144: 167-174.

166. Sazanov LA, Jackson JB. (1994) Proton-translocating transhydrogenase and NAD- and NADP-linked isocitrate dehydrogenases operate in a substrate cycle which contributes to fine regulation of the tricarboxylic acid cycle activity in mitochondria. FEBS Lett, 344: 109-116.

167. Ernster L, Navazio F. (1958) Soluble diaphorase in animal tissues. Acta Chem Scand, 12: 595-602.

168. Ernster L. (1958) Diaphorase activities in liver cytoplasmic fractions. Federation Proc, 17: 216.

169. Maerki F, Martius C. (1961) [Vitamin K reductase, from cattle and rat liver]. Biochem Z (Berlin), 334: 293-303.

170. Ernster L, Danielson L, Ljunggren M. (1962) DT diaphorase. I. Purification from the soluble fraction of rat-liver cytoplasm, and properties. Biochim Biophys Acta, 58: 171-188.

171. Wosilait WD, Nason A, Terrell AJ. (1954) Pyridine nucleotide-quinone reductase. II. Role in electron transport. J Biol Chem, 206: 271-282.

172. Wosilait WD, Nason A. (1954) Pyridine nucleotide-quinone reductase. I. Purification and properties of the enzyme from pea seeds. J Biol Chem, 206: 255-270.

173. Williams CH, Jr., Gibbs RH, Kamin H. (1959) A microsomal TPNH-neotetrazolium diaphorase. Biochim Biophys Acta, 32: 568-569.

174. Giuditta A, Strecker HJ. (1961) Purification and some properties of a brain diaphorase. Biochim Biophys Acta, 48: 10-19.

175. Giuditta A, Strecker HJ. (1959) Alternate pathways of pyridine nucleotide oxidation in cerebral tissue. J Neurochem, 5: 50-61.

176. Koli AK, Yearby C, Scott W, Donaldson KO. (1969) Purification and properties of three separate menadione reductases from hog liver. J Biol Chem, 244: 621-629.

177. Iyanagi T, Yamazaki I. (1970) One-electron-transfer reactions in biochemical systems. V. Difference in the mechanism of quinone reduction by the NADH dehydrogenase and the NAD(P)H dehydrogenase (DT-diaphorase). Biochim Biophys Acta, 216: 282-294.

178. Ernest L. (1987) DT-Diaphorase: A historical review. Chem Scripta, 27A: 1-13.

179. Vasiliou V, Ross D, Nebert DW. (2006) Update of the NAD(P)H:quinone oxidoreductase (NQO) gene family. Hum Genomics, 2: 329-335.

180. Long DJ, 2nd, Jaiswal AK. (2000) NRH:quinone oxidoreductase2 (NQO2). Chem Biol Interact, 129: 99-112.

181. Zhao Q, Yang XL, Holtzclaw WD, Talalay P. (1997) Unexpected genetic and structural relationships of a long-forgotten flavoenzyme to NAD(P)H:quinone reductase (DT-diaphorase). Proc Natl Acad Sci U S A, 94: 1669-1674.

182. Wu K, Knox R, Sun XZ, Joseph P, Jaiswal AK, Zhang D, Deng PS, Chen S. (1997) Catalytic properties of NAD(P)H:quinone oxidoreductase-2 (NQO2), a dihydronicotinamide riboside dependent oxidoreductase. Arch Biochem Biophys, 347: 221-228.

183. Dong H, Shertzer HG, Genter MB, Gonzalez FJ, Vasiliou V, Jefcoate C, Nebert DW. (2013) Mitochondrial targeting of mouse NQO1 and CYP1B1 proteins. Biochem Biophys Res Commun, 435: 727-732.

184. Bianchet MA, Faig M, Amzel LM. Structure and mechanism of NAD[P]H:quinone acceptor oxidoreductases (NQO). In: Sies H, Packer L. (ed.), Methods in Enzymology Vol. 382. Quinones and Quinone Enzymes, Part B. Academic Press, Burlington, 2004: 144-174.

185. Eliasson M, Bostrom M, DePierre JW. (1999) Levels and subcellular distributions of detoxifying enzymes in the ovarian corpus luteum of the pregnant and non-pregnant pig. Biochem Pharmacol, 58: 1287-1292.

186. Conover TE, Ernster L. (1962) DT diaphorase. II. Relation to respiratory chain of intact mitochondria. Biochim Biophys Acta, 58: 189-200.

187. Colpa-Boonstra JP, Slater EC. (1958) The possible role of vitamin K in the respiratory chain. Biochim Biophys Acta, 27: 122-133.

188. Ernster L, Ljunggren M, Danielson L. (1960) Purification and some properties of a highly dicumarol-sensitive liver diaphorase. Biochem Biophys Res Commun, 2: 88-92.

189. Danielson L, Ernster L, Ljunggren M. (1960) Selective extraction of DT diaphorase from mitochondria and microsomes. Acta Chem Scand, 14: 1837-1838.

190. Edlund C, Elhammer A, Dallner G. (1982) Distribution of newly synthesized DT-diaphorase in rat liver. Biosci Rep, 2: 861-865.

191. Conover TE, Ernster L. (1960) Mitochondrial oxidation of extra-mitochondrial TPNH1 mediated by purified DT diaphorase. Biochem Biophys Res Commun, 2: 26-30.

192. Wosilait WD. (1960) The reduction of vitamin K1 by an enzyme from dog liver. J Biol Chem, 235: 1196-1201.

193. Lind C, Hojeberg B. (1981) Biospecific adsorption of hepatic DT-diaphorase on immobilized dicoumarol. II. Purification of mitochondrial and microsomal DT-diaphorase from 3-methylcholanthrene-treated rats. Arch Biochem Biophys, 207: 217-224.

194. Ernster L. DT diaphorase. In: Estabrook RW, Pullman ME. (ed.), Methods in Enzymology Vol. 10. Oxidation and Phosphorylation. Academic Press, Burlington, 1967: 309-317.

195. Conover TE, Ernster L. (1963) DT diaphorase. IV. Coupling of extramitochondrial reduced pyridine nucleotide oxidation to mitochondrial respiratory chain. Biochim Biophys Acta, 67: 268-280.

196. Massey V. (1960) The identity of diaphorase and lipoyl dehydrogenase. Biochim Biophys Acta, 37: 314-322.

197. Klyachko NL, Shchedrina VA, Efimov AV, Kazakov SV, Gazaryan IG, Kristal BS, Brown AM. (2005) pH-dependent substrate preference of pig heart lipoamide dehydrogenase varies with oligomeric state: response to mitochondrial matrix acidification. J Biol Chem, 280: 16106-16114.

198. Reed LJ, Oliver RM. (1968) The multienzyme alpha-keto acid dehydrogenase complexes. Brookhaven Symp Biol, 21: 397-412.

199. Ide S, Hayakawa T, Okabe K, Koike M. (1967) Lipoamide dehydrogenase from human liver. J Biol Chem, 242: 54-60.

200. Bando Y, Aki K. (1992) One- and two-electron oxidation-reduction properties of lipoamide dehydrogenase. J Nutr Sci Vitaminol (Tokyo), Spec No 38: 453-456.

201. Vaubel RA, Rustin P, Isaya G. (2011) Mutations in the dimer interface of dihydrolipoamide dehydrogenase promote site-specific oxidative damages in yeast and human cells. J Biol Chem, 286: 40232-40245.

202. Chinopoulos C. (2013) Which way does the citric acid cycle turn during hypoxia? The critical role of alpha-ketoglutarate dehydrogenase complex. J Neurosci Res, 91: 1030-1043.

203. Schinzel AC, Takeuchi O, Huang Z, Fisher JK, Zhou Z, Rubens J, Hetz C, Danial NN, Moskowitz MA, Korsmeyer SJ. (2005) Cyclophilin D is a component of mitochondrial permeability transition and mediates neuronal cell death after focal cerebral ischemia. Proc Natl Acad Sci U S A, 102: 12005-12010.

204. Sims NR. (1990) Rapid isolation of metabolically active mitochondria from rat brain and subregions using Percoll density gradient centrifugation. J Neurochem, 55: 698-707.

205. Chinopoulos C, Starkov AA, Fiskum G. (2003) Cyclosporin A-insensitive permeability transition in brain mitochondria: inhibition by 2-aminoethoxydiphenyl borate. J Biol Chem, 278: 27382-27389.

206. Tyler DD, Gonze J. The preparation of heart mitochondria from laboratory animals. In: Estabrook RW, Pullman ME. (ed.), Methods in Enzymology Vol. 10. Oxidation and Phosphorylation. Academic Press, Burlington, 1967: 75-77.

207. Smith PK, Krohn RI, Hermanson GT, Mallia AK, Gartner FH, Provenzano MD, Fujimoto EK, Goeke NM, Olson BJ, Klenk DC. (1985) Measurement of protein using bicinchoninic acid. Anal Biochem, 150: 76-85.

208. Dunkley PR, Jarvie PE, Robinson PJ. (2008) A rapid Percoll gradient procedure for preparation of synaptosomes. Nat Protoc, 3: 1718-1728.

209. Chinopoulos C, Gerencser AA, Doczi J, Fiskum G, Adam-Vizi V. (2004) Inhibition of glutamate-induced delayed calcium deregulation by 2-APB and La3+ in cultured cortical neurones. J Neurochem, 91: 471-483.

210. Akerman KE, Wikstrom MK. (1976) Safranine as a probe of the mitochondrial membrane potential. FEBS Lett, 68: 191-197.

211. Valle VG, Pereira-da-Silva L, Vercesi AE. (1986) Undesirable feature of safranine as a probe for mitochondrial membrane potential. Biochem Biophys Res Commun, 135: 189-195.

212. Kamo N, Muratsugu M, Hongoh R, Kobatake Y. (1979) Membrane potential of mitochondria measured with an electrode sensitive to tetraphenyl phosphonium and relationship between proton electrochemical potential and phosphorylation potential in steady state. J Membr Biol, 49: 105-121.

213. Leyssens A, Nowicky AV, Patterson L, Crompton M, Duchen MR. (1996) The relationship between mitochondrial state, ATP hydrolysis, [Mg2+]i and [Ca2+]i studied in isolated rat cardiomyocytes. J Physiol, 496 (Pt 1): 111-128.

214. Zolkiewska A, Czyz A, Duszynski J, Wojtczak L. (1993) Continuous recording of intramitochondrial pH with fluorescent pH indicators: novel probes and limitations of the method. Acta Biochim Pol, 40: 241-250.

215. Alarcon C, Wicksteed B, Prentki M, Corkey BE, Rhodes CJ. (2002) Succinate is a preferential metabolic stimulus-coupling signal for glucose-induced proinsulin biosynthesis translation. Diabetes, 51: 2496-2504.

216. Alexandre A, Reynafarje B, Lehninger AL. (1978) Stoichiometry of vectorial H+ movements coupled to electron transport and to ATP synthesis in mitochondria. Proc Natl Acad Sci U S A, 75: 5296-5300.

217. Dennis SC, Lai JC, Clark JB. (1977) Comparative studies on glutamate metabolism in synpatic and non-synaptic rat brain mitochondria. Biochem J, 164: 727-736.

218. Konig T, Nicholls DG, Garland PB. (1969) The inhibition of pyruvate and Ls(+)-isocitrate oxidation by succinate oxidation in rat liver mitochondria. Biochem J, 114: 589-596.

219. Quagliariello E, Papa S, Saccone C, Palmieri F, Francavilla A. (1965) The oxidation of glutamate by rat-liver mitochondria. Biochem J, 95: 742-748.

220. Metallo CM, Gameiro PA, Bell EL, Mattaini KR, Yang J, Hiller K, Jewell CM, Johnson ZR, Irvine DJ, Guarente L, Kelleher JK, Vander Heiden MG, Iliopoulos O, Stephanopoulos G. (2012) Reductive glutamine metabolism by IDH1 mediates lipogenesis under hypoxia. Nature, 481: 380-384.

221. Des Rosiers C, Di Donato L, Comte B, Laplante A, Marcoux C, David F, Fernandez CA, Brunengraber H. (1995) Isotopomer analysis of citric acid cycle and gluconeogenesis in rat liver. Reversibility of isocitrate dehydrogenase and involvement of ATP-citrate lyase in gluconeogenesis. J Biol Chem, 270: 10027-10036.

222. Yoo H, Antoniewicz MR, Stephanopoulos G, Kelleher JK. (2008) Quantifying reductive carboxylation flux of glutamine to lipid in a brown adipocyte cell line. J Biol Chem, 283: 20621-20627.

223. Ehrlich RS, Colman RF. (1983) Separation, recombination, and characterization of dissimilar subunits of the DPN-dependent isocitrate dehydrogenase from pig heart. J Biol Chem, 258: 7079-7086.

224. Des Rosiers C, Fernandez CA, David F, Brunengraber H. (1994) Reversibility of the mitochondrial isocitrate dehydrogenase reaction in the perfused rat liver. Evidence from isotopomer analysis of citric acid cycle intermediates. J Biol Chem, 269: 27179-27182.

225. Comte B, Vincent G, Bouchard B, Benderdour M, Des Rosiers C. (2002) Reverse flux through cardiac NADP(+)-isocitrate dehydrogenase under normoxia and ischemia. Am J Physiol Heart Circ Physiol, 283: H1505-1514.

226. Gabriel JL, Zervos PR, Plaut GW. (1986) Activity of purified NAD-specific isocitrate dehydrogenase at modulator and substrate concentrations approximating conditions in mitochondria. Metabolism, 35: 661-667.

227. Okamoto K, Matsuzaka Y, Yoshikawa Y, Takaki A, Kulski JK, Tamiya G, Inoko H. (2003) Identification of NAD+-dependent isocitrate dehydrogenase 3 gamma-like (IDH3GL) gene and its genetic polymorphisms. Gene, 323: 141-148.

228. Kim YO, Koh HJ, Kim SH, Jo SH, Huh JW, Jeong KS, Lee IJ, Song BJ, Huh TL. (1999) Identification and functional characterization of a novel, tissue-specific NAD(+)-dependent isocitrate dehydrogenase beta subunit isoform. J Biol Chem, 274: 36866-36875.

229. Jackson JB. (1991) The proton-translocating nicotinamide adenine dinucleotide transhydrogenase. J Bioenerg Biomembr, 23: 715-741.

230. Li X, Wu F, Qi F, Beard DA. (2011) A database of thermodynamic properties of the reactions of glycolysis, the tricarboxylic acid cycle, and the pentose phosphate pathway. Database (Oxford), 2011: bar005.

231. Shi Q, Risa O, Sonnewald U, Gibson GE. (2009) Mild reduction in the activity of the alpha-ketoglutarate dehydrogenase complex elevates GABA shunt and glycolysis. J Neurochem, 109 Suppl 1: 214-221.

232. Nilsen LH, Shi Q, Gibson GE, Sonnewald U. (2011) Brain [U-13 C]glucose metabolism in mice with decreased alpha-ketoglutarate dehydrogenase complex activity. J Neurosci Res, 89: 1997-2007.

233. Tretter L, Adam-Vizi V. (2007) Uncoupling is without an effect on the production of reactive oxygen species by in situ synaptic mitochondria. J Neurochem, 103: 1864-1871.

234. Porpaczy Z, Sumegi B, Alkonyi I. (1983) Association between the alpha-ketoglutarate dehydrogenase complex and succinate thiokinase. Biochim Biophys Acta, 749: 172-179.

235. Miyadera H, Shiomi K, Ui H, Yamaguchi Y, Masuma R, Tomoda H, Miyoshi H, Osanai A, Kita K, Omura S. (2003) Atpenins, potent and specific inhibitors of mitochondrial complex II (succinate-ubiquinone oxidoreductase). Proc Natl Acad Sci U S A, 100: 473-477.

236. Harris EJ, Achenjang FM. (1977) Energy-dependent uptake of arsenite by rat liver mitochondria. Biochem J, 168: 129-132.

237. Clark JB, Land JM. (1979) Inhibitors of mitochondrial enzymes. Pharmacol Ther, 7: 351-373.

238. Pagliarini DJ, Calvo SE, Chang B, Sheth SA, Vafai SB, Ong SE, Walford GA, Sugiana C, Boneh A, Chen WK, Hill DE, Vidal M, Evans JG, Thorburn DR, Carr SA, Mootha VK. (2008) A mitochondrial protein compendium elucidates complex I disease biology. Cell, 134: 112-123.

239. Winski SL, Koutalos Y, Bentley DL, Ross D. (2002) Subcellular localization of NAD(P)H:quinone oxidoreductase 1 in human cancer cells. Cancer Res, 62: 1420-1424.

240. Martius C, Nitz-Litzow D. (1953) [The mechanism of action of dicumarol and related compounds]. Biochim Biophys Acta, 12: 134-140.

241. Giuditta A, Strecker HJ. (1963) Brain NADH-tretraazolium reductase activity, lipomide dehydrogenase and activating lipids. Biochim Biophys Acta, 67: 316-318.

242. Faig M, Bianchet MA, Winski S, Hargreaves R, Moody CJ, Hudnott AR, Ross D, Amzel LM. (2001) Structure-based development of anticancer drugs: complexes of NAD(P)H:quinone oxidoreductase 1 with chemotherapeutic quinones. Structure, 9: 659-667.

243. Tedeschi G, Chen S, Massey V. (1995) DT-diaphorase. Redox potential, steady-state, and rapid reaction studies. J Biol Chem, 270: 1198-1204.

244. Lind C, Cadenas E, Hochstein P, Ernster L. DT-diaphorase: purification, properties, and function. In: Packer L, Glazer AN. (ed.), Methods in Enzymology Vol. 186. Oxygen Radicals in Biological Systems, Part B: Oxygen Radicals and Antioxidants. Academic Press, Burlington, 1990: 287-301.

245. Dedukhova VI, Kirillova GP, Mokhova EN, Rozovskaia IA, Skulachev VP. (1986) [Effect of menadione and vicasol on mitochondrial energy during inhibition of initiation sites of the respiration chain]. Biokhimiia, 51: 567-573.

246. Kolesova GM, Karnaukhova LV, Iaguzhinskii LS. (1991) [Interaction of menadione and duroquinone with Q-cycle during DT-diaphorase function]. Biokhimiia, 56: 1779-1786.

247. Kolesova GM, Karnaukhova LV, Segal NK, Iaguzhinskii LS. (1993) [The effect of inhibitors of the Q-cycle on cyano-resistant oxidation of malate by rat liver mitochondria in the presence of menadione]. Biokhimiia, 58: 1630-1640.

248. Ernster L, Lee IY, Norling B, Persson B. (1969) Studies with ubiquinone-depleted submitochondrial particles. Essentiality of ubiquinone for the interaction of succinate dehydrogenase, NADH dehydrogenase, and cytochrome b. Eur J Biochem, 9: 299-310.

249. Flatmark T. (1967) Multiple molecular forms of bovine heart cytochrome c. V. A comparative study of their physicochemical properties and their reactions in biological systems. J Biol Chem, 242: 2454-2459.

250. Gopal D, Wilson GS, Earl RA, Cusanovich MA. (1988) Cytochrome c: ion binding and redox properties. Studies on ferri and ferro forms of horse, bovine, and tuna cytochrome c. J Biol Chem, 263: 11652-11656.

251. Preusch PC, Smalley DM. (1990) Vitamin K1 2,3-epoxide and quinone reduction: mechanism and inhibition. Free Radic Res Commun, 8: 401-415.

252. Haefeli RH, Erb M, Gemperli AC, Robay D, Courdier Fruh I, Anklin C, Dallmann R, Gueven N. (2011) NQO1-dependent redox cycling of idebenone: effects on cellular redox potential and energy levels. PLoS One, 6: e17963.

253. Danielson L, Ernster L. (1962) Lack of Relationship between Mitochondrial Oxidative Phosphorylation and the Dicoumarol-Sensitive Flavoenzyme 'Dt Diaphorase' or 'Vitamin K Reductase'. Nature, 194: 155-157.

254. Martius C, Strufe R. (1954) [Phylloquinone reductase; preliminary report]. Biochem Z (Berlin), 326: 24-25.

255. Waelsch H, Cheng SC, Cote LJ, Naruse H. (1965) CO2 fixation in the nervous system. Proc Natl Acad Sci U S A, 54: 1249-1253.

256. Cheng SC, Nakamura R. (1972) Metabolism related to the tricarboxylic acid cycle in rat brain slices. Observations on CO 2 fixation and metabolic compartmentation. Brain Res, 38: 355-370.

257. Nakamura R, Cheng SC, Naruse H. (1970) A study on the precursors of the acetyl moiety of acetylcholine in brain slices. Observations on the compartmentalization of the acetyl-coenzyme A pool. Biochem J, 118: 443-450.

258. Patel MS. (1974) The relative significance of CO2-fixing enzymes in the metabolism of rat brain. J Neurochem, 22: 717-724.

259. Salganicoff L, Koeppe RE. (1968) Subcellular distribution ot pyruvate carboxylase, diphosphopyridine nucleotide and triphosphopyridine nucleotide isocitrate dehydrogenases, and malate enzyme in rat brain. J Biol Chem, 243: 3416-3420.

260. Randle PJ, England PJ, Denton RM. (1970) Control of the tricarboxylate cycle and its interactions with glycolysis during acetate utilization in rat heart. Biochem J, 117: 677-695.

261. Toye AA, Lippiat JD, Proks P, Shimomura K, Bentley L, Hugill A, Mijat V, Goldsworthy M, Moir L, Haynes A, Quarterman J, Freeman HC, Ashcroft FM, Cox RD. (2005) A genetic and physiological study of impaired glucose homeostasis control in C57BL/6J mice. Diabetologia, 48: 675-686.

262. Adam-Vizi V, Chinopoulos C. (2006) Bioenergetics and the formation of mitochondrial reactive oxygen species. Trends Pharmacol Sci, 27: 639-645.

263. Mailloux RJ, Beriault R, Lemire J, Singh R, Chenier DR, Hamel RD, Appanna VD. (2007) The tricarboxylic acid cycle, an ancient metabolic network with a novel twist. PLoS One, 2: e690.

264. Shen X, Zheng S, Metreveli NS, Epstein PN. (2006) Protection of cardiac mitochondria by overexpression of MnSOD reduces diabetic cardiomyopathy. Diabetes, 55: 798-805.

265. Duee ED, Vignais PV. (1969) Kinetics of phosphorylation of intramitochondrial and extramitochondrial adenine nucleotides as related to nucleotide translocation. J Biol Chem, 244: 3932-3940.

266. Hafner RP, Brown GC, Brand MD. (1990) Analysis of the control of respiration rate, phosphorylation rate, proton leak rate and protonmotive force in isolated mitochondria using the 'top-down' approach of metabolic control theory. Eur J Biochem, 188: 313-319.

267. Brand MD, Harper ME, Taylor HC. (1993) Control of the effective P/O ratio of oxidative phosphorylation in liver mitochondria and hepatocytes. Biochem J, 291 (Pt 3): 739-748.

268. Woodfield K, Ruck A, Brdiczka D, Halestrap AP. (1998) Direct demonstration of a specific interaction between cyclophilin-D and the adenine nucleotide translocase confirms their role in the mitochondrial permeability transition. Biochem J, 336 (Pt 2): 287-290.

269. Luvisetto S, Basso E, Petronilli V, Bernardi P, Forte M. (2008) Enhancement of anxiety, facilitation of avoidance behavior, and occurrence of adult-onset obesity in mice lacking mitochondrial cyclophilin D. Neuroscience, 155: 585-596.

270. Jobe SM, Wilson KM, Leo L, Raimondi A, Molkentin JD, Lentz SR, Di Paola J. (2008) Critical role for the mitochondrial permeability transition pore and cyclophilin D in platelet activation and thrombosis. Blood, 111: 1257-1265.

271. Elrod JW, Wong R, Mishra S, Vagnozzi RJ, Sakthievel B, Goonasekera SA, Karch J, Gabel S, Farber J, Force T, Brown JH, Murphy E, Molkentin JD. (2010) Cyclophilin D controls mitochondrial pore-dependent Ca(2+) exchange, metabolic flexibility, and propensity for heart failure in mice. J Clin Invest, 120: 3680-3687.

272. Fournier N, Ducet G, Crevat A. (1987) Action of cyclosporine on mitochondrial calcium fluxes. J Bioenerg Biomembr, 19: 297-303.

273. Du H, Guo L, Fang F, Chen D, Sosunov AA, McKhann GM, Yan Y, Wang C, Zhang H, Molkentin JD, Gunn-Moore FJ, Vonsattel JP, Arancio O, Chen JX, Yan SD. (2008) Cyclophilin D deficiency attenuates mitochondrial and neuronal perturbation and ameliorates learning and memory in Alzheimer's disease. Nat Med, 14: 1097-1105.

274. Millay DP, Sargent MA, Osinska H, Baines CP, Barton ER, Vuagniaux G, Sweeney HL, Robbins J, Molkentin JD. (2008) Genetic and pharmacologic inhibition of mitochondrial-dependent necrosis attenuates muscular dystrophy. Nat Med, 14: 442-447.

275. Baines CP, Kaiser RA, Purcell NH, Blair NS, Osinska H, Hambleton MA, Brunskill EW, Sayen MR, Gottlieb RA, Dorn GW, Robbins J, Molkentin JD. (2005) Loss of cyclophilin D reveals a critical role for mitochondrial permeability transition in cell death. Nature, 434: 658-662.

276. Nakagawa T, Shimizu S, Watanabe T, Yamaguchi O, Otsu K, Yamagata H, Inohara H, Kubo T, Tsujimoto Y. (2005) Cyclophilin D-dependent mitochondrial permeability transition regulates some necrotic but not apoptotic cell death. Nature, 434: 652-658.

277. Basso E, Fante L, Fowlkes J, Petronilli V, Forte MA, Bernardi P. (2005) Properties of the permeability transition pore in mitochondria devoid of Cyclophilin D. J Biol Chem, 280: 18558-18561.

278. Palma E, Tiepolo T, Angelin A, Sabatelli P, Maraldi NM, Basso E, Forte MA, Bernardi P, Bonaldo P. (2009) Genetic ablation of cyclophilin D rescues mitochondrial defects and prevents muscle apoptosis in collagen VI myopathic mice. Hum Mol Genet, 18: 2024-2031.

279. Irwin WA, Bergamin N, Sabatelli P, Reggiani C, Megighian A, Merlini L, Braghetta P, Columbaro M, Volpin D, Bressan GM, Bernardi P, Bonaldo P. (2003) Mitochondrial dysfunction and apoptosis in myopathic mice with collagen VI deficiency. Nat Genet, 35: 367-371.

280. Tiepolo T, Angelin A, Palma E, Sabatelli P, Merlini L, Nicolosi L, Finetti F, Braghetta P, Vuagniaux G, Dumont JM, Baldari CT, Bonaldo P, Bernardi P. (2009) The cyclophilin inhibitor Debio 025 normalizes mitochondrial function, muscle apoptosis and ultrastructural defects in Col6a1-/- myopathic mice. Br J Pharmacol, 157: 1045-1052.

281. Merlini L, Angelin A, Tiepolo T, Braghetta P, Sabatelli P, Zamparelli A, Ferlini A, Maraldi NM, Bonaldo P, Bernardi P. (2008) Cyclosporin A corrects mitochondrial dysfunction and muscle apoptosis in patients with collagen VI myopathies. Proc Natl Acad Sci U S A, 105: 5225-5229.

282. Gledhill JR, Montgomery MG, Leslie AG, Walker JE. (2007) How the regulatory protein, IF(1), inhibits F(1)-ATPase from bovine mitochondria. Proc Natl Acad Sci U S A, 104: 15671-15676.

283. Nicholls DG, Bernson VS. (1977) Inter-relationships between proton electrochemical gradient, adenine-nucleotide phosphorylation potential and respiration, during substrate-level and oxidative phosphorylation by mitochondria from brown adipose tissue of cold-adapted guinea-pigs. Eur J Biochem, 75: 601-612.

284. Pisarenko O, Studneva I, Khlopkov V, Solomatina E, Ruuge E. (1988) An assessment of anaerobic metabolism during ischemia and reperfusion in isolated guinea pig heart. Biochim Biophys Acta, 934: 55-63.

285. Peuhkurinen KJ, Takala TE, Nuutinen EM, Hassinen IE. (1983) Tricarboxylic acid cycle metabolites during ischemia in isolated perfused rat heart. Am J Physiol, 244: H281-288.

286. Sanborn T, Gavin W, Berkowitz S, Perille T, Lesch M. (1979) Augmented conversion of aspartate and glutamate to succinate during anoxia in rabbit heart. Am J Physiol, 237: H535-541.

287. Pisarenko O, Studneva I, Khlopkov V. (1987) Metabolism of the tricarboxylic acid cycle intermediates and related amino acids in ischemic guinea pig heart. Biomed Biochim Acta, 46: S568-571.

288. Hunter FE, Jr. (1949) Anaerobic phosphorylation due to a coupled oxidation-reduction between alpha-ketoglutaric acid and oxalacetic acid. J Biol Chem, 177: 361-372.

289. Randall HM, Jr., Cohen JJ. (1966) Anaerobic CO2 production by dog kidney in vitro. Am J Physiol, 211: 493-505.

290. Chance B, Hollunger G. (1960) Energy-linked reduction of mitochondrial pyridine nucleotide. Nature, 185: 666-672.

291. Penney DG, Cascarano J. (1970) Anaerobic rat heart. Effects of glucose and tricarboxylic acid-cycle metabolites on metabolism and physiological performance. Biochem J, 118: 221-227.

292. Wilson MA, Cascarano J. (1970) The energy-yielding oxidation of NADH by fumarate in submitochondrial particles of rat tissues. Biochim Biophys Acta, 216: 54-62.

293. Taegtmeyer H, Peterson MB, Ragavan VV, Ferguson AG, Lesch M. (1977) De novo alanine synthesis in isolated oxygen-deprived rabbit myocardium. J Biol Chem, 252: 5010-5018.

294. Taegtmeyer H. (1978) Metabolic responses to cardiac hypoxia. Increased production of succinate by rabbit papillary muscles. Circ Res, 43: 808-815.

295. Chick WL, Weiner R, Cascareno J, Zweifach BW. (1968) Influence of Krebs-cycle intermediates on survival in hemorrhagic shock. Am J Physiol, 215: 1107-1110.

296. Weinberg JM, Venkatachalam MA, Roeser NF, Saikumar P, Dong Z, Senter RA, Nissim I. (2000) Anaerobic and aerobic pathways for salvage of proximal tubules from hypoxia-induced mitochondrial injury. Am J Physiol Renal Physiol, 279: F927-943.

297. Gerencser AA, Chinopoulos C, Birket MJ, Jastroch M, Vitelli C, Nicholls DG, Brand MD. (2012) Quantitative measurement of mitochondrial membrane potential in cultured cells: calcium-induced de- and hyperpolarization of neuronal mitochondria. J Physiol, 590: 2845-2871.

298. Zacharias NM, Chan HR, Sailasuta N, Ross BD, Bhattacharya P. (2012) Real-time molecular imaging of tricarboxylic acid cycle metabolism in vivo by hyperpolarized 1-(13)C diethyl succinate. J Am Chem Soc, 134: 934-943.

299. Alves TC, Jarak I, Carvalho RA. (2012) NMR methodologies for studying mitochondrial bioenergetics. Methods Mol Biol, 810: 281-309.

300. Tretter L, Adam-Vizi V. (2000) Inhibition of Krebs cycle enzymes by hydrogen peroxide: A key role of [alpha]-ketoglutarate dehydrogenase in limiting NADH production under oxidative stress. J Neurosci, 20: 8972-8979.

301. McKenna MC. (2007) The glutamate-glutamine cycle is not stoichiometric: fates of glutamate in brain. J Neurosci Res, 85: 3347-3358.

302. Allen DA, Ottaway JH. (1986) Succinate thiokinase in pigeon breast muscle mitochondria. FEBS Lett, 194: 171-175.

303. Rouslin W, Erickson JL, Solaro RJ. (1986) Effects of oligomycin and acidosis on rates of ATP depletion in ischemic heart muscle. Am J Physiol, 250: H503-508.

304. Rouslin W, Broge CW, Grupp IL. (1990) ATP depletion and mitochondrial functional loss during ischemia in slow and fast heart-rate hearts. Am J Physiol, 259: H1759-1766.

305. Estabrook RW, Sacktor B. (1958) alpha-Glycerophosphate oxidase of flight muscle mitochondria. J Biol Chem, 233: 1014-1019.

306. Tretter L, Takacs K, Kover K, Adam-Vizi V. (2007) Stimulation of H(2)O(2) generation by calcium in brain mitochondria respiring on alpha-glycerophosphate. J Neurosci Res, 85: 3471-3479.

307. Preusch PC, Siegel D, Gibson NW, Ross D. (1991) A note on the inhibition of DT-diaphorase by dicoumarol. Free Radic Biol Med, 11: 77-80.

308. Hodnick WF, Sartorelli AC. (1993) Reductive activation of mitomycin C by NADH:cytochrome b5 reductase. Cancer Res, 53: 4907-4912.

309. Traver RD, Siegel D, Beall HD, Phillips RM, Gibson NW, Franklin WA, Ross D. (1997) Characterization of a polymorphism in NAD(P)H: quinone oxidoreductase (DT-diaphorase). Br J Cancer, 75: 69-75.

310. Beyer RE, Segura-Aguilar J, Di Bernardo S, Cavazzoni M, Fato R, Fiorentini D, Galli MC, Setti M, Landi L, Lenaz G. (1996) The role of DT-diaphorase in the maintenance of the reduced antioxidant form of coenzyme Q in membrane systems. Proc Natl Acad Sci U S A, 93: 2528-2532.

311. Lenaz G, Fato R, Degli Esposti M, Rugolo M, Parenti Castelli G. (1985) The essentiality of coenzyme Q for bioenergetics and clinical medicine. Drugs Exp Clin Res, 11: 547-556.

312. Kolesova GM, Vishnivetskii SA, Iaguzhinskii LS. (1989) [A study of the mechanism of cyanide resistant oxidation of succinate from rat liver mitochondria in the presence of menadione]. Biokhimiia, 54: 103-111.

313. Kolesova GM, Kapitanova NG, Iaguzhinskii LS. (1987) [Stimulation by quinones of cyanide-resistant respiration in rat liver and heart mitochondria]. Biokhimiia, 52: 715-719.

314. Yue Y, Krenz M, Cohen MV, Downey JM, Critz SD. (2001) Menadione mimics the infarct-limiting effect of preconditioning in isolated rat hearts. Am J Physiol Heart Circ Physiol, 281: H590-595.

315. Chan TS, Teng S, Wilson JX, Galati G, Khan S, O'Brien PJ. (2002) Coenzyme Q cytoprotective mechanisms for mitochondrial complex I cytopathies involves NAD(P)H: quinone oxidoreductase 1(NQO1). Free Radic Res, 36: 421-427.

316. Cresteil T, Jaiswal AK. (1991) High levels of expression of the NAD(P)H:quinone oxidoreductase (NQO1) gene in tumor cells compared to normal cells of the same origin. Biochem Pharmacol, 42: 1021-1027.

317. Giorgio M, Migliaccio E, Orsini F, Paolucci D, Moroni M, Contursi C, Pelliccia G, Luzi L, Minucci S, Marcaccio M, Pinton P, Rizzuto R, Bernardi P, Paolucci F, Pelicci PG. (2005) Electron transfer between cytochrome c and p66Shc generates reactive oxygen species that trigger mitochondrial apoptosis. Cell, 122: 221-233.

318. Ventura A, Maccarana M, Raker VA, Pelicci PG. (2004) A cryptic targeting signal induces isoform-specific localization of p46Shc to mitochondria. J Biol Chem, 279: 2299-2306.

319. Chapple SJ, Siow RC, Mann GE. (2012) Crosstalk between Nrf2 and the proteasome: therapeutic potential of Nrf2 inducers in vascular disease and aging. Int J Biochem Cell Biol, 44: 1315-1320.

320. Rushmore TH, Kong AN. (2002) Pharmacogenomics, regulation and signaling pathways of phase I and II drug metabolizing enzymes. Curr Drug Metab, 3: 481-490.

321. Gomez-Diaz C, Buron MI, Alcain FJ, Gonzalez-Ojeda R, Gonzalez-Reyes JA, Bello RI, Herman MD, Navas P, Villalba JM. (2003) Effect of dietary coenzyme Q and fatty acids on the antioxidant status of rat tissues. Protoplasma, 221: 11-17.

322. Sack MN, Finkel T. (2012) Mitochondrial metabolism, sirtuins, and aging. Cold Spring Harb Perspect Biol, 4: a013102.

323. Sasaki N, Sato T, Marban E, O'Rourke B. (2001) ATP consumption by uncoupled mitochondria activates sarcolemmal K(ATP) channels in cardiac myocytes. Am J Physiol Heart Circ Physiol, 280: H1882-1888.

324. Karschin A, Brockhaus J, Ballanyi K. (1998) KATP channel formation by the sulphonylurea receptors SUR1 with Kir6.2 subunits in rat dorsal vagal neurons in situ. J Physiol, 509 (Pt 2): 339-346.

325. Ballanyi K, Doutheil J, Brockhaus J. (1996) Membrane potentials and microenvironment of rat dorsal vagal cells in vitro during energy depletion. J Physiol, 495 (Pt 3): 769-784.

326. Trapp S, Ballanyi K. (1995) KATP channel mediation of anoxia-induced outward current in rat dorsal vagal neurons in vitro. J Physiol, 487 (Pt 1): 37-50.

327. Rouslin W, Broge CW. (1989) Regulation of mitochondrial matrix pH and adenosine 5'-triphosphatase activity during ischemia in slow heart-rate hearts. Role of Pi/H+ symport. J Biol Chem, 264: 15224-15229.

328. King MP, Attardi G. (1989) Human cells lacking mtDNA: repopulation with exogenous mitochondria by complementation. Science, 246: 500-503.

329. Appleby RD, Porteous WK, Hughes G, James AM, Shannon D, Wei YH, Murphy MP. (1999) Quantitation and origin of the mitochondrial membrane potential in human cells lacking mitochondrial DNA. Eur J Biochem, 262: 108-116.

330. St-Pierre J, Brand MD, Boutilier RG. (2000) Mitochondria as ATP consumers: cellular treason in anoxia. Proc Natl Acad Sci U S A, 97: 8670-8674.

DOI:10.14753/SE.2015.1713

10. LIST OF PUBLICATIONS

Publications related to the present thesis

1. Chinopoulos C, Gerencsér AÁ, Mándi M, Máthé K, Törőcsik B, Dóczi J, Turiák L, **Kiss G**, Konrád C, Vajda S, Vereczki V, Oh RJ, Ádám-Vizi V. (2010) Forward operation of adenine nucleotide translocase during F_0F_1-ATPase reversal: critical role of matrix substrate-level phosphorylation. FASEB J, 24: 2405-2416.

   Impact factor: 6.515

2. Chinopoulos C, Konrád C, **Kiss G**, Metelkin E, Törőcsik B, Zhang SF, Starkov AA. (2011) Modulation of F_0F_1-ATP synthase activity by cyclophilin D regulates matrix adenine nucleotide levels. FEBS J, 278: 1112-1125.

   Impact factor: 3.790

3. **Kiss G**, Konrád C, Dóczi J, Starkov AA, Kawamata H, Manfredi G, Zhang SF, Gibson GE, Beal MF, Ádám-Vizi V, Chinopoulos C. (2013) The negative impact of alpha-ketoglutarate dehydrogenase complex deficiency on matrix substrate-level phosphorylation. FASEB J, 27: 2392-2406.

   Impact factor: 5.704 (2012)

4. **Kiss G**, Konrád C, Pour-Ghaz I, Mansour JJ, Németh B, Starkov AA, Ádám-Vizi V, Chinopoulos C. (2014) Mitochondrial diaphorases as NAD^+ donors to segments of the citric acid cycle that support substrate-level phosphorylation yielding ATP during respiratory inhibition. FASEB J, 28: 1682-1697.

   Impact factor: 5.704 (2012)

Publications not related to the present thesis

5. Vajda S, Mándi M, Konrád C, **Kiss G**, Ambrus A, Ádám-Vizi V, Chinopoulos C. (2009) A re-evaluation of the role of matrix acidification in uncoupler-induced Ca^{2+} release from mitochondria. FEBS J, 276: 2713-2724.

   Impact factor: 3.042

6. Dóczi J, Turiák L, Vajda S, Mándi M, Törőcsik B, Gerencsér AÁ, **Kiss G**, Konrád C, Ádám-Vizi V, Chinopoulos C. (2011) Complex contribution of cyclophilin D to Ca^{2+}-induced permeability transition in brain mitochondria, with relation to the bioenergetic state. J Biol Chem, 286: 6345-6353.

   Impact factor: 4.773

7. Konrád C, **Kiss G**, Törőcsik B, Lábár JL, Gerencsér AÁ, Mándi M, Ádám-Vizi V, Chinopoulos C. (2011) A distinct sequence in the adenine nucleotide translocase from Artemia franciscana embryos is associated with insensitivity to bongkrekate and atypical effects of adenine nucleotides on Ca^{2+} uptake and sequestration. FEBS J, 278: 822-836.

   Impact factor: 3.790

8. Konrád C, **Kiss G**, Törőcsik B, Ádám-Vizi V, Chinopoulos C. (2012) Absence of Ca^{2+}-induced mitochondrial permeability transition but presence of bongkrekate-sensitive nucleotide exchange in C. crangon and P. serratus. PLoS One, **7**: e39839.

   Impact factor: 3.730

9. Chinopoulos C, **Kiss G**, Kawamata H, Starkov AA. Measurement of ADP-ATP exchange in relation to mitochondrial transmembrane potential and oxygen consumption. In: Galluzzi L, Kroemer G. (ed.), Methods in Enzymology Vol. 542. Conceptual Background and Bioenergetic/Mitochondrial Aspects of Oncometabolism. Academic Press, Burlingon, 2014: 333-348.

   Impact factor: 2.002 (2012)

DOI:10.14753/SE.2015.1713

11. ACKNOWLEDGEMENTS

I would like to thank first and foremost my tutor and supervisor; **Dr. Christos Chinopoulos** who introduced me not only to the field of bioenergetics but to scientific research in general with endless patience, enthusiasm, determination and honesty. His prodigious knowledge and experience in mitochondriology, straightforward criticism and insightful suggestions together provided for clear direction in the completion of my research and the preparation of this thesis.

I wish to express my gratitude to **Prof. Veronika Ádám-Vizi** who provided me the opportunity to work at the Department of Medical Biochemistry at Semmelweis University. As a fair and exemplary leader she supported the accomplishment of our projects in so many ways. My thanks go also to all my colleagues in the department for their encouragement, friendship and helpful discussions.

I am indebted to **Dr. Csaba Konrád** whom I have learnt and worked together with for 8 years as undergraduate, then PhD students. Our collaboration under the guidance of Christos gave rise to 8 publications as well as provided a solid basis for both of our theses. I also wish to thank him for his friendship and the stimulating discussions we have had.

Furthermore, I would like to give my gratitude to the various funding agencies for their financial support during the course of this research including the U.S. National Institutes of Health (NIH), Országos Tudományos Kutatási Alapprogram (OTKA), Magyar Tudományos Akadémia (MTA), Egészségügyi Tudományos Tanács (ETT) and Astellas Pharma Research Grant offered through the Kerpel-Fronius Ödön Talent Support Program of Semmelweis University.

Finally, but most important of all, I am honestly thankful to my loving wife **Judit** for her remarkable patience, understanding and support over the last few years but especially during the preparation of this thesis. I also wish to thank my family for their love, support and never failing faith in me.